UNCLASSIFIED

AD NUMBER
AD340137
CLASSIFICATION CHANGES
TO: unclassified
FROM: secret
LIMITATION CHANGES
TO: Approved for public release, distribution unlimited
FROM: Distribution authorized to U.S. Gov't. agencies and their contractors; Administrative/Operational Use; 30 APR 1958. Other requests shall be referred to Air Force Wright Air Development Center, Aircraft Laboratory, Wright-Patterson AFB, OH 45433.
AUTHORITY
dna ltr 27 oct 1980; dna ltr 27 oct 1980

THIS PAGE IS UNCLASSIFIED

SECRET
RESTRICTED DATA

AD 340137L

DEFENSE DOCUMENTATION CENTER
FOR
SCIENTIFIC AND TECHNICAL INFORMATION
CAMERON STATION, ALEXANDRIA, VIRGINIA

RESTRICTED DATA
SECRET

NOTICE: When government or other drawings, specifications or other data are used for any purpose other than in connection with a definitely related government procurement operation, the U. S. Government thereby incurs no responsibility, nor any obligation whatsoever; and the fact that the Government may have formulated, furnished, or in any way supplied the said drawings, specifications, or other data is not to be regarded by implication or otherwise as in any manner licensing the holder or any other person or corporation, or conveying any rights or permission to manufacture, use or sell any patented invention that may in any way be related thereto.

NOTICE:

THIS DOCUMENT CONTAINS INFORMATION AFFECTING THE NATIONAL DEFENSE OF THE UNITED STATES WITHIN THE MEANING OF THE ESPIONAGE LAWS, TITLE 18, U.S.C., SECTIONS 793 and 794. THE TRANSMISSION OR THE REVELATION OF ITS CONTENTS IN ANY MANNER TO AN UNAUTHORIZED PERSON IS PROHIBITED BY LAW.

SECRET
RESTRICTED DATA
SPACE TECHNOLOGY LABORATORIES, INC.
10636 Copy 176
WT-1134
This document consists of 129 pages
No. 176 of 240 copies, Series A
AFBMD Technical Library HQARDC
AFBMD Technical Library HQARDC
AIR FORCE BALLISTIC MISSILE DIVISION TECHNICAL LIBRARY
Document No. 8-7314
Copy No. 1
rule 6
RESTRICTED DATA
This document contains restricted data as defined in the Atomic Energy Act of 1954. Its transmittal or the disclosure of its contents in any manner to an unauthorized person is prohibited.
EXCLUDED FROM AUTOMATIC REGRADING: DOD DIR 5200.10 DOES NOT APPLY
RESTRICTED DATA
SECRET
AFSWP-1637
USAF

Operation TEAPOT

NEVADA TEST SITE

February – May 1955

Project 5.4

EVALUATION OF FIREBALL LETHALITY USING BASIC MISSILE STRUCTURES (C)

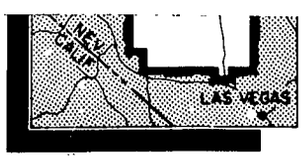

HEADQUARTERS FIELD COMMAND, ARMED FORCES SPECIAL WEAPONS PROJECT
SANDIA BASE, ALBUQUERQUE, NEW MEXICO

RESTRICTED DATA
SECRET

Inquiries relative to this report may be made to

Chief, Armed Forces Special Weapons Project
Washington, D. C.

When no longer required, this document may be destroyed in accordance with applicable security regulations.

DO NOT RETURN THIS DOCUMENT

AEC Technical Information Service Extension
Oak Ridge, Tennessee

(4) NM (5) 242 900

(6) NA

SECRET

Restricted Data

REG. NO. 18301 X

LOG. NO. 8-9446

WDSOT

RESTRICTED DATA

AFBMD
Technical Library
HQARDC

(18) DASA (20) S-RD

(19) Rept. No. WT-1134

(21) Report and

OPERATION TEAPOT—PROJECT 5.4 [U]

AFBMD
Technical Library
HQARDC

(9) NA

Report to the Test Director

(7) # EVALUATION OF FIREBALL LETHALITY USING BASIC MISSILE STRUCTURES (C)

(8)

(11) 30 Apr 58

(10) by

J. E. Kester and
R. B. Ferguson, Capt., USAF

University of Dayton
Dayton, Ohio

Aircraft Laboratory
Wright Air Development Center
Dayton Ohio

(12) 129 p.

(13) NA

(14-17) NA

"This document contains information affecting the National Defense of the United States within the meaning of the Espionage Laws, Title 18, U. S. C., Section 793 and 794. Its transmission or the revelation of its contents in any manner to an unauthorized person is prohibited by law."

Issuance Date: April 30, 1958

Lde

RESTRICTED DATA

This document contains restricted data as defined in the Atomic Energy Act of 1954. Its transmittal or the disclosure of its contents in any manner to an unauthorized person is prohibited.

SUMMARY OF SHOT DATA, OPERATION TEAPOT

Shot	Code Name	Date	Time*	Area	Type	Latitude and Longitude of Zero Point
1	Wasp	18 February	1200	T–7–4†	762-ft Air	37° 05' 11.6856" 116° 01' 18.7368"
2	Moth	22 February	0545	T–3	300-ft Tower	37° 02' 52.2654" 116° 01' 15.6967"
3	Tesla	1 March	0530	T–9b	300–ft Tower	37° 07' 31.5737" 116° 02' 51.0977"
4	Turk	7 March	0520	T–2	500-ft Tower	37° 08' 18.4944" 116° 07' 03.1679"
5	Hornet	12 March	0520	T–3a	300-ft Tower	37° 02' 25.4043" 116° 01' 31.3674"
6	Bee	22 March	0505	T–7–1a	500-ft Tower	37° 05' 41.3880" 116° 01' 25.5474"
7	ESS	23 March	1230	T–10a	67-ft Underground	37° 10' 06.1263" 116° 02' 37.7010"
8	Apple	29 March	0455	T–4	500-ft Tower	37° 05' 43.3200" 116° 06' 09.9040"
9	Wasp'	29 March	1000	T–7–4‡	740-ft Air	37° 05' 11.6856" 116° 01' 18.7368"
10	HA	6 April	1000	T–5§	36,620-ft MSL Air	37° 01' 43.3642" 116° 03' 28.2624"
11	Post	9 April	0430	T–9c	300-ft Tower	37° 07' 19.6965" 116° 02' 03.8860"
12	MET	15 April	1115	FF	400-ft Tower	36° 47' 52.6887" 115° 55' 44.1086"
13	Apple 2	5 May	0510	T–1	500-ft Tower	36° 03' 11.1095" 116° 06' 09.4937"
14	Zucchini	15 May	0500	T–7–1a	500-ft Tower	37° 05' 41.3880" 116° 01' 25.5474"

* Approximate local time, PST prior to 24 April, PDT after 24 April.
† Actual zero point 36 feet north, 426 feet west of T–7–4.
‡ Actual zero point 94 feet north, 62 feet west of T–7–4.
§ Actual zero point 36 feet south, 397 feet west of T–5.

ABSTRACT

Even though future atomic attack via intercontinental ballistic missiles is an evident possibility, there exists at present no known system of defense. It is apparent that any defense system will require a warhead with a large lethal radius; hence, the possibility of using a nuclear warhead is being strongly considered. The test described herein was conducted to provide preliminary information on the thermal lethality of a nuclear explosion.

Solid steel and aluminum spheres and hollow steel cylinders were exposed atop lightweight television towers at five different ranges within the fireball of Shot 12. All of the tower mounted specimens were recovered, and it was possible to obtain curves of depth of metal loss versus distance from the burst point for each of the specimen types. The maximum metal loss from the steel spheres was 0.4 inch; from the aluminum spheres, 1.3 inch; and from the steel cylinders, 0.26 inch (at the center). Several types of ceramics were inserted in some of the aluminum spheres; however, because of heavy blast damage, the data on ceramics vulnerability were only qualitative, indicating only that the ceramics were somewhat less vulnerable to material loss than aluminum. Because of the limited scope of the lethality-study program, relatively few specific conclusions and recommendations can be made on the basis of test results alone; however, since this method of testing was shown to be feasible, additional tests which are more comprehensive should be conducted.

In addition to the specimens exposed within the fireball, small samples of molybdenum, graphite, and two ceramic materials were exposed at ranges external to the fireball. The purpose of these exposures was to determine the thermal-shock-resistant characteristics of various materials, designed for use as protective surfaces for intercontinental ballistic missiles, under conditions of rapid heating such as would be experienced during re-entry of the missile into the atmosphere. A parabolic reflector was used at the farthest range to concentrate the thermal energy on the specimens. The ceramics at the parabolic reflector were severely glazed, but no thermal-shock damage was observed. The materials directly exposed at closer ranges sustained sufficient blast damage to obscure any thermal damage which may have been inflicted on the specimens.

FOREWORD

This report presents the final results of one of the 56 projects comprising the Military Effects Program of Operation Teapot, which included 14 test detonations at the Nevada Test Site in 1955.

For overall Teapot military-effects information, the reader is referred to "Summary Report of the Technical Director, Military Effects Program," WT-1153, which includes the following: (1) a description of each detonation including yield, zero-point environment, type of device, ambient atmospheric conditions, etc.; (2) a discussion of project results; (3) a summary of the objectives and results of each project; and (4) a listing of project reports for the Military Effects Program.

PREFACE

The test described herein was the first test of its kind to be conducted and as such was designed to be rather exploratory in nature. Hence, only a limited amount of data was obtained. The fact that the vulnerability data were obtained only for several types of specimens and under particular environmental conditions should be remembered when using these data to predict damage under different exposure conditions.

In order to minimize the amount of descriptive detail and the number of photographs in the main body of the report, Appendix A was included to serve as a repository for the description and photographs of the damage to each individual specimen. The major results and general descriptions of the damage are summarized in Chapter 3. Consequently, only the reader interested in the peculiarities of the damage to individual specimens need refer to Appendix A. Appendix B comprises a discussion of the trajectories of the lethality-study specimens and Appendix C, a brief description of the damage to the various shot towers used during Operation Teapot.

Project 5.4 was conducted under the direction of the Project Officer, Captain R. B. Ferguson, USAF, of Wright Air Development Center. Contractual support was provided by the University of Dayton on Contract AF 33(616)-2664 under the supervision of E. J. Freeh with the author acting as Project Engineer. Among the many who contributed significantly during the initial planning of the Project were: J. F. Magee, University of Notre Dame; E. J. Zadina, Special Weapons Center; B. R. Suydam, Los Alamos Scientific Laboratory.

The support of R. D. Holbrook, W. B. Graham, and B. W. Augenstein of Rand Corporation in assisting in the design of the lethality study is gratefully acknowledged. W. F. Radcliffe and M. L. Streiff of Convair were instrumental in bringing the thermal-shock study of ceramics to practical completion. The author wishes to thank the personnel of the U. S. Naval Radiological Defense Laboratory, Thermal Radiation Branch, for supplying the specially designed radiometers and calorimeters to Project 5.4 and, also, for their suggestion of using the parabolic reflector. The interest, generous assistance, and outstanding cooperation of the Program 5 Director, Cdr. Charles C. Hoffman, USN, contributed immeasurably to the successful completion of the test.

CONTENTS

ABSTRACT 5

FOREWORD 6

PREFACE 7

CHAPTER 1 INTRODUCTION 15
1.1 Objective 15
1.2 Military Significance 15
1.3 Background and Theory 16

CHAPTER 2 PROCEDURE 18
2.1 Lethality Study 18
2.1.1 Spherical Specimens 20
2.1.2 Cylindrical Specimens 21
2.2 Thermal-Shock Study 24
2.3 Instrumentation 28

CHAPTER 3 RESULTS 30
3.1 Lethality Study 30
3.1.1 Spherical Specimens 33
3.1.2 Steel Cylinders 37
3.1.3 Ceramic Inserts 47
3.2 Thermal-Shock Study 50
3.3 Instrumentation and Thermal Inputs 54

CHAPTER 4 DISCUSSION 58
4.1 Lethality Study 58
4.2 Thermal-Shock Study 66

CHAPTER 5 CONCLUSIONS AND RECOMMENDATIONS 69
5.1 Conclusions 69
5.1.1 Lethality Study 69
5.1.2 Thermal-Shock Study 70
5.2 Recommendations 70
5.2.1 Lethality Study 70
5.2.2 Thermal-Shock Study 71

APPENDIX A DESCRIPTION OF DAMAGE TO LETHALITY-STUDY SPECIMENS 72
A.1 Steel Spheres 72
A.1.1 Tower 1 (Ref. Figure A.1) 72
A.1.2 Tower 2 (Ref. Figure A.2) 72
A.1.3 Tower 3 (Ref. Figure A.3) 72
A.1.4 Tower 4 (Ref. Figure A.4) 72
A.1.5 Tower 5 (Ref. Figure A.5) 72

A.1.6 Base of Tower 1 73
A.2 Aluminum Spheres 73
A.2.1 Tower 1 (Ref. Figure A.6) 73
A.2.2 Tower 2 (Ref. Figure A.7) 73
A.2.3 Tower 3 (Ref. Figure A.8) 73
A.2.4 Tower 4 (Ref. Figure A.9) 73
A.2.5 Tower 5 (Ref. Figure A.10) 76
A.3 Ceramic Insert Spheres 76
A.3.1 Tower 1 (Ref. Figure A.11) 76
A.3.2 Tower 2 (Ref. Figure A.12) 77
A.3.3 Tower 3 (Ref. Figure A.13) 81
A.3.4 Tower 4 (Ref. Figure A.14) 82
A.3.5 Tower 5 (Ref. Figure A.15) 83
A.4 Steel Cylinders 85
A.4.1 Tower 1, Left Side, 1-in. Hole (Ref. Figure A.19) 85
A.4.2 Tower 1, Right Side, 1-in. Hole (Ref. Figure 3.20) 90
A.4.3 Tower 2, Left Side, 1-in. Hole (Ref. Figure A.21(a), (b), and (c) 90
A.4.4 Tower 2, Right Side, 2-in. Hole (Ref. Figure A.21(d), (e), and (f) 90
A.4.5 Tower 3, Left Side, 2-in. Hole (Ref. Figure A.22) 91
A.4.6 Tower 3, Right Side, 3-in. Hole (Ref. Figure A.23)..... 91
A.4.7 Tower 4, Left Side, 3-in. Hole (Ref. Figure A.24)..... 92
A.4.8 Tower 4, Right Side, 4-in. Hole (Ref. Figure A.25)..... 96

APPENDIX B TRAJECTORIES OF LETHALITY-STUDY SPECIMENS 97
B.1 Derivation of Equations 97
B.2 Summary of Trajectory Data 99

APPENDIX C DESCRIPTION OF SHOT TOWER DAMAGE 111
C.1 Description of Towers 111
C.2 Summary of Tower Damage 116
C.2.1 Shot 2 (300-ft, Triangular Tower) 116
C.2.2 Shot 3 (300-ft, 30-ton Square Tower) 116
C.2.3 Shot 4 (500-ft, 100-ton Square Tower)..... 117
C.2.4 Shot 5 (300-ft, 100-ton Square Tower)..... 119
C.2.5 Shot 6 (500-ft, 100-ton Square Tower)..... 120
C.2.6 Shot 8 (500-ft, 100-ton Square Tower)..... 121
C.2.7 Shot 11 (300-ft, 100-ton Square Tower)..... 122
C.2.8 Shot 12 (400-ft, 100-ton Square Tower)..... 123
C.2.9 Television Towers 125

ILLUSTRATIONS
2.1 Layout for Lethality Study and Thermal-Shock Test 19
2.2 Typical Tower Installation 22
2.3 Ceramic-Insert Sphere 22
2.4 Construction Details of Spheres and Cylinders 23
2.5 Hollow Steel Cylinder 23
2.6 Delta-Wing Pylon 24
2.7 Parabolic Mirror, Range 6,500 Feet 25
2.8 Support Structures for Exposure of Ceramic Materials 26
2.9 Relative Dimensions of Delta-Wing Pylons 26

2.10 Test Specimens for Thermal-Shock Study 27
2.11 Typical Test Exposure of Materials for Thermal-Shock Study 27
2.12 Magnification of Ceramic Specimens in Mirror 27
2.13 Instrumentation Schematic 29
3.1 General Debris of Shot Tower and TV Towers 32
3.2 Typical Post-Shot Locations of Test Specimens 33
3.3 Schematic of Recovery Area Showing Post-Shot Locations of Test Specimens 36
3.4 Overall Views of Each Type of Spherical Specimen Showing Gradation in Size 38
3.5 Profiles of Steel Spheres 38
3.6 Profiles of Solid Aluminum Spheres 39
3.7 Profiles of Ceramic-Insert Spheres 39
3.8 Overall View of Steel Cylinders 41
3.9 Longitudinal Profiles of Cylinder From Right Side of Tower 1 42
3.10 Longitudinal Profile of Cylinder From Right Side of Tower 2 43
3.11 Longitudinal Profile of Cylinder From Right Side of Tower 3 43
3.12 End Face of Cylinder From Left Side of Tower 1 44
3.13 Pock Marks on Cylinders 44
3.14 Cross Section at Center of Cylinder From Left Side of Tower 1 46
3.15 Cross Section at Center of Cylinder From Right Side of Tower 1 46
3.16 Cross Sections of Hemispherical Holes on Cylinders 48
3.17 Hemispherical Holes on Cylinders With 1-in. Walls From Towers 3 and 4 49
3.18 Maximum Observed Protrusion of Battelle and Graphite Inserts 49
3.19 Once-Molten Aluminum Covering Three Front Ceramic Inserts, Tower 2 49
3.20 Battelle and Armour Ceramics From Focal Point of Mirror 52
3.21 Post-Shot Photographs of Specimens Exposed on Pylons and Pipe Mount 53
3.22 Calculated Radiant Exposure and Peak Irradiance versus Ground Range 55
3.23 Sequence of Frames From a Film Showing Engulfment of Tower Specimens by Fireball 56
4.1 Variation of Weight Loss With Distance From the Burst Point for Aluminum and Steel Spheres 62
4.2 Variation of Reduction-of-radius With Distance From the Burst Point for Aluminum and Steel Spheres 62
4.3 Variation of Weight Loss With Distance From the Burst Point for Steel Cylinders 62
4.4 Variation of Average Metal Loss at the Center of the Cylinders (Reduction-in-wall-thickness) With Distance From the Burst Point for Steel Cylinders 63

4.5	Apparent Material Loss From Armour Ceramic, Battelle Ceramic, and Graphite Inserts	63
A.1	Steel Sphere, Tower 1	74
A.2	Steel Sphere, Tower 2	74
A.3	Steel Sphere, Tower 3	74
A.4	Steel Sphere, Tower 4	75
A.5	Steel Sphere, Tower 5	75
A.6	Aluminum Sphere,Tower 1	75
A.7	Aluminum Sphere, Tower 2	75
A.8	Aluminum Sphere, Tower 3	78
A.9	Aluminum Sphere, Tower 4	78
A.10	Aluminum Sphere, Tower 5	79
A.11	Ceramic-Insert Sphere, Tower 1	79
A.12	Ceramic-Insert Sphere, Tower 2	84
A.13	Ceramic-Insert Sphere, Tower 3	84
A.14	Ceramic-Insert Sphere, Tower 4	84
A.15	Ceramic-Insert Sphere, Tower 5	85
A.16	Armour Ceramic Inserts After Exposure	86
A.17	Battelle Ceramic Inserts After Exposure	87
A.18	Graphite Inserts After Exposure	88
A.19	Cylinder From Tower 1, Left Side, 1-in.-diameter Hole	89
A.20	Cylinder From Tower 1, Right Side, 1-in.-diameter Hole	92
A.21	Cylinders From Left Side (1-in. Hole) and Right Side (2-in. Hole) of Tower 2	93
A.22	Cylinder From Tower 3, Left Side, 2-in. Hole	94
A.23	Cylinder From Tower 3, Right Side, 3-in. Hole	94
A.24	Cylinder From Tower 4, Left Side, 3-in. Hole	95
A.25	Cylinder From Tower 4, Right Side, 4-in. Hole	95
B.1	Reference Sketch for Trajectory Calculations	102
B.2	Variation of Angle of Departure of Specimen From Tower With Distance From Burst Point	102
B.3	Variation of Initial Velocities of Spheres With Distance From the Burst Point	104
B.4	Variation of Impact Velocity With Distance Penetrated in Ground for 10-in.-diameter Steel and Aluminum Spheres	104
B.5	Variation of Distance From Apparent Fireball Center With Time After Detonation for Steel Spheres	107
B.6	Variation of Distance From Apparent Fireball Center With Time After Detonation for Aluminum Spheres	107
B.7	Variation of Distance From Apparent Fireball Center With Time After Detonation for Ceramic-Insert Spheres	108
B.8	Variation of Distance From Apparent Fireball Center With Time After Detonation for Cylinders From Left Side of the Towers	108
B.9	Variation of Distance From Apparent Fireball Center With Time After Detonation for Cylinders From Right Side of the Towers	109
B.10	Rise of Fireball Center Above Burst Point as a Function of Time After Detonation	109
C.1	Typical Tower Construction	114
C.2	Pre-Shot Views of Typical Towers	115

C.3 Close-Up Views of Various Towers 117
C.4 Shot 2 Tower Wreckage 118
C.5 Shot 3 Tower Wreckage 119
C.6 Shot 4 Tower Wreckage 120
C.7 Shot 5 Tower Wreckage 121
C.8 Shot 6 Tower Wreckage 122
C.9 Shot 8 Tower Wreckage 123
C.10 Shot 11 Tower Wreckage 124
C.11 Shot 12 Tower Wreckage 125

TABLES

2.1 Deployment of Spherical and Cylindrical Test Specimens 20
2.2 Summary of Materials Used in Fabrication of Specimens 22
2.3 Deployment of Materials and Predicted Thermal Inputs 28
3.1 Summary of Depth of Penetration and Horizontal Distance Traveled for Spheres and Cylinders 34
3.2 Summary of Pre-Shot and Post-Shot Measurements of Spherical Specimens 37
3.3 Summary of Sphere Diameters 40
3.4 Summary of Cylinder Data 45
3.5 Summary of Protrusion and Loss of Material for Ceramic Inserts 51
3.6 Summary of Pre-Shot and Post-Shot Masses of Thermal-Shock Study Specimens 54
3.7 Estimated Thermal Inputs for Thermal-Shock Study 57
4.1 Summary of External Pressures Required to Yield Cylinders Under Static Conditions 64
B.1 List of Symbols 100
B.2 Summary of Individually Calculated Departure Angles, A 100
B.3 Summary of Trajectory Parameters 106
B.4 Comparison of Terminal Velocities of Spheres 106
C.1 Summary of Data for Tower Shots 112
C.2 Summary of Main Support Member, Tension Member, and Guy Cable Sizes for Square Towers 113
C.3 Distribution of Weight and Material for the 400 Ft, 100 Ton Tower (Shot 12)..... 116
C.4 Summary of Damage to Tower Legs and Guy Cables..... 126

Chapter I
INTRODUCTION

1.1 OBJECTIVE

Project 5.4 comprised two investigations: a lethality study and a thermal-shock study. The objective of the lethality study was to determine the thermal lethality of a nuclear fireball as applied to basic missile structures such as spheres and cylinders. This knowledge should permit a preliminary estimation of the lethal range of a nuclear fireball employed to defend friendly target areas against enemy intercontinental ballistic missiles of the Atlas type or smaller missiles of the V-2 class which may be capable of carrying nuclear warheads.

The purpose of the thermal-shock study was to determine the thermal shock resistance of various ceramic materials exposed to thermal flux intensities of approximately the same magnitude as fluxes produced by the aerodynamic heating of an intercontinental ballistic missile of the Atlas type during re-entry of the missile into the atmosphere. The data obtained from exposure of these ceramic materials will be of primary value in the design of heat-resistant coatings for intercontinental ballistic missiles.

1.2 MILITARY SIGNIFICANCE

The fact that intercontinental ballistic missiles are nearing reality, with the consequent threat to the security of the nation, makes the development of an adequate defense system an urgent requirement. Considerable thought has been given to the problem of protecting against hostile intercontinental ballistic missiles; however, partly because of the scarcity of vulnerability data, there is at present no positive method of defense. Because of the high velocity and the variety of evasive tactics that can be employed, the problem of intercepting and destroying a ballistic missile of the Atlas type imposes severe requirements on the hypothetical defense system. Because of the magnitude of the anticipated average miss distance, it is doubtful that conventional warheads have sufficiently large lethal radii to give a reasonable overall probability of successful interception.

It was speculated that a nuclear warhead may have a greater lethal range of destruction than conventional warheads in the application of ballistic missile defense. However, because of the lack of factual

information on the capabilities of nuclear weapons employed in this manner, it was suggested that an experimental test be conducted.

1.3 BACKGROUND AND THEORY

Determination of the capabilities of a nuclear weapon used as a defensive warhead for interception of intercontinental ballistic missiles has been strongly advocated by many since the initial test proposal in December of 1953. This proposal stemmed from suggestions by Project Wizard personnel of the Willow Run Research Center who were working on the general problem of missile defense. The propoced test was comprehensive and included using various types of rockets fired in several salvos so as to enter the fireball at predetermined times after detonation.

As a result of several meetings held in connection with the problem of ballistic missile defense, it was agreed that the proposal was more comprehensive than was warranted for an initial investigation and that a simple and more basic type of test should be conducted. The test suggested was designed primarily to investigate the thermal lethality of a nuclear explosion with respect to basic metal and ceramic structures. Spheres were selected as the primary test structure because of their simplicity, insensitivity to orientation, and moderate coefficient of drag. Analysis of the missile defense problem indicates that interception would probably take place at high altitude, in which event, because of the low air density, the overpressure and drag forces may be considerably less effective than the accompanying thermal energy in destroying a ballistic missile. A small-yield weapon was detonated at 36,620 feet during this operation and should provide some useful data pertinent to this problem. A higher-altitude burst is being planned for a future test and should yield information from which it will be possible to predict more accurately the lethal range of a nuclear explosion at high altitude.

Personnel working on the problem of ballistic missile defense suggested that hollow steel cylinders also be exposed at ranges within the fireball to investigate the possibility of a thermally induced shock wave in the cylinder wall causing internal failure or spalling and also to investigate metal loss from this type of configuration.

At the time of the planning phase of this program there had been little theoretical work done on evaluating the response of a ballistic missile in the vicinity of a nuclear fireball because of lack of factual information on thermal and blast phenomena of a nuclear explosion at high altitude and because of insufficient information regarding the behavior of materials exposed to high thermal fluxes. It is generally agreed that in order to intercept effectively an intercontinental ballistic missile it must be intercepted early in its re-entry stage, probably above 100,000 feet. Although altitude and yield scaling laws do exist, there are many who question their validity, and, as a consequence, calculations based on these scaled inputs have been looked upon

with skepticism. It is, however, agreed that at high burst altitudes the partition of energy released would change and yield less blast energy and more thermal energy. It was for this reason that it was decided to evaluate primarily the effects of thermal energy on ballistic missiles.

An important factor in determining the amount of metal lost from the surface of a missile exposed to high intensity thermal radiation is the opacity of the vaporized metal lost during the initial radiation. This factor is probably the least well known, and it was believed that the only way to obtain values of metal loss would be actually to measure the metal loss during a full-scale nuclear test program. It was speculated that, from analyses of measurements of the metal loss incurred in a nuclear fireball, it would be possible to obtain relative values of opacities of particular materials.

Effects based on a theoretical analysis of the problem of fireball lethality, even for the simple case of material loss from a solid sphere, are at best only estimates. Some of the factors that are presently not well enough understood to permit accurate calculation are: an adequate knowledge of conditions within the fireball as a function of distance and time for various burst altitudes; the methods of heat transfer into the material; the response of material subjected to heat fluxes of the magnitude expected; the opacity and, therefore, the thermal attenuation caused by the vaporized material; and the influence of chemical reaction. From the empirical data obtained in this test, it may be possible to deduce qualitative information regarding most of the above factors; further theoretical and experimental work will be required for the quantitative conclusions ultimately desired.

The thermal-shock study using ceramic specimens was an outgrowth of work on the design of heat-dissipative systems for friendly intercontinental ballistic missiles of the Atlas type. Because of the high velocity of such missiles upon re-entry into the atmosphere, there is a great problem of dissipating the energy generated by aerodynamic heating. Theoretical calculations of the aerodynamic heating indicated that the intensity was of approximately the same magnitude as the thermal flux obtained in the proximity of a nuclear fireball.

Among the proposed methods of coping with the high heat fluxes experienced during re-entry were (1) the evaporation of a coolant as in porous cooling, (2) the use of materials capable of withstanding the high temperatures and, (3) allowing the surface material to absorb the energy with the consequent loss of metal through melting, vaporizing, oxidizing, or other processes. Because porous cooling appeared to offer the best promise, it was initially suggested that model nose-cone sections with porous cooling be exposed. However, primarily because of insufficient time, it was decided that nose-cone models could not be incorporated in the test; as a consequence, it was proposed that specimens of ceramics designed for coating various parts of the missile-structure be exposed to study their behavior when subjected to extremely high thermal fluxes.

Chapter 2
PROCEDURE

The test specimens for the lethality study were solid spheres 10 inches in diameter and hollow cylinders 10 inches long and 5 inches in diameter. These were exposed within a nuclear fireball to determine the vulnerability of these configurations to such an exposure. Both steel and aluminum were selected to be tested in the spherical structures; however, only steel was used in fabricating the cylinders. Several types of ceramics were also exposed in the form of inserts in some of the aluminum spheres. These specimens represent some basic structures and materials which could be an integral part of a typical intercontinental ballistic missile. The specimens were mounted atop each of five light television towers. Four of the tower tops were positioned so as to be in the fireball and the fifth just outside the fireball of Shot 12, the military-effect tower shot. The predicted yield of the shot was 26 KT.

The specimens for the thermal shock study were flat ceramic plates rigidly mounted at four ranges external to the fireball in order to determine the thermal-shock resistance under high thermal fluxes. At three ranges the ceramic specimens were directly exposed on rigid mounts; whereas at the fourth, the most-remote range, the specimens were positioned at the focal point of a large parabolic mirror, which was oriented towards the burst point. A pictorial presentation of the overall test array is given in Figure 2.1. There was no time-history response instrumentation attempted on any of the test specimens. Two measurements of the thermal inputs were attempted at the closer station of the thermal-shock study.

2.1 LETHALITY STUDY

The spherical and cylindrical specimens used for the lethality study were exposed atop towers having heights of 348, 296, 244, 192, and 140 feet positioned at ground ranges of 60, 120, 180, 240, and 300 feet, respectively. A line through the tops of the towers and the shot cab was at an angle of elevation of 41°. These towers were standard lightweight guyed television towers made by the Dresser Equipment Co., Florence, California. The towers were of triangular cross-section, 2 feet on a side, and were fabricated in 20-ft lengths, which were bolted together during erection. The towers were relatively inexpensive; the total cost including bases and erection on the site was about $20,000.

The positioning of the towers was determined from the predicted rate of fireball rise and growth so that the four towers which were

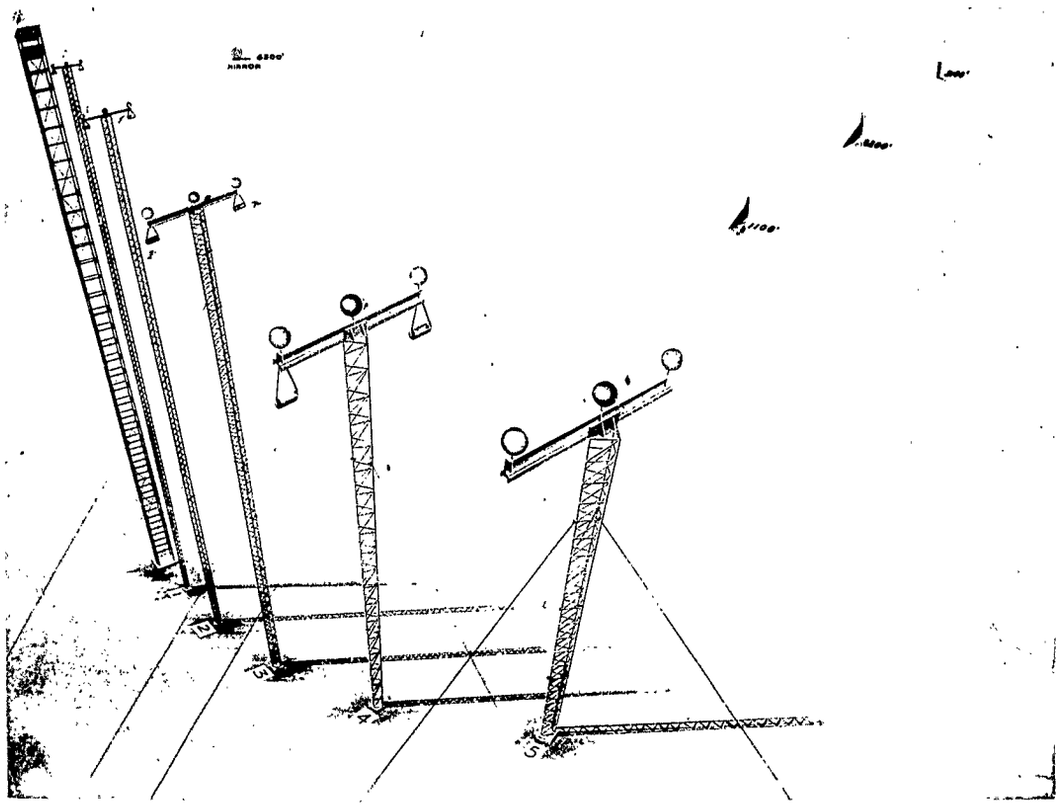

Figure 2.1 Layout for Lethality Study and Thermal-Shock Test

nearest to the shot tower would be in the fireball and the farthest tower just outside the fireball. In order that the test specimens would not interfere or collide with one another during exposure, the towers were positioned on separate azimuths from ground zero at 5° intervals. In an attempt to extend the lethality data to closer ranges, one steel and one aluminum sphere were placed in the shot cab. To determine if a fireball spike might travel down the TV towers, a solid steel ball was placed on the base of Tower 1. The deployment of the specimens for the lethality study is given in Table 2.1. Figure 2.2 shows a typical tower installation and the relative spacing of the specimens. The specimen mounts were designed to minimize the transmittal of forces from the crossbeam and mounting fixtures to the specimens. A 1/2 in. bolt was used to support each sphere such that the bottom of the sphere was 3 inches above the crossbeam. Each cylinder was attached to the steel mounting strap by two 1/4 in. machine screws. The mounting straps were 1/4 in. thick and 1-in. wide and were spaced about 1/8 inch from the end of the cylinder by two 1/4 in. washers.

In order that the test specimens could be distinguished from one another after exposure in such an extreme environment as the fireball of a nuclear explosion, it was necessary to provide means of post-shot

identification. To accomplish this a numbered slug was inserted in the center of each specimen. If the specimens remained intact after exposure, the numbered slug could be removed and positive identification affected. In the event that only small portions of the specimens would be found, the specimens were made from materials selected so as to have

TABLE 2.1 DEPLOYMENT OF SPHERICAL AND CYLINDRICAL TEST SPECIMENS

Tower No.	Tower Height (ft)	Ground Range (ft)	Azimuth	Steel Spheres	Aluminum Spheres	Ceramic Insert Spheres	Cylinder Wall Thickness (in.)	
							Left*	Right*
Shot Tower	400	12.3	N45E	X	X			
1	348	60	N70E	X	X	X	2.0	2.0
2	296	120	N65E	X	X	X	2.0	1.5
3	244	180	N60E	X	X	X	1.5	1.0
4	192	240	N55E	X	X	X	1.0	0.5
5	140	300	N50E	X	X	X		
1 (base)	0	60	N70E	X				

* Facing the Shot Tower

different but closely related compositions. Comparison of pre-shot and post-shot chemical analysis could then provide identification of the specimens. The materials selected for the steel specimens were in the range of from 1015 to 1060 steel. The aluminum specimens were made from two different heats each of three different aluminum alloys,

TABLE 2.2 SUMMARY OF MATERIALS USED IN FABRICATION OF SPECIMENS

Tower No.	Spheres			Steel Cylinders	
	Steel	Aluminum	Ceramic Insert	Left	Right
Shot Tower	1025	2014-T6			
1	1033	7075-T6	7075-T6	1015	1045
2	1050	6061-T6	6061-T6	1025	1055
3	1015	2014-T6*	2014-T6*	1020	1045
4	1040	7075-T6*	7075-T6*	1018	1055
5	1055	6061-T6*	6061-T6*		
1 (base)	1060				

* These materials were from a different heat than their corresponding alloys.

2014-T6, 6061-T6 and 7075-T6. A summary of the particular material used for each specimen is given in Table 2.2.

2.1.1 Spherical Specimens. Three different types of spherical specimens were exposed: solid steel, solid aluminum, and aluminum with ceramic inserts, all of which were 10 inches in diameter. The latter spheres contained two inserts of a ceramic developed by the Battelle

Memorial Institute, two inserts of a ceramic developed by the Armour Research Foundation, and two inserts of Speer, grade 250, graphite, as shown in Figures 2.3 and 2.4. The Battelle ceramic was an unfired ceramic containing 90 percent fuzed magnesium oxide powder, 5 percent asbestos fiber and 5 percent sodium silicate. The Armour ceramic was a pressed and sintered product made from Norton Magnorite No. 46F. This ceramic was sintered at about 1000°C and matured at about 1700°C. The constituents were: magnesium oxide, 97 percent; silicone dioxide, 1 1/2 percent; and calcium oxide, 1 1/2 percent. The graphite was designated as Speer Grade 250. One of each of the three types of spheres was placed at the top of each of the five TV towers, as shown in Figure 2.2. Also, one steel sphere and one aluminum sphere were positioned in the corner of the shot cab at a range of about 13 feet from the weapon which was about 3 feet above the cab floor. The ceramic-insert spheres were oriented such that three specimens, one of each type ceramic, were facing the shot cab with equal incidence angles (45 degrees), while the second specimen of each type ceramic faced away from the tower, as seen in Figures 2.3 and 2.4.

The ceramic inserts were 4-in. long tapering from a diameter of 1 inch on the exposed end to 1 1/8 inch on the end near the center of the sphere. The inserts were held in the sphere by the insert retainer, an externally threaded aluminum cylinder 1 1/2 inch in diameter and 4-in. long, internally tapered to accommodate the ceramic insert. The ceramic inserts were identified only by the sphere in which they were contained, because it was believed that if the inserts were detached from the containing sphere, they would be heavily damaged and probably not recovered.

2.1.2 Cylindrical Specimens. All of the cylindrical specimens were hollow steel cylinders provided with threaded end caps to protect the ends and inside of the cylinders, as seen in Figures 2.4 and 2.5. In order to evaluate the effect of wall thickness on interval spalling or failure, the wall thickness of the cylinders varied, in 1/2 in. increments, from 1/2 in. to 2-in. In addition, thicker wall cylinders were believed necessary for survival at the closer ranges. A total of eight cylinders were exposed; two on each of the first four towers, as indicated in Table 2.1. The cylinders were suspended below the cross-beam on top of the tower, as shown in Figure 2.2. The deployment of the cylinders was selected as far as possible so that at a given station there would be two cylinders with different wall thicknesses to compare the damage variation with this parameter and so that two cylinders with the same wall thickness would be exposed at two adjacent ranges in order to determine the variation of damage with range.

In order to investigate the effects of hypersonic fluid flow over small indentations, three 3/8 in.-diameter and three 3/16 in.-diameter hemispherical holes were machined on the surface of two cylinders, one from Tower 3 and the other from Tower 4. Both of the cylinders selected had 1-in.-thick walls. The holes were positioned on the surface of the

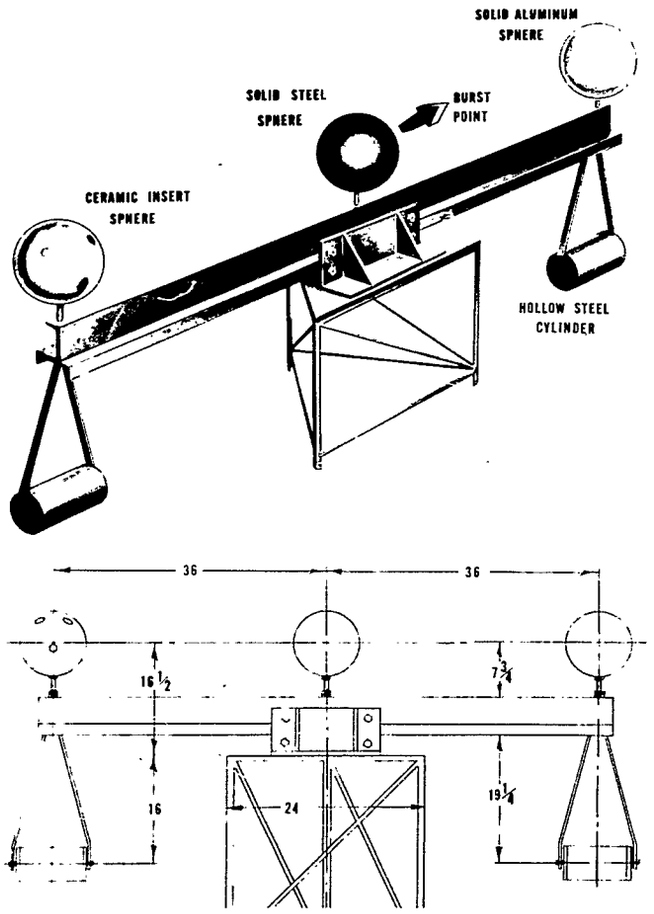

Figure 2.2 Typical Tower Installation

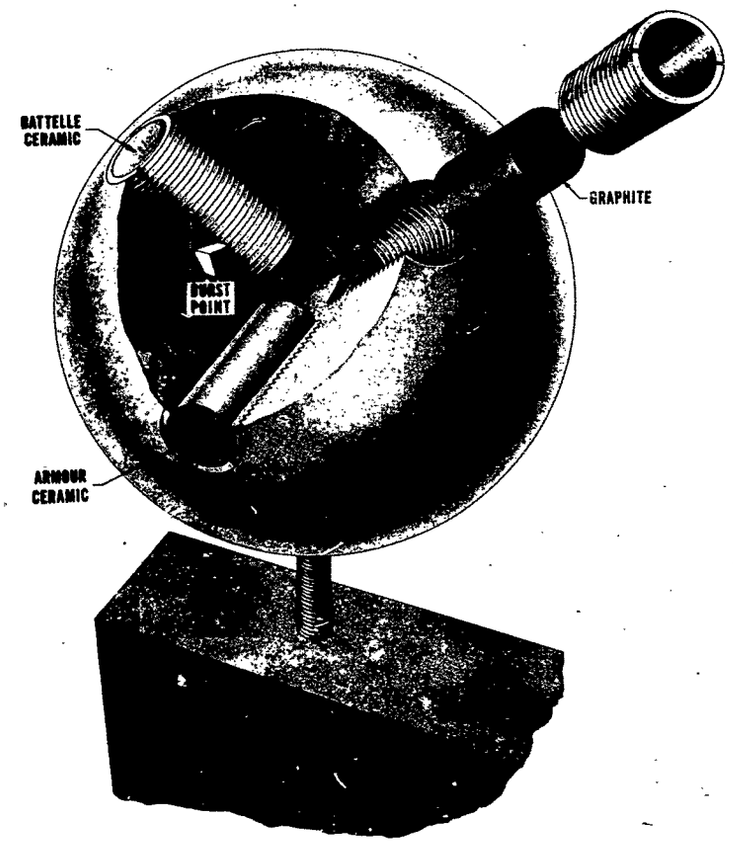

Figure 2.3 Ceramic-Insert Sphere

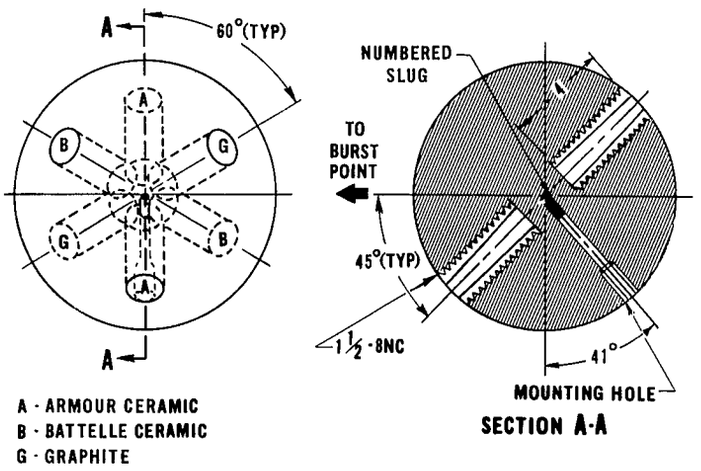

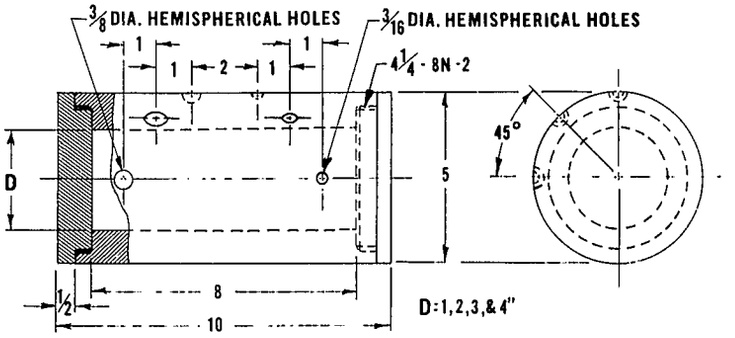

Figure 2.4 Construction Details of Spheres and Cylinders

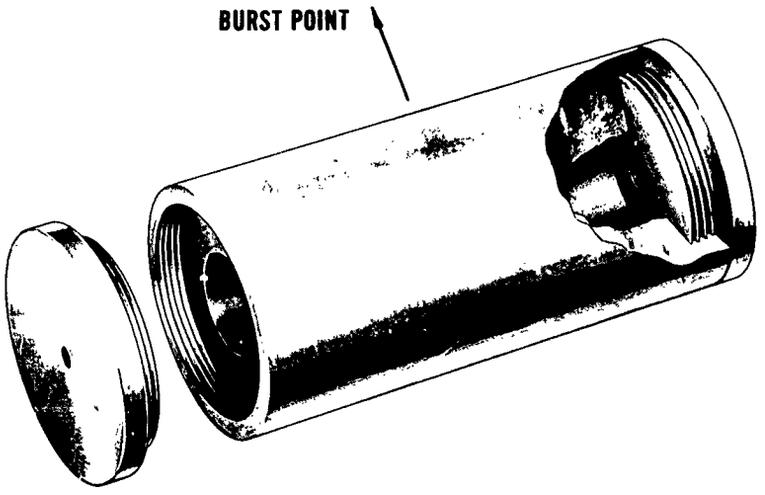

Figure 2.5 Hollow Steel Cylinder

cylinder so that one of each size would realize tangential flow; another set, 45-degree flow; and the remaining set, flow directly into the holes (normal incidence) as shown in Figure 2.4.

2.2 THERMAL-SHOCK STUDY

Small samples of various materials being developed for possible use as protective surfaces for intercontinental ballistic missiles were exposed to high-intensity thermal radiation to determine their thermal-shock-resistance characteristics. The samples were exposed in the form of thin flat plates rigidly mounted at four different ranges external to the fireball.

In order to obtain the high thermal intensities required for this investigation, it was realized that either the exposure stations would have to be relatively close to the nuclear explosion, and as a consequence in a region of high blast force, or else a means of magnifying the radiant flux would be necessary. Both methods of attack were investigated and two somewhat nonconventional exposure techniques were utilized: first, support structures of a delta-wing design, as seen in Figure 2.6, were used at the two closest exposure stations (1,100 and

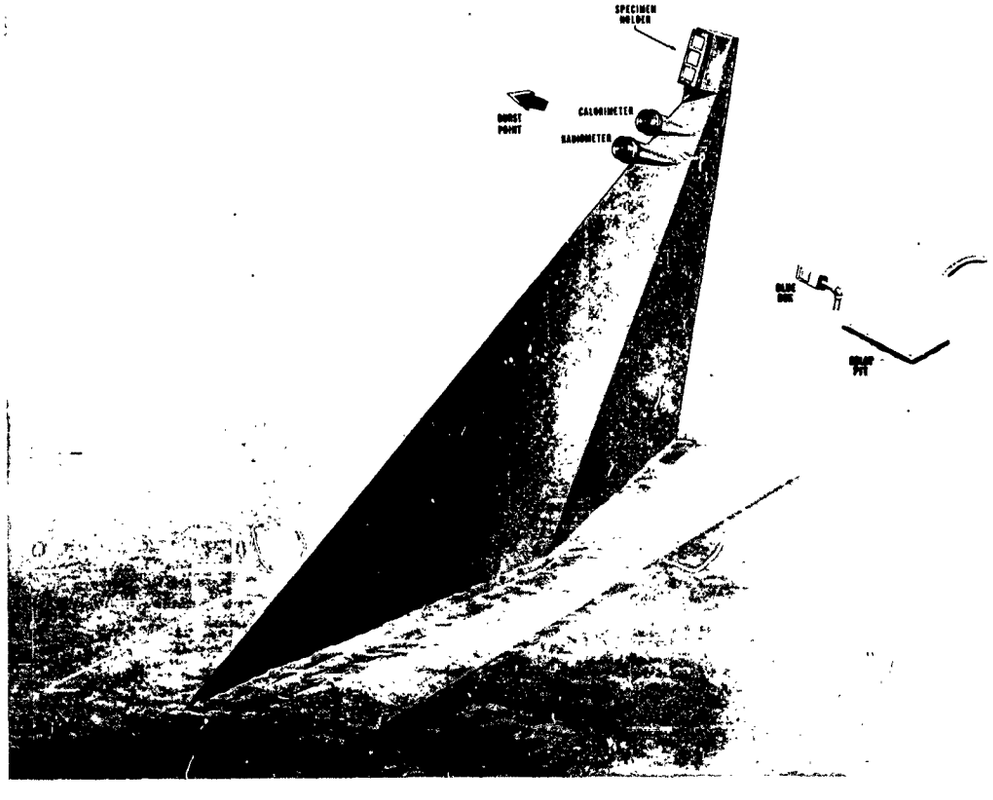

Figure 2.6 Delta-Wing Pylon

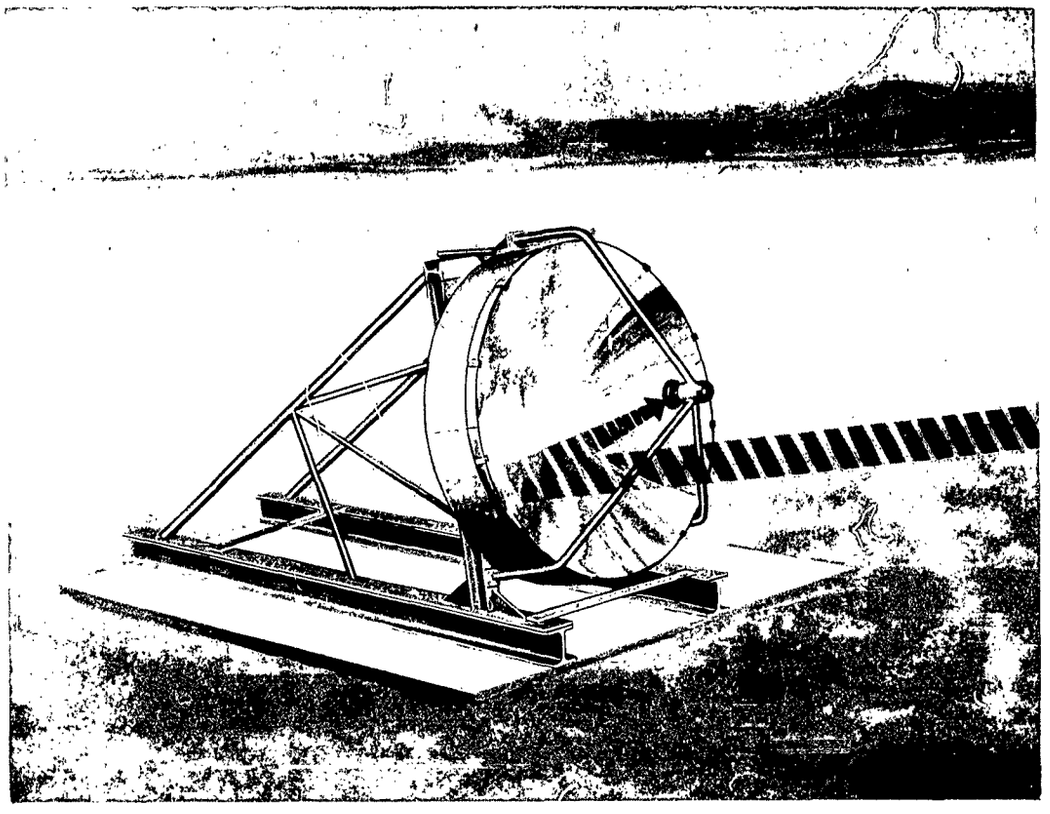

Figure 2.7 Parabolic Mirror, Range 6,500 Feet

2,200 feet) to reduce the effectiveness of high drag forces; and second, a parabolic reflector, as shown in Figures 2.7 and 2.8, was used to magnify the thermal flux at a remote range to obtain extremely high fluxes over a small area at the focal point. Both of these techniques were used in exposing the various ceramic materials; and although it was not a primary objective of the test, it was believed that an evaluation of these two exposure techniques was worth while.

The delta-wing pylons consisted of a relatively light substructure, covered with 1/2 in. steel plate and filled with concrete. The relative dimensions of both pylons were the same and are shown in Figure 2.9. Two pylons were fabricated, one 6-ft. high and the other 3 1/2 ft high, and were positioned at ranges of 1,100 and 2,200 feet respectively. On-site erection consisted of properly orienting the pylons and welding them to the metal base plate plate provided in the concrete pad. A 6-in., double extra-strong pipe, 6 feet in height, was used for the support structure at the 3,100-ft range. Photographs of the pylons and the pipe mount are shown in Figure 2.8.

The parabolic mirror was a surplus reflector from a 60-in. search light and had a focal length of 25.56 inches. The reflector was mounted rigidly by a relatively simple superstructure on an existing concrete

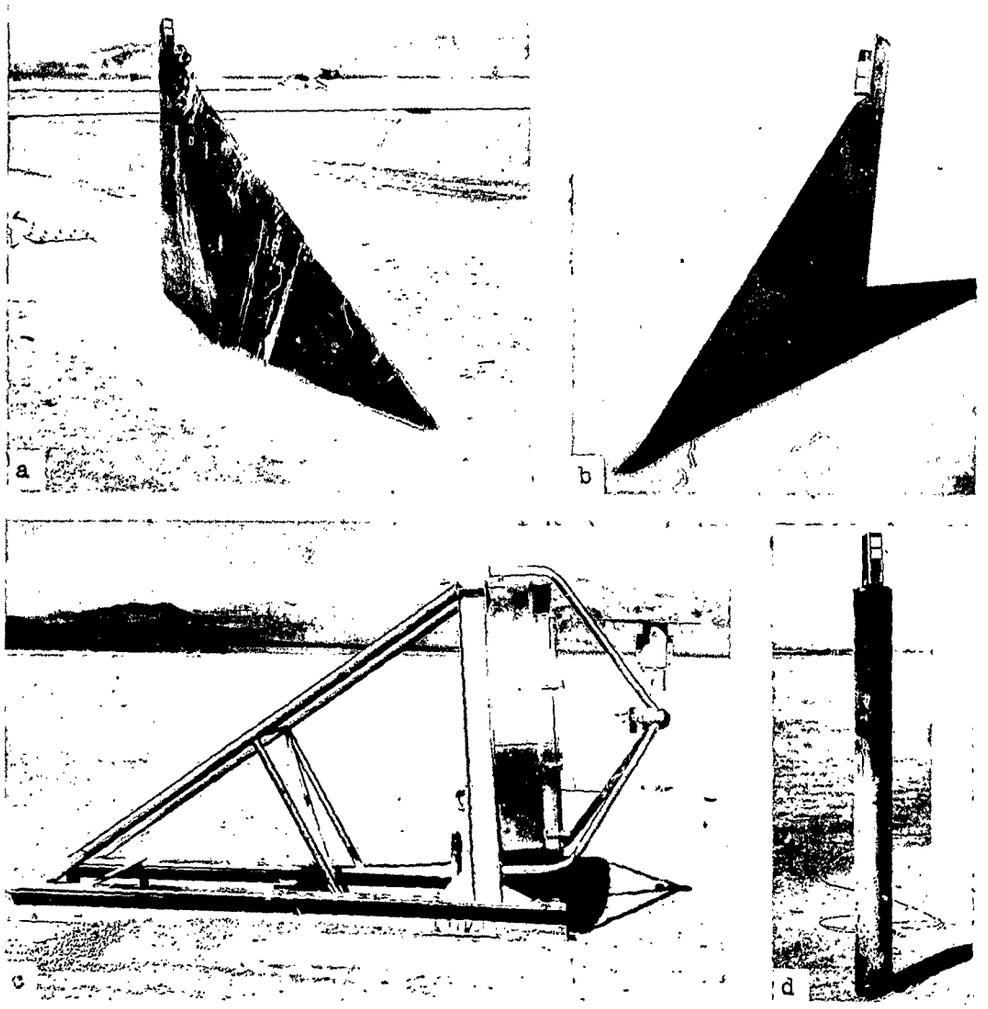

Figure 2.8 Support Structures for Exposure of Ceramic Materials. (a) 6-ft Pylon (1100 feet) (b) $3\frac{1}{2}$-ft Pylon (2200 feet) (c) Parabolic Reflector (6500 feet) (d) 6-ft Pipe Mount (3100 feet)

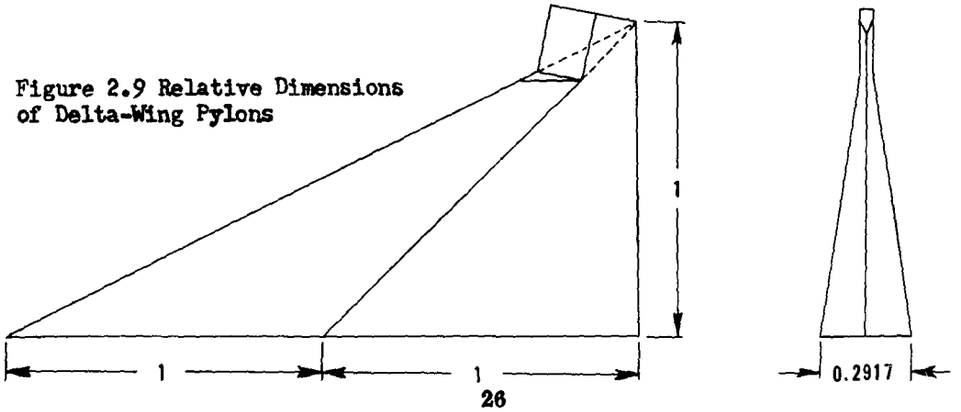

Figure 2.9 Relative Dimensions of Delta-Wing Pylons

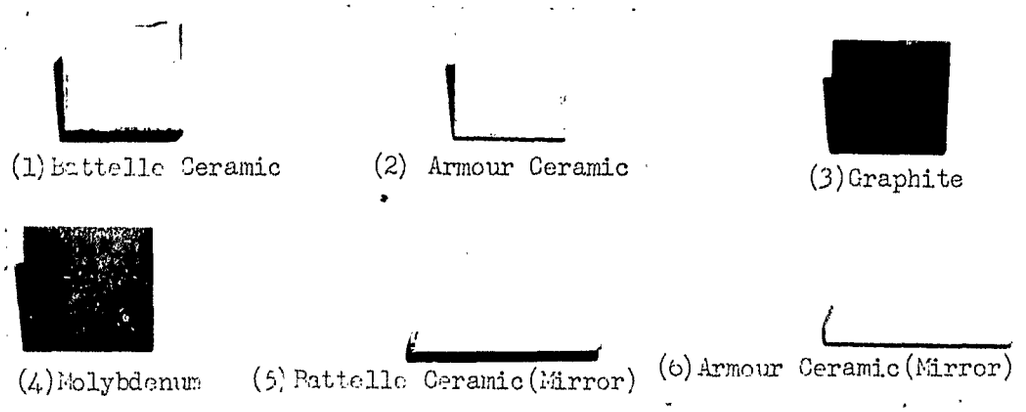

Figure 2.10 Test Specimens for Thermal-Shock Study

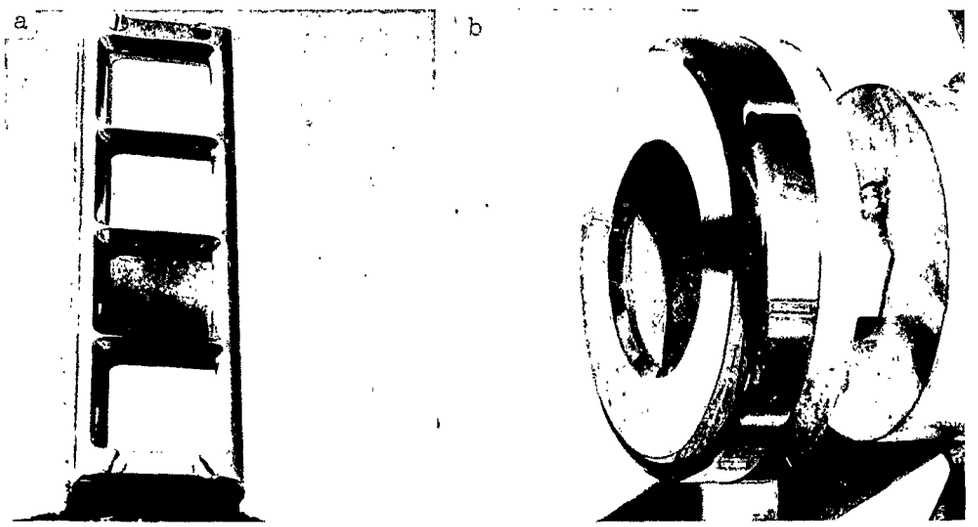

Figure 2.11 Typical Test Exposure of Materials for Thermal-Shock Study.
(a) At Pylons and Pipe Mount
(b) At Mirror

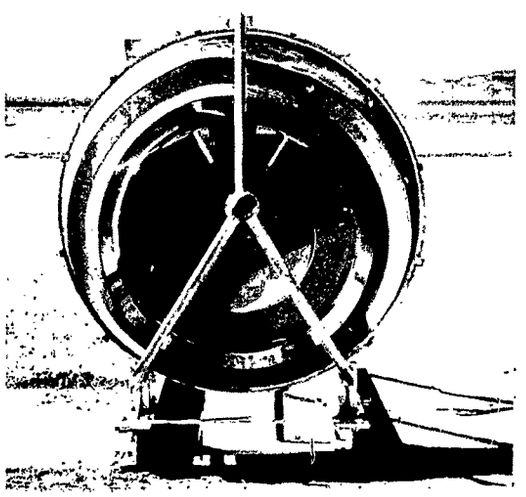

Figure 2.12 Magnification of Ceramic Specimens in Mirror

base at a range of 6,500 feet from ground zero. The mirror was oriented with its optical axis aligned with a point 70 feet above air zero, so that the image of the fireball would fall on the ceramic specimens for a greater portion of the fireball rise time.

The materials selected for exposure were Battelle ceramic Type 88-5, Armour ceramic, graphite, and molybdenum. The Armour and Battelle ceramics were of the same type as used in the spherical specimens. The graphite, which was made by Speer Carbon Company, was designated as Grade 3474D. The molybdenum was of high purity grade and was made by the Fansteel Metallurgical Corporation. The Battelle ceramics were 5/8 in. thick and encased on the sides and unexposed face by a steel container, so as to provide additional mechanical strength during exposure. The Armour ceramics and the graphite were prepared in 1/4 in. thicknesses and the molybdenum plates were 1/8 in. thick. All of the test samples were 2-in. square, except the specimens exposed at the focal point of the parabolic mirror (which were prepared in the form of

TABLE 2.3 DEPLOYMENT OF MATERIALS AND PREDICTED THERMAL INPUTS

Ground Range (ft)	Predicted Thermal[a]		Materials Exposed			
	Radiant[b] Exposure (Cal/sq cm)	Peak Irradiance (Cal/sq cm/sec)	Battelle Ceramic	Armour Ceramic	Graphite	Molyb-denum
1,100	260	1,300	X	X	X	
2,200	110	370	X	X	X	X
3,100	71	160	X	X	X	X
6,500 (Mirror)	1,200[c]	2,700[c]	X	X		

(a) 26-KT device
(b) Prior to blast arrival
(c) An approximate magnification factor of 80 was used.

3-in.-diameter semicircles). The test samples are shown in Figure 2.10. The deployment of the specimens and the predicted thermal inputs at the various ranges are shown in Table 2.3.

The specimen holders in which the ceramics were mounted were made of highly polished stainless steel (Figure 2.11). The size of exposed area of the samples was 1 3/4 in. by 1 3/4 in. The remaining 1/8 inch around the periphery was covered by the stainless-steel frame. Similarly, 1/8 inch around the periphery of the semicircular test samples was used to hold the specimens in position; there was, thus, a 2 3/4 in.-diameter area for specimen exposure. A photograph of the mirror assembly showing the reflection of the ceramic specimens and the stainless-steel holder in the mirror is shown in Figure 2.12.

2.3 INSTRUMENTATION

Time-history instrumentation was limited to thermal radiation measurements at the pylon, 1,100 feet from ground zero. The instrumentation comprised one total thermal-energy measurement, made with a disk-

type calorimeter, and one thermal-energy-intensity measurement, made with a foil radiometer. These instruments were similar to the standard type made by the Naval Radiological Defense Laboratory (NRDL). The basic function of these instruments is measuring, by means of a thermocouple, the temperature rise of a metal disk in the calorimeters, and of a foil in the radiometer. Descriptions of these standard instruments may be

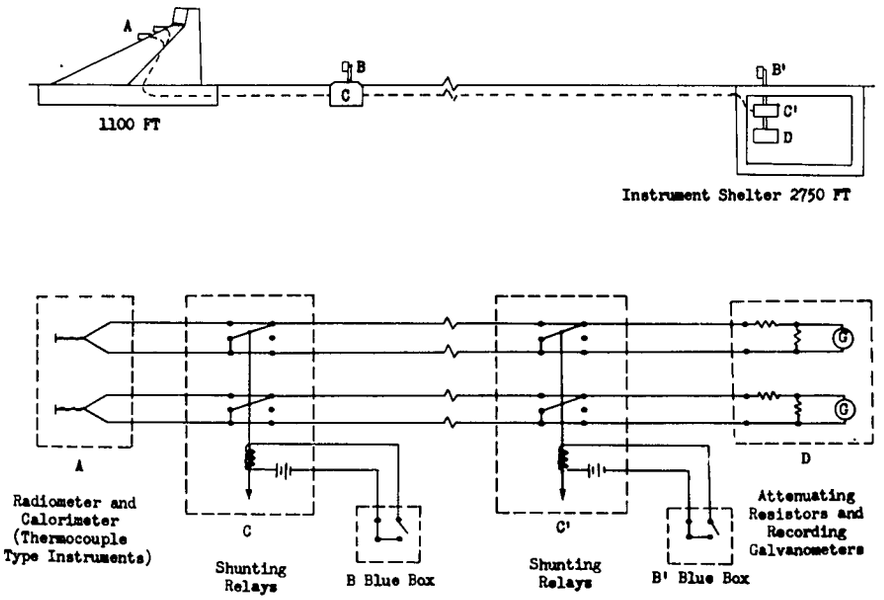

Figure 2.13 Instrumentation Schematic

found in "The Thermal Data Handbook" (AFSWP 700). Two of the standard type instruments were especially modified and calibrated by NRDL to measure the required thermal inputs.

The outputs of these instruments were recorded on an oscillograph located in an instrument shelter, 2,750 feet from ground zero. Use of such a remote recording station necessitated that the instruments and recording galvanometers be protected from currents which might be generated by the electromagnetic pulse at time zero. To afford this protection, the lead wires were shunted immediately behind the pylon and also immediately forward of the oscillograph. These shunts were removed approximately 16 msec after detonation by means of time-delay relays actuated by the commonly used photocell systems called "blue boxes," made by Edgerton, Germeshausen and Grier, Inc., Boston, Massachusetts. A schematic of the recording system is given in Figure 2.13.

Motion-picture coverage of the ceramic specimens at the 3,100-ft range was provided in an attempt to observe any fracture of the ceramic materials which might occur prior to blast arrival. High-speed motion-picture coverage of the engulfment of the tower specimens by the fireball was also provided in conjunction with other fireball-photography programs. No other zero-time photographic coverage was attempted.

Chapter 3
RESULTS

Shot 12 was detonated atop a 400-ft tower on 15 April 1955. The yield of the burst was reported to be 23 ± 1.5 KT, which was slightly lower than predicted. This reduced yield was still sufficient for fulfilling the primary objectives of this program. Various other data relative to this detonation are summarized in Appendix C, Table C.1.

No portion of the shot tower or the five specimen towers was left standing; however, nearly 225 feet of the main support members of the shot tower were still intact and layed out radially from their original position. About 150 feet of both Tower 1 and Tower 2, though in a twisted, almost unrecognizable form, were still intact and attached to their bases. General pictures of the debris near ground zero are given in Figure 3.1. Approximately 100 feet of twisted television tower, believed to be from Tower 3, was still intact and found about 70 feet behind its base. For the most part, however, what remained of the towers was found at ranges beyond 800 feet with isolated pieces at ranges of over 2,000 feet. Further information on damage to the shot tower and to other shot towers used during Operation Teapot is given in Appendix C.

Inspection of tower guys and support members where fireball spikes were expected indicated that there was no obviously greater damage in these areas than in areas where spikes would not have been developed. Analysis of high-speed motion-picture photographs of the fireball growth showed that there were large spikes coming down the legs and the main guys of the shot tower and a few small spikes on the maze of specimen tower guys. However, no fireball spikes were observed traveling down the television towers themselves. Further evidence indicating the absence of spikes on the specimen towers was the almost unscathed condition of the steel sphere positioned at the base of the first tower. The machine marks were still quite visible on the surface of this sphere. The ball of fire, as seen on the film, touched the ground and extended to a ground range of about 530 feet, or to a slant range of about 650 feet, thus placing all of the specimens well within the apparent fireball.

Little thermal damage was inflicted on the ceramics used for the thermal-shock study, with the exception of those at the focal point of the mirror. All mounts and fixtures stood up well during the test except the pylon at the closest range. This pylon was torn from its base and came to rest about 10 feet behind the concrete slab. The failure was in the reinforcing rods in the concrete base just below the weld attaching them to the base plate in the slab.

3.1 LETHALITY STUDY

Specimen recovery for the lethality study far surpassed expectations, the only specimens not recovered being the solid aluminum and

solid steel spheres positioned on the floor of the shot cab at a range of about 13 feet. Specimen recovery was accomplished on 11 May 1955, 26 days after the shot in approximately 8 man-hours, by the use of hand tools alone. The specimen impact holes, for the most part, were readily located from characteristic humps in the ground accompanied by soft powderly earth, as seen in Figure 3.2 (b). The radiation level in the recovery area varied from about 0.5 to 0.7 r/hr. After being hosed with clear water, the steel specimens read from about 0.1 to 0.7 r/hr and the aluminum specimens read from approximately 0.01 to 0.4 r/hr. Identification of the test specimens was accomplished easily in the impact area from visual assessment of the amount of metal loss and from the approximate range and azimuth of their post-shot locations. The identification as reported in the preliminary report was correct, except for the two cylinders from Tower 1, whose trajectories apparently crossed prior to impact. These identifications were verified by the numbered slugs located in the specimens. Chemical analysis, which was the alternate method of identification provided, was not necessary.

It is believed that all of the tower-mounted specimens, except possibly three, were found in their initial impact holes. The three exceptions were: (1) the steel cylinder on the right side (facing G. Z.) of Tower 4, (2) the solid aluminum sphere from Tower 2 (see Figure 3.2a), and (3) the ceramic-insert sphere from Tower 1. The latter sphere was broken in half and the two pieces were found at ranges differing by about 32 feet. The depths below the surface that the specimens were found varied from on the surface as mentioned above, to 37 inches as shown in Figure 3.2 (d). Several specimens were partly buried, such as the one seen in Figure 3.2 (b). Table 3.1 summarizes the approximate depths below the surface to which the bottoms of the specimens penetrated and the distances the specimens traveled from their respective towers. Figure 3.3 shows the post-shot locations of all specimens, the majority of which were found close to their original azimuth and followed a reasonable pattern of the closer-in specimens receiving higher velocities and, hence, traveling farther from their respective towers. The obvious exceptions to this scheme were the ceramic-insert spheres from Towers 1 and 2 and the solid aluminum spheres from Towers 1 and 3 which did not travel far enough relative to the other spheres. The solid aluminum sphere from Tower 2, shown in Figure 3.2 (a), was found above ground; although no evidence of impact was observed forward of this position, it is believed that this sphere skipped out of its initial impact hole and rolled to its post-shot location. There were other peculiar post-shot locations observed, not the least of which was that, at each of Towers 2, 3, and 4, the heavier of the two cylinders went farther than the lighter cylinder, even though the orientation and external dimensions were identical. Probable trajectories of the various specimens are discussed in Appendix B.

What appeared to be fuzed silica was splattered over the upper surface of partly buried specimens and the specimens which were found above ground, as can be seen in Figure 3.2 (a) and (b). The aluminum sphere from Tower 2 (Figure 3.2a) was the most-heavily coated. This material came off easily with brushing and washing. There was apparently only a

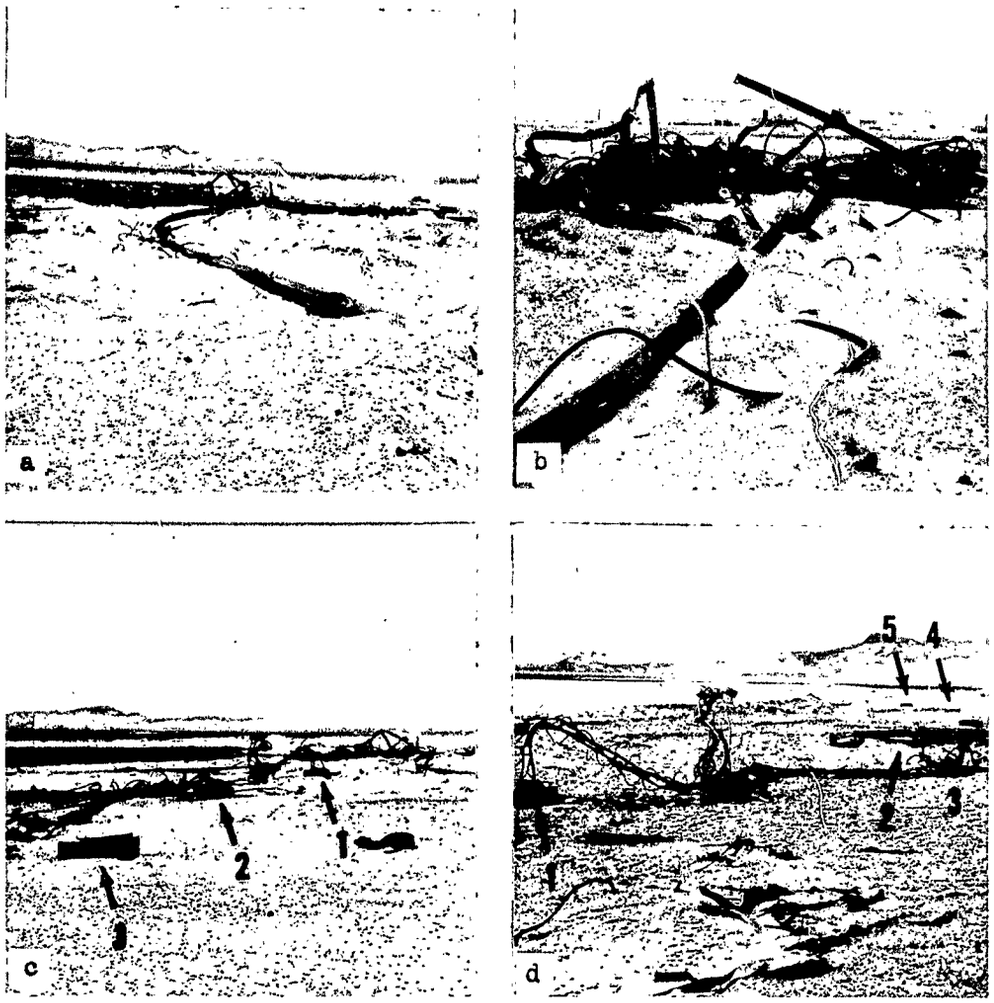

Figure 3.1 General Debris of Shot Tower and TV Towers. (a) General View of Shot Tower Werckage. (b) Close-up View of Shot Tower Wreckage (c) Debris near TV Tower Bases 1, 2, and 3, Looking Toward G.Z. (d) TV Tower Wrekage Looking away from G.Z. Note Five TV Tower Bases.

small amount of foreign material adhering to the surface of even the deepest-buried specimens. All specimens were soaked in a solution of sodium citrate, scrubbed with soap and water, and protected with a strippable coating of clear plastic to prevent further loss of surface material.

After washing, there still remained surface material which could be easily chipped from the surface. Chemical analysis of several such samples indicated that the material was largely parent material, i.e., aluminum or steel. The aluminum content of samples from aluminum spheres varied from 72 to 95 percent, and the iron content in the surface material from a steel specimen was about 97 percent. The maximum silica content observed was about 16 percent. There was evidence that the

Armour and Battelle ceramic inserts had a surface glaze about 1/32 in. deep; however, most of this was chipped off, probably upon impact or during recovery.

3.1.1 Spherical Specimens. All of the spheres retained an approximately spherical configuration and were, for the most part, fairly smooth. The steel spheres were not reduced in size as much as the spheres made of aluminum and were, in general, more smooth and round in appearance. The surface of the spheres appeared to be uniform, except close to the inserts on the ceramic-insert spheres, where in some instances there was less damage and in others there was excessive damage. Overall views of each of the three types of spherical specimens are shown in Figure 3.4. There were only three instances of damage other than metal loss

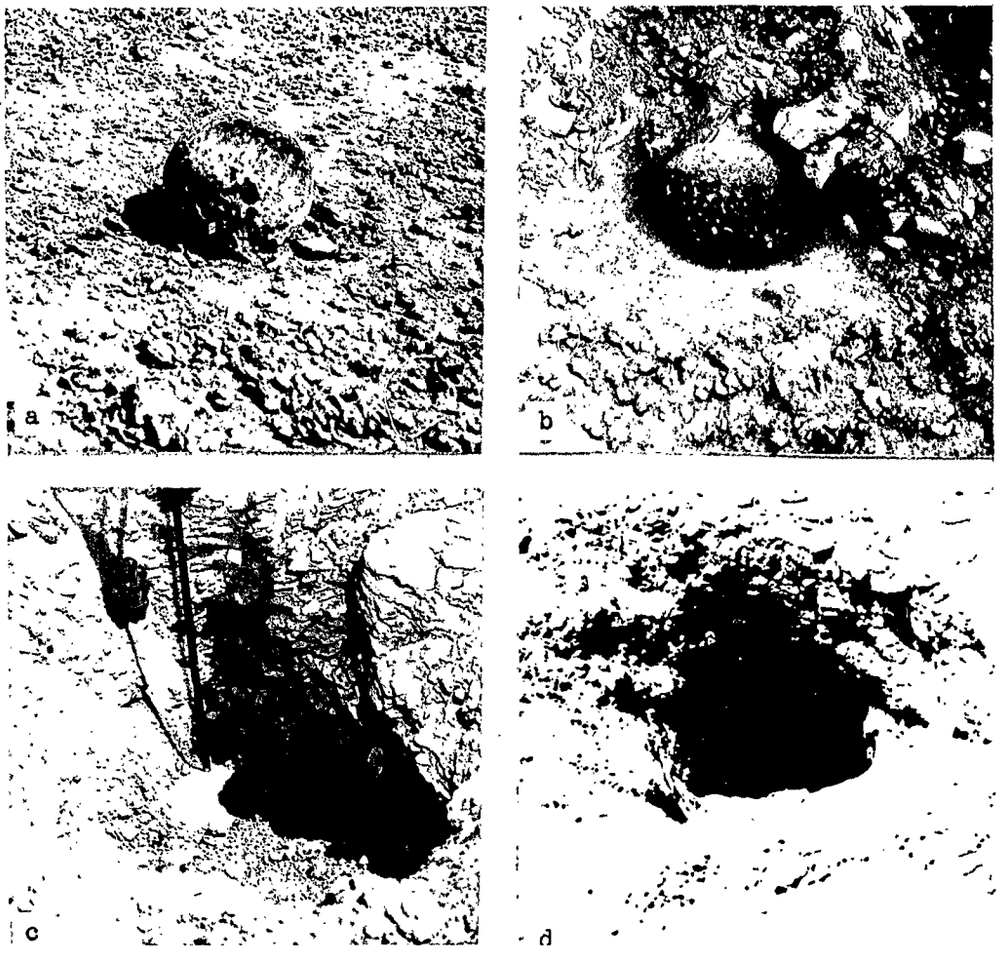

Figure 3.2 Typical Post-Shot locations of Test Specimens. (a) Solid Aluminum Sphere, Tower 2, found above ground. (b) Solid Aluminum Sphere, Tower 5 , found semi-buried. (c) Solid Steel Sphere, Tower 4, found buried approximately 30 in. deep. (d) Solid Steel, Tower 1, found buried approximately 37 in. deep.

from the surface: (1) the ceramic-insert sphere from Tower 1 was broken into two pieces, probably somewhere along its trajectory, as evidenced by the metal loss on the surface of the fracture; (2) the ceramic insert sphere from Tower 3 was cracked all the way around but was still intact; and (3) the solid aluminum sphere from Tower 1 sustained a deep cut (approx. 1 1/4 in. deep, 1 1/4 in. wide, and 3 1/2 in. long) which extended into a crack nearly two-thirds the way around the sphere. The

TABLE 3.1 SUMMARY OF DEPTH OF PENETRATION AND HORIZONTAL DISTANCE TRAVELED FOR SPHERES AND CYLINDERS

Tower No.	Horizontal Distance Traveled From Tower (ft)					Depth of Penetration (in.)				
	1	2	3	4	5	1	2	3	4	5
Steel Sphere	394.1	268.1	183.4	128.2	90.0	37	16	13	30	10
Alum. Sphere	245.0	369.8	235.8	223.8	166.5	14	0	9	10	11
Ceramic Sphere	261.4*	254.7	269.1	224.3	177.5	0	12	13	12	11
Cylinder Left**	302.2	263.7	219.6	177.5		30	22	12	11	
Right**	287.0	257.0	204.7	175.0		20	17	25	9	

* Mid point of two halves
** Facing Ground Zero

location of this cut was about 45° above the horizontal plane through the center of the sphere. It is possible that this was the first point of impact with the shock wave. Since there was evidence of metal loss and there were no sharp corners on the cut, it is believed that this occurred before penetration into the ground and probably at or near time of shock impact by flying debris in the shock wave. A visual damage assessment of each specimen including individual photographs is given in Appendix A.

There was evidence of molten metal flow and splattering of varying degree on the surface of nearly all of the spheres. In this regard, the ceramic-insert sphere from Tower 2 was the most prominent, being spattered with molten aluminum over nearly the entire front half of the specimen, in some places about 1/2 in. high. The coating completely covered the front three ceramics. The steel sphere from Tower 4 was unique in regard to metal splashes on the steel spheres. It was completely covered with molten steel in the form of paint runs, whereas the other steel spheres were relatively clean and smooth. Shiny streaming areas were observed on the surface of many of the aluminum spheres, as can be seen in Figure 3.4 and are indicated in Appendix A. These areas appeared as though there was radial streaming from a point on the surface of the sphere. In most instances, the centers of these areas were located on the sphere in a position which was not close to the point of first impact with the shock wave. It is thus believed that these streaming patterns were caused by impact with the ground. Some streaming patterns were noticed also on the steel spheres and cylinders but were not evidenced by being shiny as observed on the aluminum spheres. These streaming patterns are noted in the individual visual damage analyses in Appendix A. The surfaces of some of the spheres were finely checked.

This was observed mostly over the shiny streaming patterns where the surface was smooth and is believed to have been caused by cracking of the surface during cooling.

The metal loss from the spherical test specimens, which was the primary objective of the test, is presented as an apparent reduction in radius determined by two different methods, both of which assume post-shot spherical symmetry. The first method utilizes the post-shot circumference measurement from which the radius of an equivalent sphere can be directly calculated. The difference between this radius and the pre-shot radius is the metal loss. The second method uses the post-shot weight of the specimen from which the radius of an equivalent sphere can be calculated, again, the difference between pre-shot and post-shot radii being the metal loss. In this second method it was assumed that the density did not change during the test. This assumption appears reasonable, since the post-shot densities of several close-in specimens were calculated from measurements of their volume and weight and were found to remain invariant within 1 percent, which was within the accuracy of the weight measurements. Using this assumption, the following equation for reduction-in-radius can be derived.

$$\text{Rad Loss (in.)} = r_o\left[1-(w/w_o)^{1/3}\right] \qquad (3.1)$$

where w = Post-shot weight (lb)
w_o = Pre-shot weight (lb)
r_o = Pre-shot radius (in.)

A summary of various pre-shot and post-shot measurements of each of the spherical test specimens including the calculated reduction-in-radius is presented in Table 3.2. The 1.3-in. metal loss on the ceramic insert sphere from Tower 1, as calculated from weight measurements, is probably an overestimate for surface material loss, because the sphere broke into two pieces and apparently lost metal from the fractured surfaces. In addition, portions of some of the ceramic inserts in this sphere were broken out and lost. No special consideration was given the ceramic-insert spheres in regard to metal loss as the densities of the ceramics were of about the same magnitude as the aluminum. Further, the volume occupied by the ceramics was less than 4 percent of the total volume.

It can be seen that the radius loss, as calculated from circumference measurements, is generally less than the corresponding value calculated from weight measurements. This difference is attributed to the protrusion of surface materials, causing the circumference measurements to be too large. It is believed that the reduction in radius as calculated from weight measurements is the most representative for average metal loss.

Table 3.3 gives a summary of three mutually perpendicular diameter measurements for each sphere. It can be seen that there is a considerable variation in diameters over the sphere; however, no definite trend

of heavy or light metal loss can be attributed to any particular diameter. The error in these measurements may be as much as 1/16 inch, because of possible surface variations and because of the difficulties in locating the end points of a true diameter. The diameters D_3 and D_5 for the solid aluminum and solid steel spheres are mutually perpendicular in a hori-

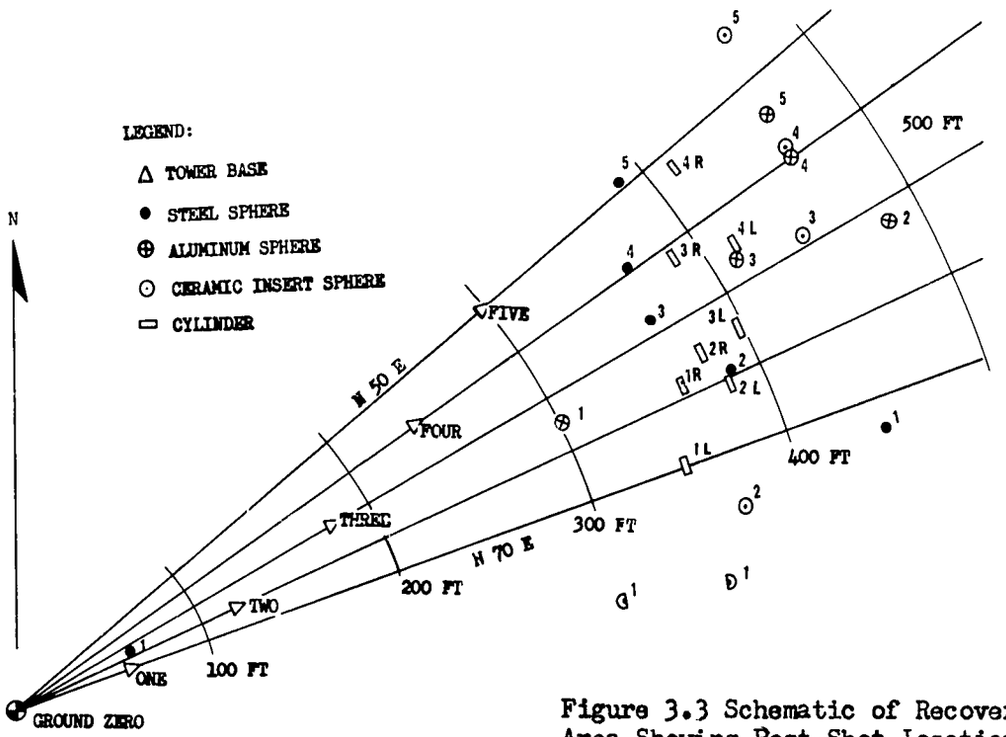

Figure 3.3 Schematic of Recovery Area Showing Post-Shot Locations of Test Specimens

zontal plane; but D_5 does not necessarily point toward the shot tower, since the orientation of these spheres with respect to the shot tower could not be determined.

Profiles or cross sections of some of the steel spheres, solid aluminum spheres, and ceramic insert spheres, are presented in Figures 3.5, 3.6, and 3.7, respectively, in order to portray the irregularity of the surfaces. These profiles represent cross sections of the spheres in a horizontal plane through the center of the sphere. The profiles of the spheres are shown plotted approximately concentric; however, the exact center of the spheres could be in error by as much as 1/8 inch, because of mislocation of the mounting hole during fabrication of the specimens. The profiles of the ceramic-insert spheres (Figure 3.7) are all positioned with the direction of the shot tower being directly up on the drawing. The solid aluminum spheres and steel spheres contained only the mounting hole on the bottom; hence, their orientation with respect to the shot tower cannot be determined. It can be seen that there are flat spots on the sides nearest to the shot tower on the

ceramic-insert spheres from the Towers 2 and 3; however, this is probably a local effect caused by the proximity of the ceramic inserts. The front and rear Armour ceramic inserts were positioned approximately in the horizontal plane, as indicated in Figure 3.7.

3.1.2 Steel Cylinders. The cylinders retained a roughly cylindrical configuration, and the surfaces were quite smooth, as with the steel spheres, except for certain relatively small areas where pock marks were

TABLE 3.2 SUMMARY OF PRE-SHOT AND POST-SHOT MEASUREMENTS OF SPHERICAL SPECIMENS

Specimen Type	Tower No.	Slant Range (ft)	PRE-SHOT		POST-SHOT			Weight[a] Loss (lbs)	Reduction in Radius (in.)	
			Weight[a] (lb)	Radius (in.)	Weight[a] (lb)	Apparent Radius (in.)				
						From Circumference Measurements	From Weight Measurements		From Circumference Measurements	From Weight Measurements
Steel	1	80	148.0	5.003	115.5	4.60 - 4.66	4.60	32.5	0.34 - 0.40	0.40
	2	160	148.0	5.003	122.5	4.70 - 4.75	4.69	25.5	0.25 - 0.30	0.31
	3	239	148.0	4.996	136.0	4.86 - 4.89	4.86	12.0	0.11 - 0.14	0.14
	4	319	148.0	5.004	144.5	4.94 - 4.99	4.96	3.5	0.01 - 0.06	0.04
	5	398	148.5	5.001	147.5	4.97 - 5.01	4.99	1.0	0.00 - 0.04	0.01
	1 (base)	406	148.0	5.004	148.0	4.99 - 5.00	---	0.0	0.00 - 0.01	0.00
Aluminum (Solid)	1	80	53.5	5.006	23.5	3.83 - 3.85	3.81	30.0	1.16 - 1.18	1.20
	2	160	51.5	5.005	26.8	4.03 - 4.08	4.02	24.7	0.92 - 0.97	0.98
	3	239	53.0	5.000	38.5	4.51 - 4.54	4.49	14.5	0.46 - 0.49	0.51
	4	319	53.5	5.007	49.8	4.89 - 4.92	4.89	3.7	0.09 - 0.11	0.12
	5	398	51.5	4.999	50.5	4.97 - 4.99	4.97	1.0	0.01 - 0.03	0.03
Aluminum (With Ceramic Inserts)	1	80	52.5	5.006	21.3	3.90	---	31.2	1.11	1.30
	2	160	50.5	4.998	26.5	4.06 - 4.10	4.03	24.0	0.90 - 0.94	0.97
	3	239	52.5	4.999	38.5	4.54 - 4.62	4.51	14.0	0.38 - 0.46	0.49
	4	319	52.5	5.000	49.0	4.91 - 4.93	4.89	3.5	0.07 - 0.09	0.11
	5	398	50.5	5.002	49.8	4.97 - 4.99	4.97	0.7	0.01 - 0.03	0.03

Note: [a] The estimated accuracy of weight measurements is ± 0.5 lb. The order of accuracy of the other data is indicated by the number of significant figures in which the data are reported.

observed. A group photograph of the cylinders is shown in Figure 3.8. The metal loss was noticeably nonuniform along the length of the cylinder, there being considerably more metal loss near the ends than at the center, giving a barrel shaped appearance. This barreling was pronounced at the two closest ranges, was measurable at Tower 3, but practically nil at the fourth tower, where there was little metal loss. Longitudinal cross

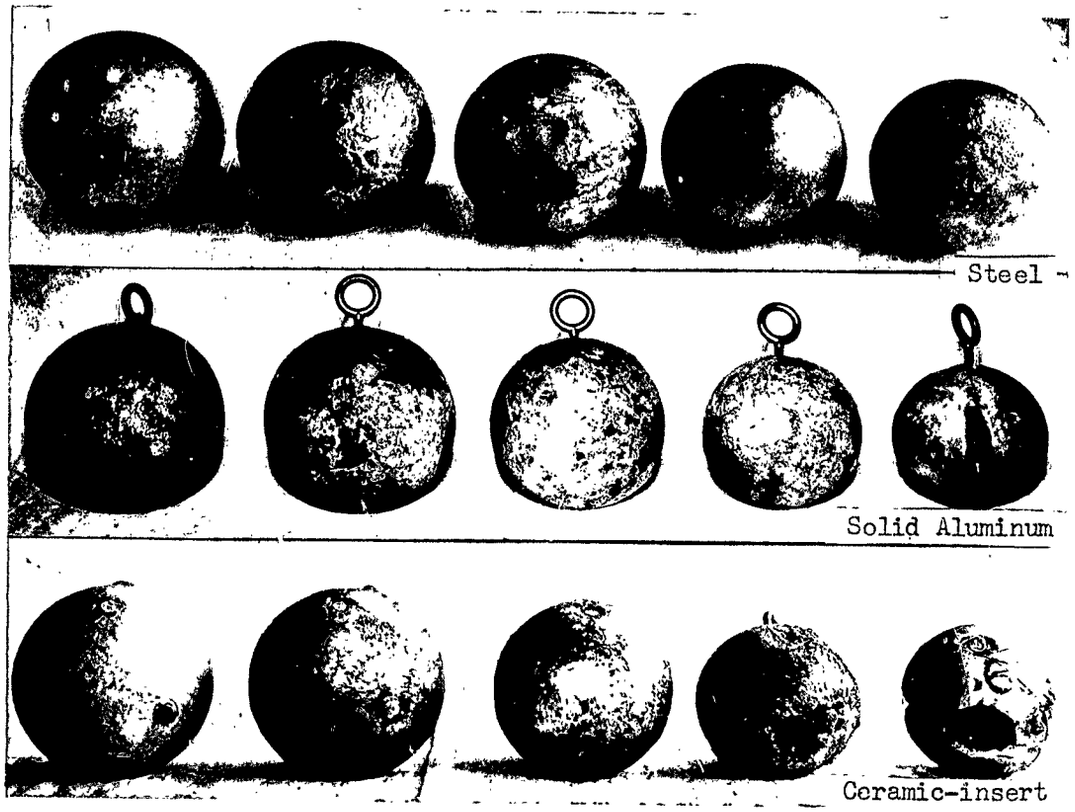

Figure 3.4 Overall Views of Each Type of Spherical Specimen Showing Gradation in Size. Left to Right, Towers 5, 4, 3, 2, 1.

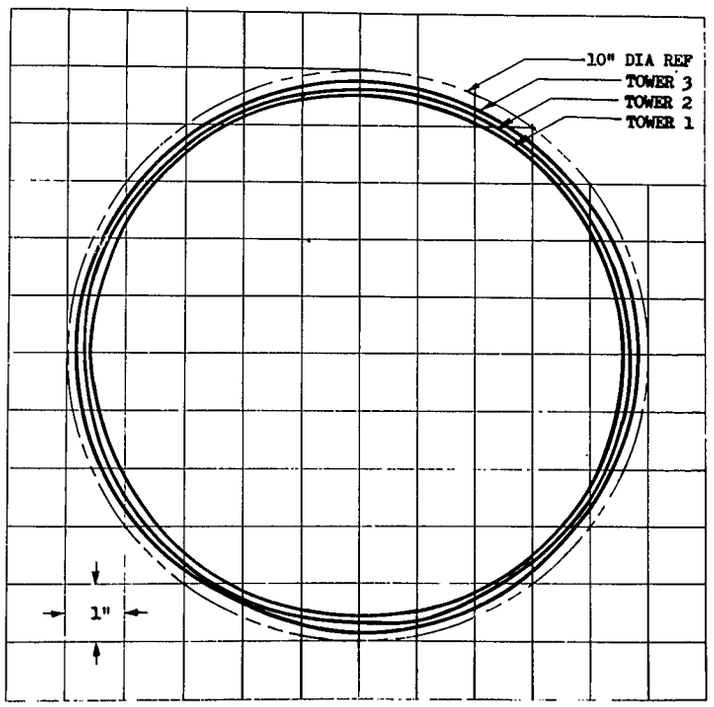

Figure 3.5 Profiles of Steel Spheres

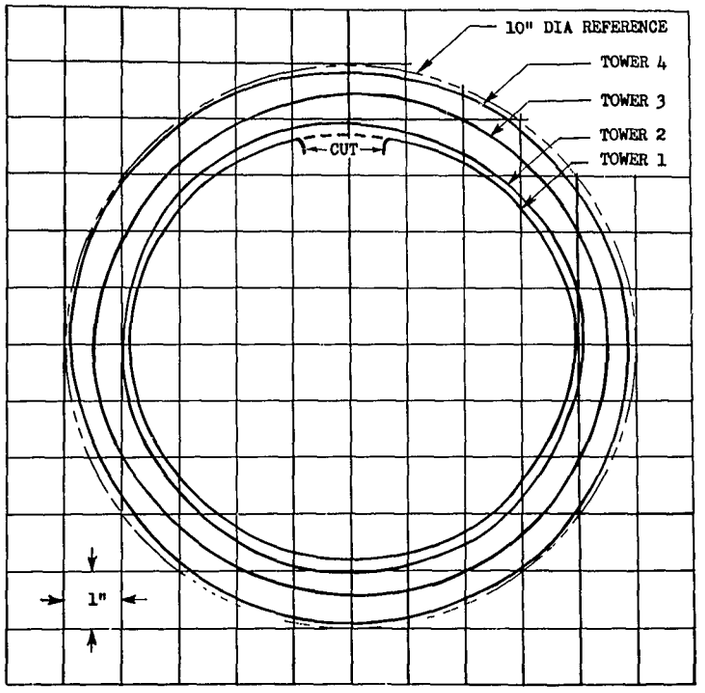

Figure 3.6 Profiles of Solid Aluminum Spheres

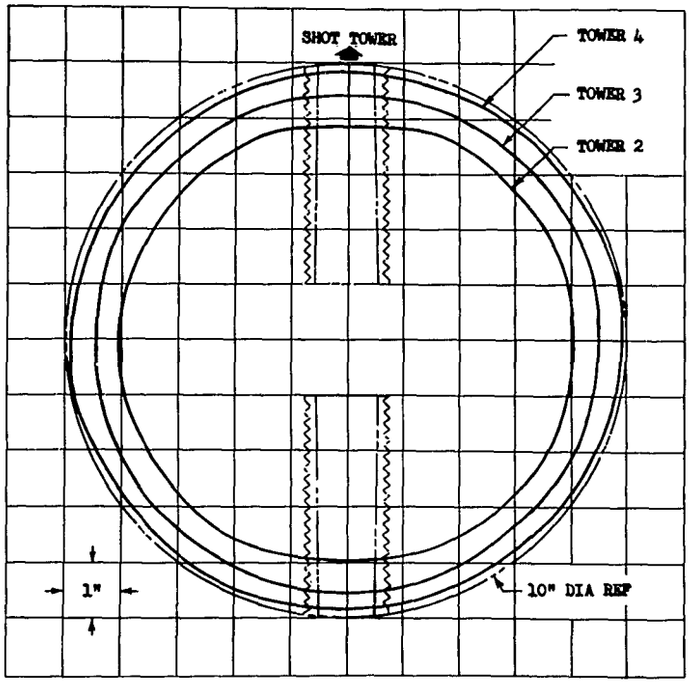

Figure 3.7 Profiles of Ceramic-Insert Spheres

TABLE 3.3 SUMMARY OF SPHERE DIAMETERS

Specimen and Tower No.	Diameters[a] (in.)				
	D_1	D_2	D_3[b]	D_4	D_5[b]
Steel Spheres					
1			9.12	9.03	9.15
2			9.16	9.31	9.37
3			9.69	9.63	9.65
4			9.79	9.83	9.86
5			9.97	9.87	9.97
Aluminum Spheres					
1	7.66[c]	7.38[c]	7.42	7.58	7.80
2			8.00	7.98	8.00
3			9.00	9.02	9.03
4			9.73	9.60	9.71
5			9.87	9.86	9.91
Ceramic-insert Spheres					
1	(d)	(d)	(d)		
2	8.06	7.84	8.16		
3	9.17	9.12	8.94		
4	9.67	9.78	9.81		
5	9.90	9.87	9.90		

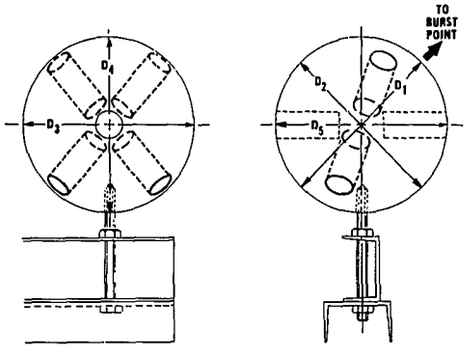

(a) Estimated reliability 0.06 in. For location of diameters see sketch below.
(b) The diameters D_3 and D_5 for the solid aluminum and solid steel spheres are mutually perpendicular in a horizontal plane, but D_5 does not necessarily point towards the shot tower.
(c) This assumes that the large cut was first point of impact by shock front.
(d) Sphere broke into two pieces.

SECRET

sections or profiles of various cylinders are given in Figures 3.9, 3.10, and 3.11. The outline of the pre-shot configuration is shown superimposed over the profiles for comparison purposes. At the two closest stations the metal loss was sufficient to remove the entire shoulder of the thread and, consequently, leave the cap unattached. The caps from both the cylinders from Tower 2 were detached from the cylinders; however, both caps of the left cylinder and one cap from the right cylinder from Tower 1 were still attached. These caps were welded on by once-molten metal that streamed under the cap, such as seen in Figure 3.12. Both caps from the left cylinder were removed by striking the caps with a

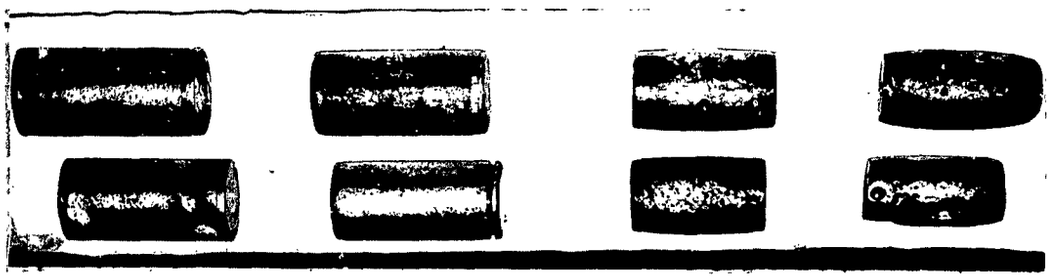

Figure 3.8 Overall View of Steel Cylinders. Left to Right, Towers 1, 2, 3, 4.

hammer until the weld broke, but the single cap from the right cylinder could not be detached. The cylinders from Tower 1 were distorted such that the length of the cylinder on one side was greater than on the other side, i.e., the two end faces were no longer parallel, as seen in Figure 3.9. One may observe that the maximum length of the cylinder occurs on the side of the cylinder containing the indentations or pock marks discussed below and, therefore, it may be possible to conclude that this was the side of the cylinder which faced the burst point. However, positive orientation could not be determined on any of the cylinders, except the two provided with the hemispherical holes. There was no bending of the cylinders along the longitudianl axis that could be detected visually with a straight edge.

There were large indentations or pock marks on the surface of the cylinders from Towers 1 and 2. Some of these indentations measured about 7/16 in. deep by 1 3/8 in. in diameter at the first tower and at the second tower about 7/32 in. deep by 1/2 in. diameter. There were pock marks on the cylinders from Tower 3, though lesser in number and magnitude. No pock marks were noted on the specimens from Tower 4. Photographs of two of the more-severely indented cylinders are presented in Figure 3.13. In general, the pock marks occurred only in small areas. The largest area was on the cylinder on the left side of Tower 1 (Figure 3.13a) and was extremely irregular over nearly the entire half of the cylinder. The sides opposite the pock-mark areas were relatively smooth.

The two cylinders from Tower 1 were severely squashed and had approximately elliptical cross sections, as seen in Figures 3.12, 3.14, and 3.15. Both of these cylinders had hole diameters of 1 inch and are

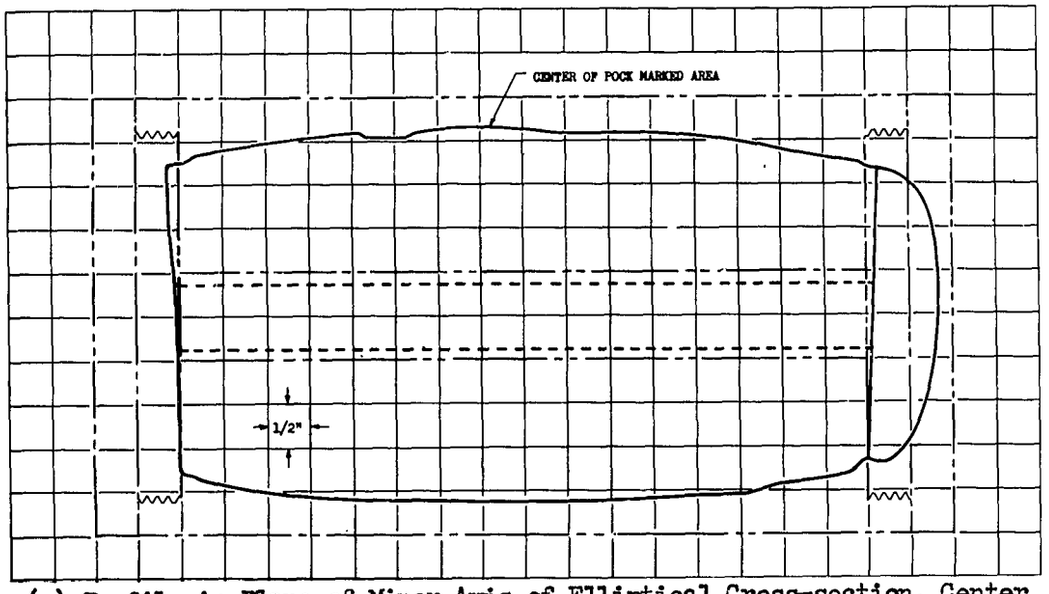

(a) Profile in Plane of Minor Axis of Elliptical Cross-section. Center of Pock-Mark Area is at Top of Profile.

Figure 3.9 Longitudinal Profiles of Cylinder From Right Side of Tower 1

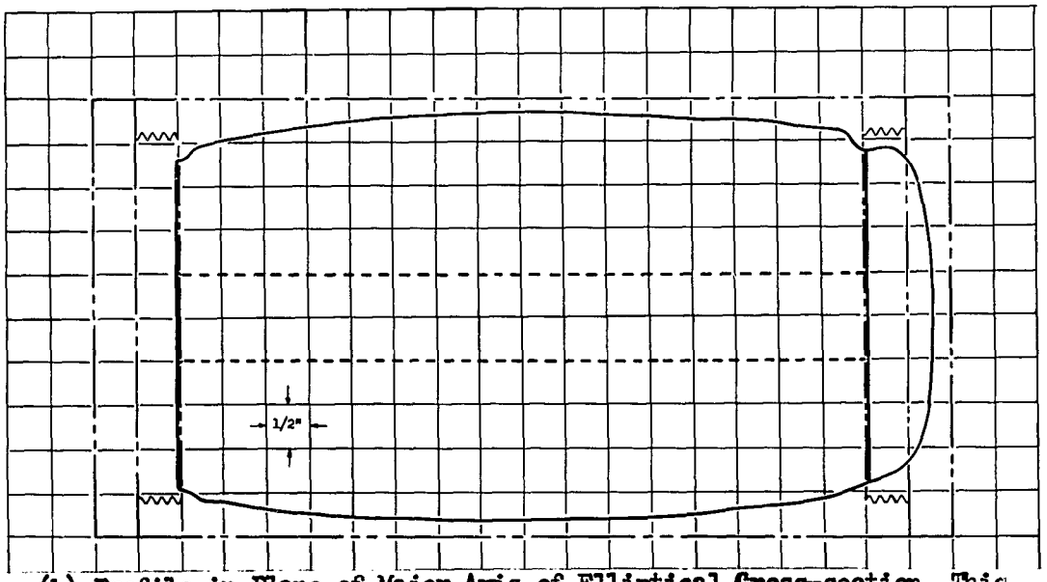

(b) Profile in Plane of Major Axis of Elliptical Cross-section. This Profile is at 90° to Profile (a) Above.

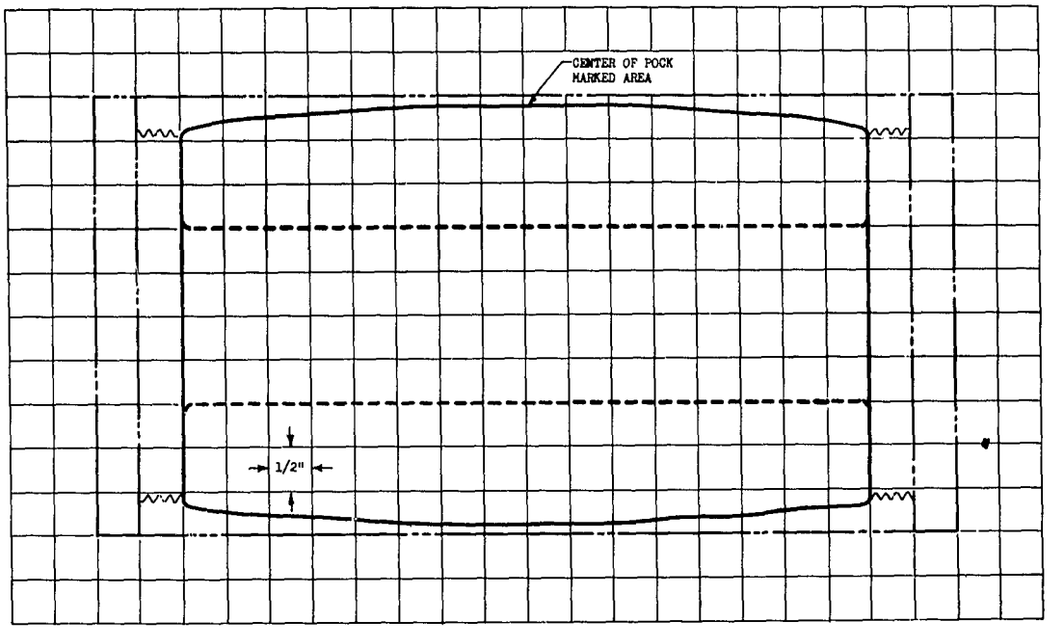

Figure 3.10 Longitudinal Profile of Cylinder From Right Side of Tower 2. Center of pock-mark area is at top of page.

Figure 3.11 Longitudinal Profile of Cylinder From Right Side of Tower 3. The two hemispherical holes shown were on side of cylinder facing the burst point.

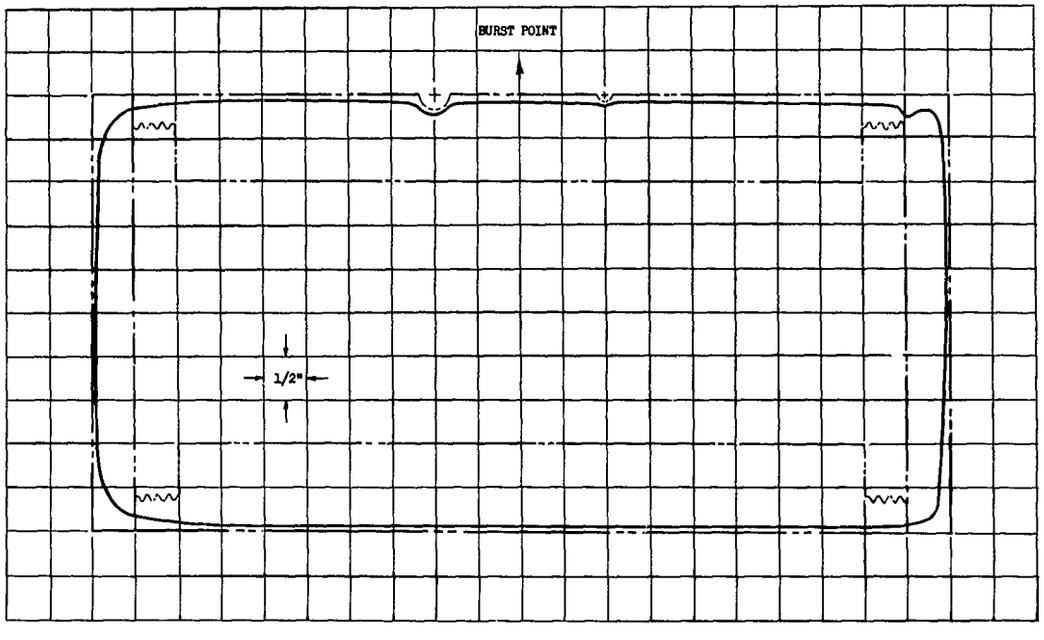

now elliptical with a major diameter of less than 1 inch. The cylinders from Tower 2, one having a 1-in.-diameter hole, the other a 2-in.-diameter hole, were elliptical only to a slight extent, with differences

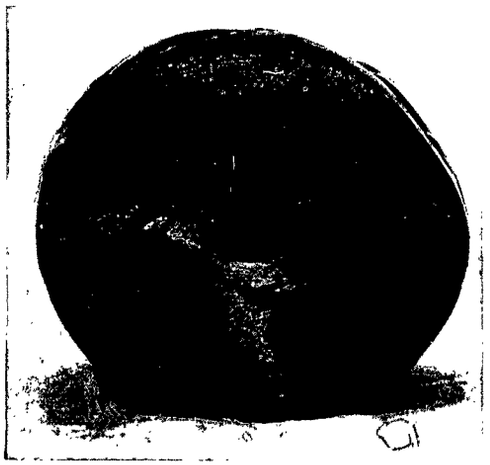

Figure 3.12 End Face of Cylinder From Left Side of Tower 1. Note elliptical cross-section and molten metal flow on face

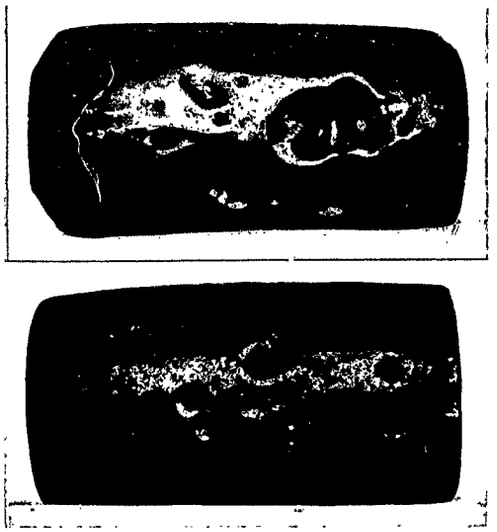

Figure 3.13 Pock Marks on Cylinders. These ar most extremely indented cylinders. Top: Tower 1 (2-in. wall) Bottom: Tower 2 (2-in. wall)

between major and minor diameters of 0.004 inches and 0.024 inches, respectively. There was no measurable deformation at Towers 3 or 4. On all specimens where squashing of the cylinders was noticed, the minor axis of the elliptical cross section pointed toward the center of the pock-marked area, as shown in Figures 3.14 and 3.15. A summary of the various pre-shot and post-shot measurements of the cylinders, including the variation of wall thickness around the circumference, is given in Table 3.4. Individual damage assessments and photographs are presented in Appendix A.

One of the primary purposes of the cylinder exposures, in addition to material loss, was to determine if there would be any internal spalling or failure caused by a thermally induced shock wave passing through the cylinders, but the results in this regard were entirely negative. The inside of all the cylinders were smooth and straight with no observable pitting. On the cylinders on which the caps were missing, there was some discoloration of the material inside, but apparently no metal loss or pitting, as evidenced by the clearly visible machine marks.

On the two cylinders with 1-in. wall thickness, one on Tower 3 and the other on Tower 4, hemispherical holes 3/8 inch and 3/16 inch in diameter were machined in the surfaces to determine the effects of hypersonic flow over such indentations. All of the holes became slightly elliptical in appearance, but there was no appreciable erosion or

TABLE 3.4 SUMMARY OF CYLINDER DATA

Tower No.	Slant Range (ft)	PRE-SHOT				POST-SHOT								Metal[c] Loss at Center (in.)
		Outside Dia.(in.)	Hole Dia.(in.)	Wall Thickness (in.)	Weight[a] (lbs)	Weight[a] (lbs)	Section[b]	Sta.[b] (in.) / Hole Dia.(in.)	Outside Diameter (in.) 0	1	2	3	4	
1 Left	82	4.999	1.022	1.989	53.5	33.0	A-A	0.66	4.18	4.17	4.12	3.96	3.59	0.23
							B-B	0.90	4.35	4.35	4.32	4.19	3.73	0.26
Right		4.999	1.017	1.991	53.5	33.3[d]	A-A	0.75	4.35	4.30	4.27	4.03	3.59	0.19
							B-B	0.97	4.57	4.52	4.32	4.20	3.75	0.19
2 Left	162	4.998	1.032	1.984	53.5	34.0[d]	A-A	1.021	4.62	4.59	4.53	4.41	4.15	0.18
							B-B	1.025	4.65	4.61	4.55	4.42	4.14	0.17
Right		5.000	2.004	1.498	49.0	29.5[e]	A-A	1.984	4.66	4.65	4.55	4.43	4.08	0.16
							B-B	2.008	4.70	4.73	4.64	4.52	4.24	0.15
3 Left	241	4.998	2.048	1.475	48.0	41.8	Typical	2.048	4.81	4.82	4.81	4.80	4.73	0.10
Right		4.998	2.987	1.006	40.0	34.3	Typical	2.987	4.85	4.83	4.84	4.82	4.80	0.08
4 Left	321	5.001	3.037	0.982	39.0	37.5	Typical	3.037	4.96[f]					0.02
Right		5.001	4.001	0.500	27.0	26.0	Typical	4.001	4.97[f]					0.02

(a) The estimated accuracy of weight measurements ± 0.5 lb. The order of accuracy of the other data is indicated by the number of significant figures to which the data are reported.
(b) See sketch for location.
(c) Calculated as pre-shot wall thickness minus post-shot wall thickness at Station 0°.
(d) One end cap was not recovered. Estimated weight of lost cap is 1½ lb.
(e) Neither end cap was recovered. Estimated weight of lost caps is 2½ lb ea.
(f) Cylinder profile was flat within 0.01 in.

Variation of Wall Thickness Around Circumference About 1 Inch From End

Tower No.	Wall Thickness[g] (in.) 0°	45°	90°	135°	180°
1 Left	1.63		1.70		1.65
Right	1.61		1.63		1.61
2 Left	1.688	1.700	1.706	1.705	1.710
Right	1.188	1.198	1.243	1.264	1.260
3 Left	1.348	1.370	1.375	1.359	1.379
Right[h]	0.899	0.902	0.925	0.926	0.918
4 Left[h]	0.937	0.942	0.966	0.973	0.979
Right[i]	0.466	0.474	0.491	0.492	0.486

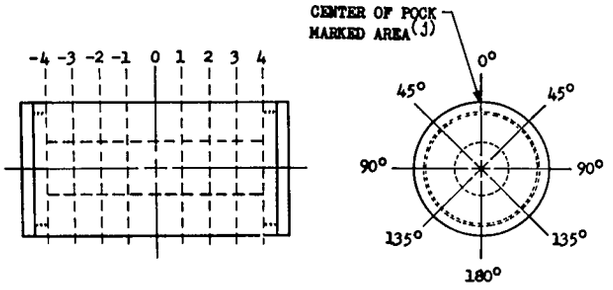

(g) These data represent, in most instances, average values for both ends and for plus and minus stations from 0 as seen in the sketch.
(h) Station 0° was definitely on side facing burst point as determined from location of hemispherical holes.
(i) Station 0° was arbitrarily taken at shiny metal flow area (see Figure A.25 a).
(j) Station 0° was taken at center of pock marked area on surface of cylinder except as noted in (h) and (i) above.

SECRET

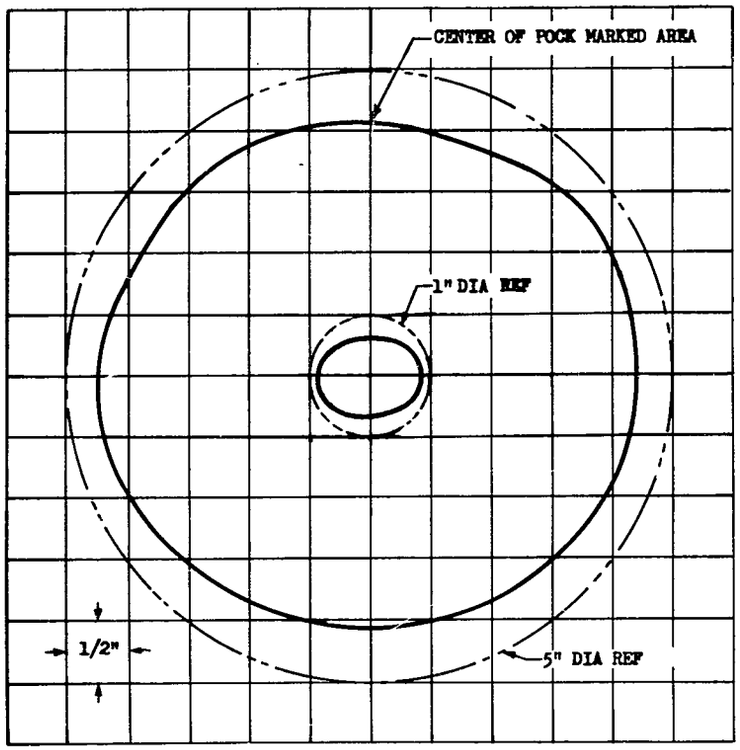

Figure 3.14 Cross Section at Center of Cylinder From Left Side of Tower 1

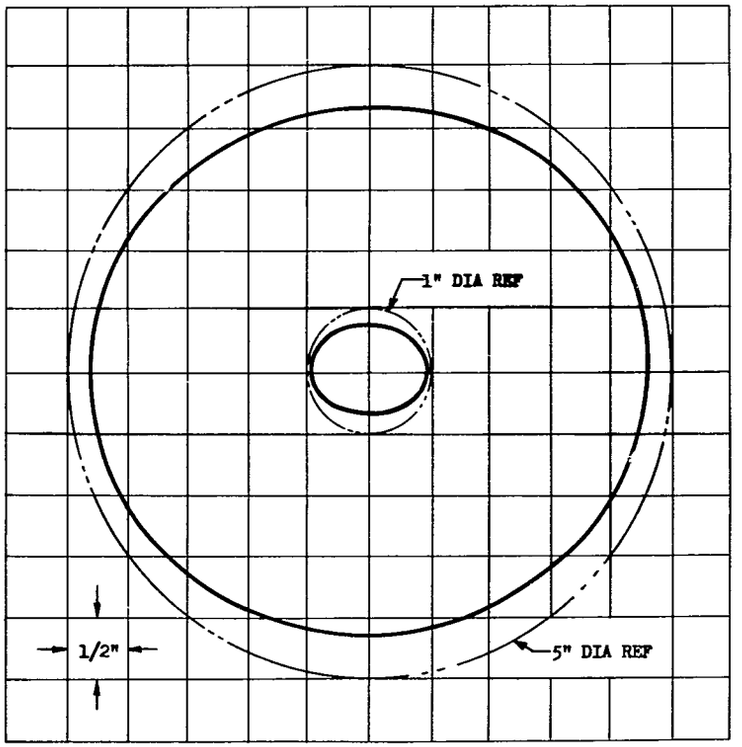

Figure 3.15 Cross Section at Center of Cylinder From Right Side of Tower 1

streaming effect noticed. There was little difference in damage between the holes which had tangential flow and the other holes, as can be seen from the cross sections in Figure 3.16. Photographs of the hemispherical holes are shown in Figure 3.17. The 3/16 in.-diameter holes on the cylinder from Tower 3 were practically undistinguishable, as seen in Figures 3.16 and 3.17 (a) and (b) because the gross metal loss on this cylinder was of about the same magnitude as the depth of the holes (3/32 inch). In several instances there was some molten flow into the hemispherical holes, which gave them the appearance of being slightly shallow. This was observed in particular on the holes which had tangential flow across them.

3.1.3 Ceramic Inserts. The ceramics exposed in the fireball exhibited surprisingly high mechanical shock resistance for the particular conditions of exposure. Some of the inserts were protruding appreciably above the surface of the containing sphere, as seen in Figure 3.18. The maximum protrusion of the Battelle ceramics was about 1/8 inch on the sphere from Tower 2. There was a considerable amount of metal loss immediately surrounding this insert extending to a depth of 5/8 inch below the nominal surface of the sphere, as seen in Figure 3.18 (a) and 3.19. The top of the ceramic was thus about 3/4 inch above the aluminum in the immediate vicinity. Nominal surface as used in this section means the average spherical surface of the aluminum in the vicinity of the insert, neglecting surface irregularities. The maximum protrusion observed for the graphite inserts was 7/16 inch; this occurred on Tower 3. One small corner of an Armour ceramic from Tower 3 protruded about 1/8 inch which was the maximum. The remainder of the surface was broken off, showing the undamaged parent material underneath. A summary of the approximate amount of protrusion of each insert above the containing sphere is given in Table 3.5. Table 3.5 also gives the apparent reduction in length of the inserts. This is given as the difference between the radius loss for the containing sphere, as given in Table 3.2, and the protrusion. There was a large amount of once-molten aluminum which covered the three ceramics on the front of the sphere from Tower 2, as shown in Figure 3.18 (a) and 3.19. There was apparently little if any molten aluminum covering any of the other ceramics. Close-up photographs of the various ceramics are shown in Appendix A, Figures A.16, A.17 and A.18. There was evidence that all of the Armour and Battelle ceramics were covered with a glaze of once-molten ceramic about 1/32 in. thick; however, the glaze was practically all missing, probably being chipped off during impact with the ground and during recovery. The graphite inserts sustained no apparent glazing and only little charring of the surfaces. In all instances the amount of protrusion given in Table 3.5 was measured from the nominal surface of the containing sphere to the maximum protrusion of any portion of the surface of the material, whether it was glaze or undamaged parent material.

The glazed surfaces of all but two of the Armour ceramic inserts were absent, leaving the parent material exposed. The two exceptions were the front insert from Tower 2, which was covered with aluminum, and the rear insert from Tower 1, which had a dark-green glaze over the entire surface. Several small areas of the parent material on the front insert

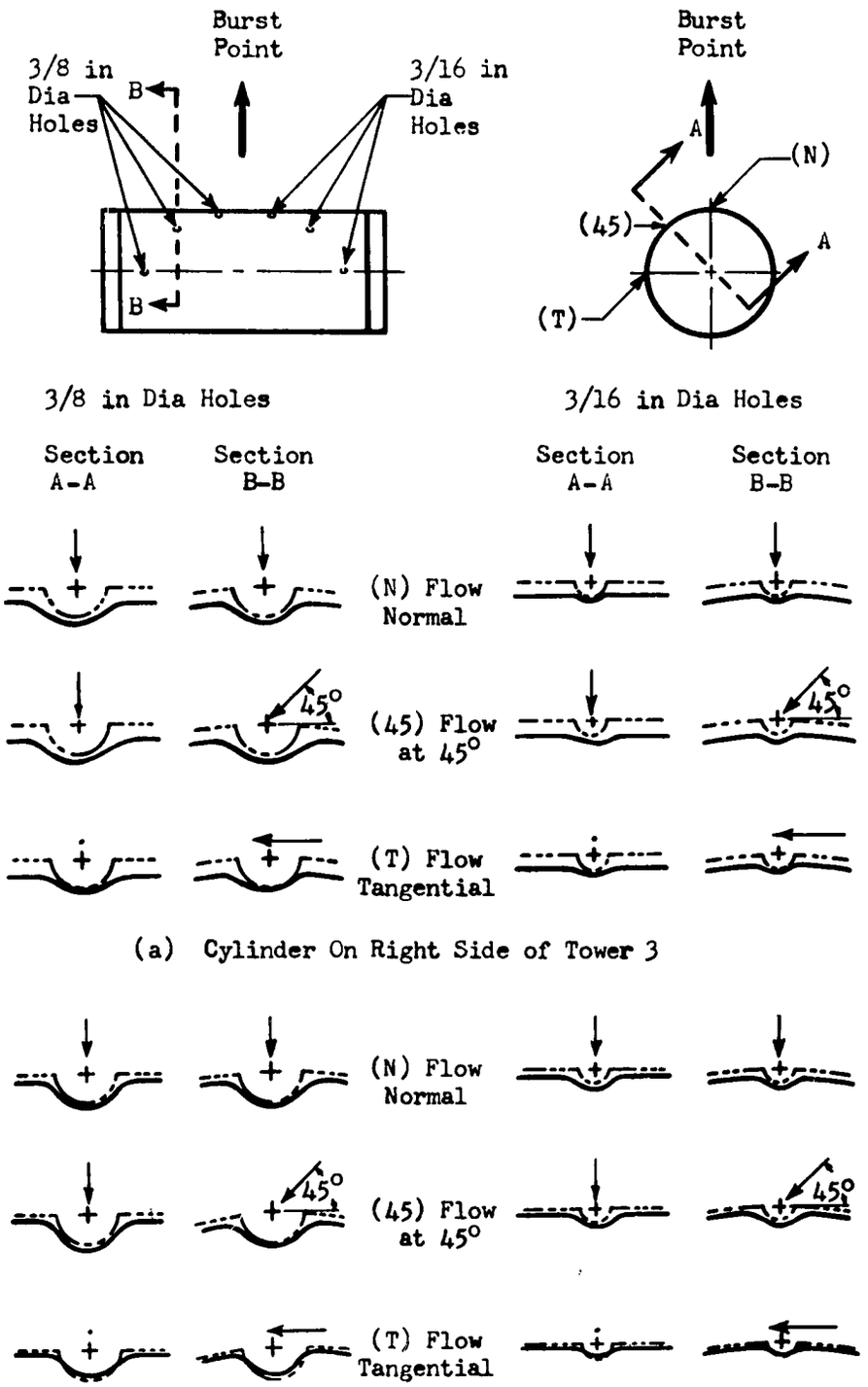

(a) Cylinder On Right Side of Tower 3

(b) Cylinder On Left Side of Tower 4

Figure 3.16 Cross Section of Hemispherical Holes on Cylinders

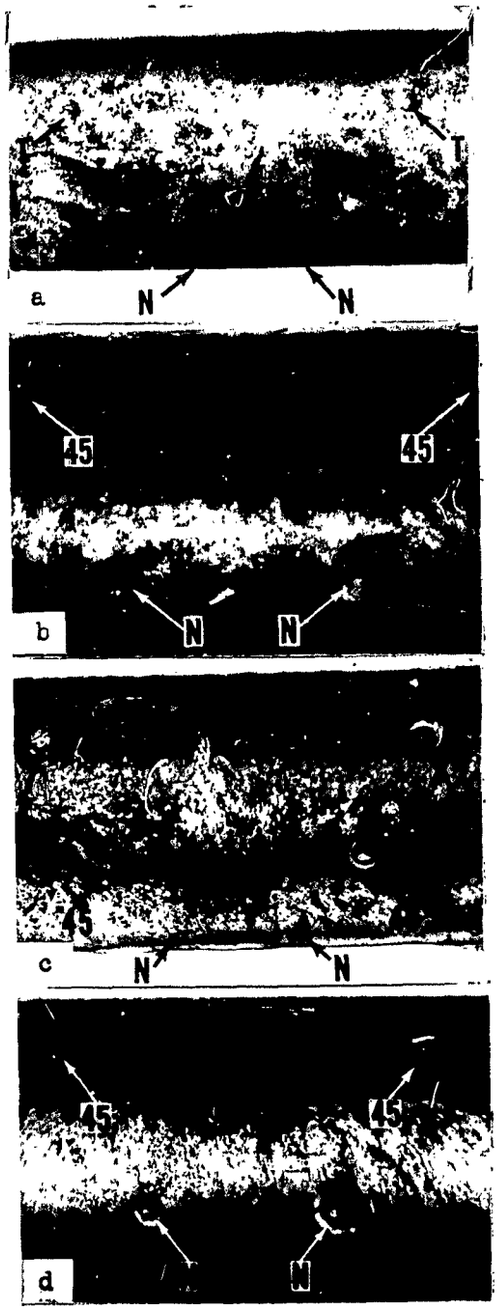

Figure 3.17 **Hemispherical Holes** on Cylinders with 1-in. walls from Towers 3 and 4. T-Tangential Flow, 45-Holes receiving 45° flow, and N-Flow directly into Holes-normal Flow. (a) and (b) Tower 3. (c) and (d) Tower 4.

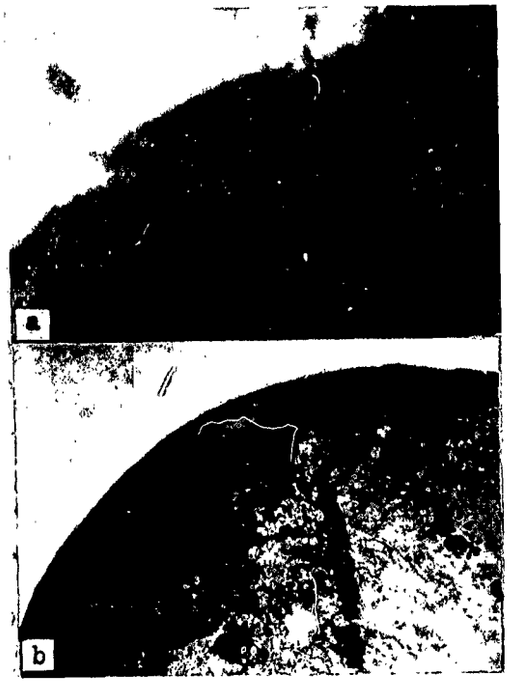

Figure 3.18 Maximum Observed Protrusion of Battelle and Graphite Inserts (a) Front Battelle, Tower-2 (b) Rear Graphite, Tower-3

Figure 3.19 Once-Molten Aluminum Covering Three Front Ceramic Inserts, Tower 2

from Tower 2 could be seen at a depth of less than 1/16 inch under the once-molten aluminum. The Armour ceramics on the front of each sphere were flush or below the surface of the sphere. Of the rear ceramics, only three, as listed in Table 3.5, had any portion remaining above the surface of the containing sphere, the remaining two inserts at the highest point were flush. The average surface of all Armour ceramics was below the nominal surface of the containing sphere. It is believed that impact with the ground broke off any portion of the ceramic which may have been above the surface.

The Battelle ceramic inserts, which under ordinary conditions exhibit less mechanical shock resistance than the Armour ceramics, appeared to withstand the exposure in the fireball much better than the Armour ceramics. There were several inserts which protruded 1/8 inch above the surface of the containing sphere, and all but three of the total ten inserts exposed were still protruding to varying degree. Of the remaining three, two were about flush with the surface. As with the Armour ceramics, there was evidence that all of the inserts were covered with a glaze. Some of the inserts still had a glaze covering part of the surface of the ceramics.

In general, the surface of the graphite inserts protruded farther than the other inserts. The amount of protrusion varied from 3/64 inch to 7/16 inch, with seven of the total ten inserts still protruding above the surface of the containing sphere. Of the other three inserts, one was about flush, one was broken off about 1/2 inch below the surface, and the other was broken out completely. The surface of the graphite inserts was not noticeably glazed, but there was some charring noticed on a few of the inserts. Several inserts had a macroscopically thin layer of aluminum over a portion of their surfaces, such as seen in Figure A.18 (i). A more-detailed description of the damage sustained by each insert is given in Appendix A.

3.2 THERMAL-SHOCK STUDY

Very little thermal damage was apparent on any of the materials, except those exposed at the focal point of the parabolic reflector. Post-shot photographs of all of the specimens are given in Figures 3.20 and 3.21. A summary of the pre-shot and post-shot masses of the specimens is given in Table 3.6. Both the pre-shot and the post-shot masses were obtained after oven drying the specimens at about 250°F for 3/4 hour to remove any moisture.

The ceramics at the focal point of the mirror were severely glazed and had slumped slightly in the holder indicating melting. The Battelle ceramic had a light olive-colored glaze and had three major surface cracks believed to have been caused by cooling of the glaze. The surface was pitted or pock marked. Most of these indentations were darker than the rest of the surface. The Armour ceramic had a relatively smooth glaze, almost white in color, over the surface and was finely checked as though cracked during cooling. There was a crack all the

way through the Armour ceramic along the edge adjacent to the metal case of the Battelle ceramic. This crack, it is believed, was not a result of thermal shock but was caused by a difference in thermal expansion between the ceramic and the metal case. The glaze and surface cracks on both ceramics extended to a depth of about 0.04 inch. Below this depth, the material was essentially undamaged parent ceramic material. The metal case of the Battelle ceramic which separated the two ceramics

TABLE 3.5 SUMMARY OF PROTRUSION AND LOSS OF MATERIAL FOR CERAMIC INSERTS

Tower No.	Location on Sphere	Maximum Protrusion Above Sphere (in.)			Apparent Material Loss From End*(in.)		
		Armour	Battelle	Graphite	Armour	Battelle	Graphite
1	Front	---	---	---	---	---	---
	Rear	0	0	---	1.3	1.3	---
2	Front	---	1/8	1/8	---	0.84	0.84
	Rear	0	1/16	0	0.97	0.91	0.97
3	Front	0	1/32	3/32	0.49	0.46	0.40
	Rear	1/8	5/32	7/16	0.36	0.33	0.05
4	Front	---	1/8	11/64	---	0	0
	Rear	1/32	5/64	7/64	0.08	0.03	0
5	Front	---	1/32	3/64	---	0	0
	Rear	1/32	0	1/16	0	0.03	0

* Calculated as the difference between the metal loss from containing sphere and the amount of protrusion.

Dash line means surface of ceramic was below nominal surface of containing sphere.

was partially melted and had run down toward the bottom. The lower portion of the stainless-steel specimen holder was nearly black in appearance and showed evidence of melting and flowing toward the bottom of the holder. The top half of the holder was covered with a dense, white deposit believed to be smoke from the Armour ceramic. There was apparently little, if any, damage to the parabolic reflector.

The ceramics at the 6-ft. pylon (range 1,100 feet) were severely eroded on the surface, probably because of impact of sand and larger particles carried by the shock wave. This pylon was torn from its base and was found about 13 feet to the rear and slightly to the left (facing ground zero) of its original position. The top of the pylon where the ceramics were mounted was buried under mud and water, and because of the high radiation level, it was not possible to recover the specimens until 5 days after the test. All of the test samples were still in the specimen holder; however, upon removal of the specimens, the Armour ceramic practically disintegrated, as seen in Figure 3.20. An unexposed test sample of the Armour ceramic was left to soak in water for 7 days and showed no tendency to disintegrate or change its physical properties. It is thus believed that the ceramic sustained a maze of microscopically small cracks during the test. There was no glaze or other evidence of thermal damage on any of these materials. If any thermal damage had been inflicted on these specimens, it was obscured by the heavy mechanical damage. The stainless-steel specimen holder was pitted, probably by debris carried along by the shock wave. The right side of the holder (facing ground zero) appeared to be more-heavily pitted than the left side, which may indicate that the shock flow was from the right side.

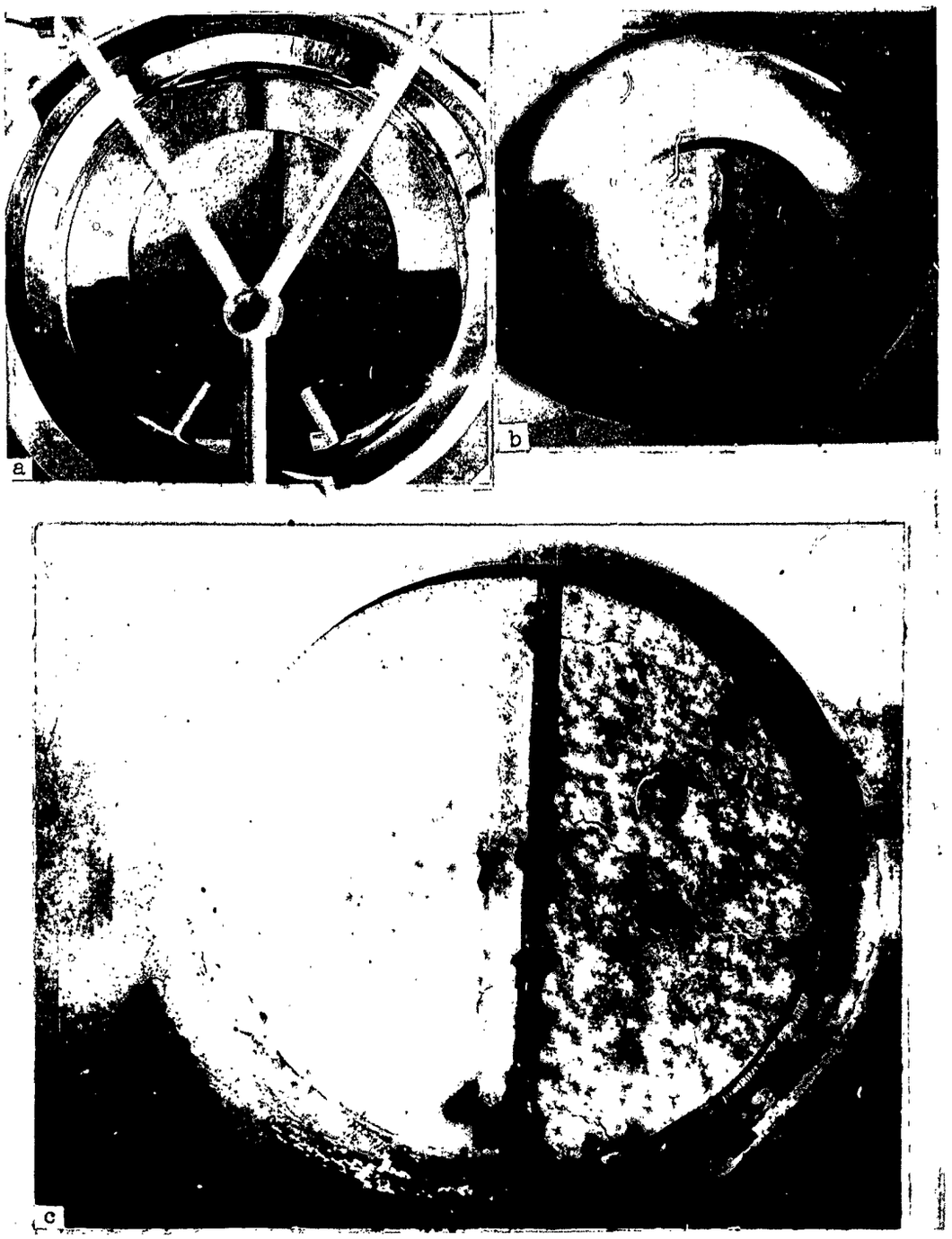

Figure 3.20 Battelle and Armour Ceramics from Focal Point of Mirror. Armour Ceramic is on left in each photograph. (a) Pre-Shot View; (b) Post-Shot View; (c) Close-up View of Ceramics.

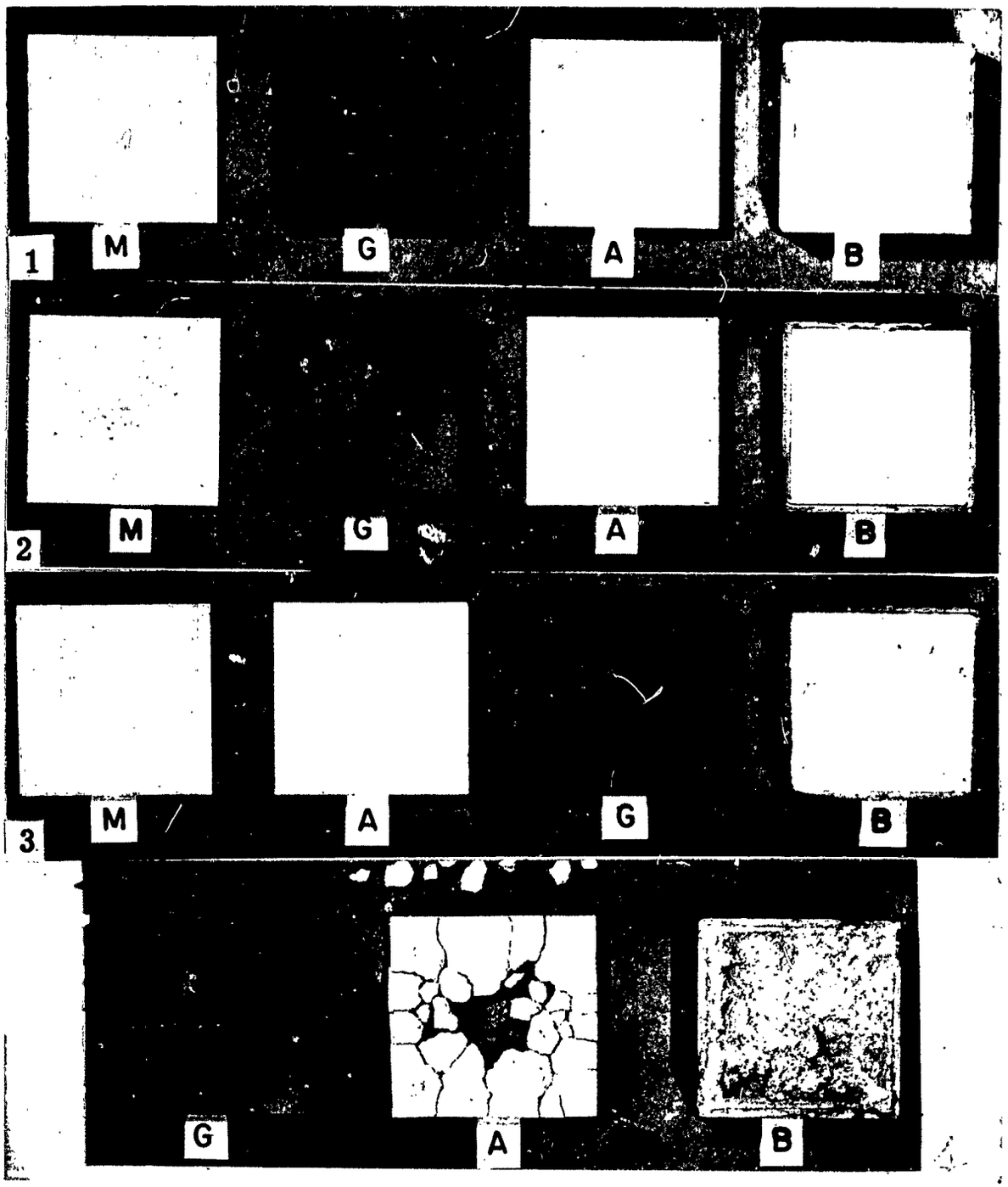

Figure 3.21 Post-Shot Photographs of Specimens Exposed on Pylons and Pipe Mount. B-Battelle; A-Armour; G-Graphite; M-Molybdenum. (1) Typical Pre-shot Specimens. (2) Range 3,100 feet (After Exposure). (3) Range 2,200 feet (After Exposure).(4) Range 1,100 feet (After Exposure).

The post-shot location of the pylon also suggests that the shock flow came from the right side of the pylon, since its post-shot location was slightly to the left of its original position.

There was essentially no thermal damage observed at either the 2,200-ft or 3,100-ft ranges. The Battelle ceramic at the small pylon, (2,200 feet), sustained mild pitting or spalling, which is believed to have been caused by impact of sand and other material in the shock wave.

TABLE 3.6 SUMMARY OF PRE-SHOT AND POST-SHOT MASSES OF THERMAL-SHOCK STUDY SPECIMENS

Range (ft)	Material	Mass (gms)		Mass Loss (gms)
		Pre-shot	Post-shot	
1,100	Armour	45.65	40.75	4.90
	Battelle	155.94	150.79	5.15
	Graphite	26.90	26.46	0.44
2,200	Armour	45.84	45.66	0.18
	Battelle	154.76	154.60	0.16
	Graphite	27.77	27.77	0.00
	Molybdenum	82.63	82.57	0.06
3,100	Armour	44.02	44.00	0.02
	Battelle	154.51	154.48	0.03
	Graphite	26.77	26.77	0.00
	Molybdenum	83.67	83.59	0.08
6,500	Armour	40.72	40.30	0.42
	Battelle	139.03	138.44	0.59

A slight amount of pitting was also observed on the graphite sample at 2,200 feet and the Battelle ceramic at 3,100 feet. There was a slight amount of pitting observed on the stainless-steel specimen holders at both of these ranges.

3.3 INSTRUMENTATION AND THERMAL INPUTS

No thermal-input data were recorded by this project, due to the failure of the recording galvanometers at time zero. The galvanometers began to rotate or oscillate rapidly and broke in less than 2 msec, even before the blue box had operated. The blue box, which actuated the relay system for removal of the shunts from across the instrumentation cables, required about 4 msec for operation. The relay system required about 12 msec for operation, giving a total time delay of 16 msec for removal of the shunts. A schematic of the instrumentation wiring, showing the location of the shunts, is given in Figure 2.13. All check lists and post-shot analyses of the circuits indicated that the relays were properly set prior to the shot. It is believed, however, that the galvanometers should have been adequately protected if the shunts were across the cables at time zero; as a consequence, it is concluded that either there was some malfunction of the relay system when the reset buttons were pushed prior to the shot or, for some unknown reason, the relays were prematurely actuated, causing the shunts to be removed.

The total radiant exposure, radiant exposure prior to blast arrival, and peak irradiance as a function of ground range were calculated for

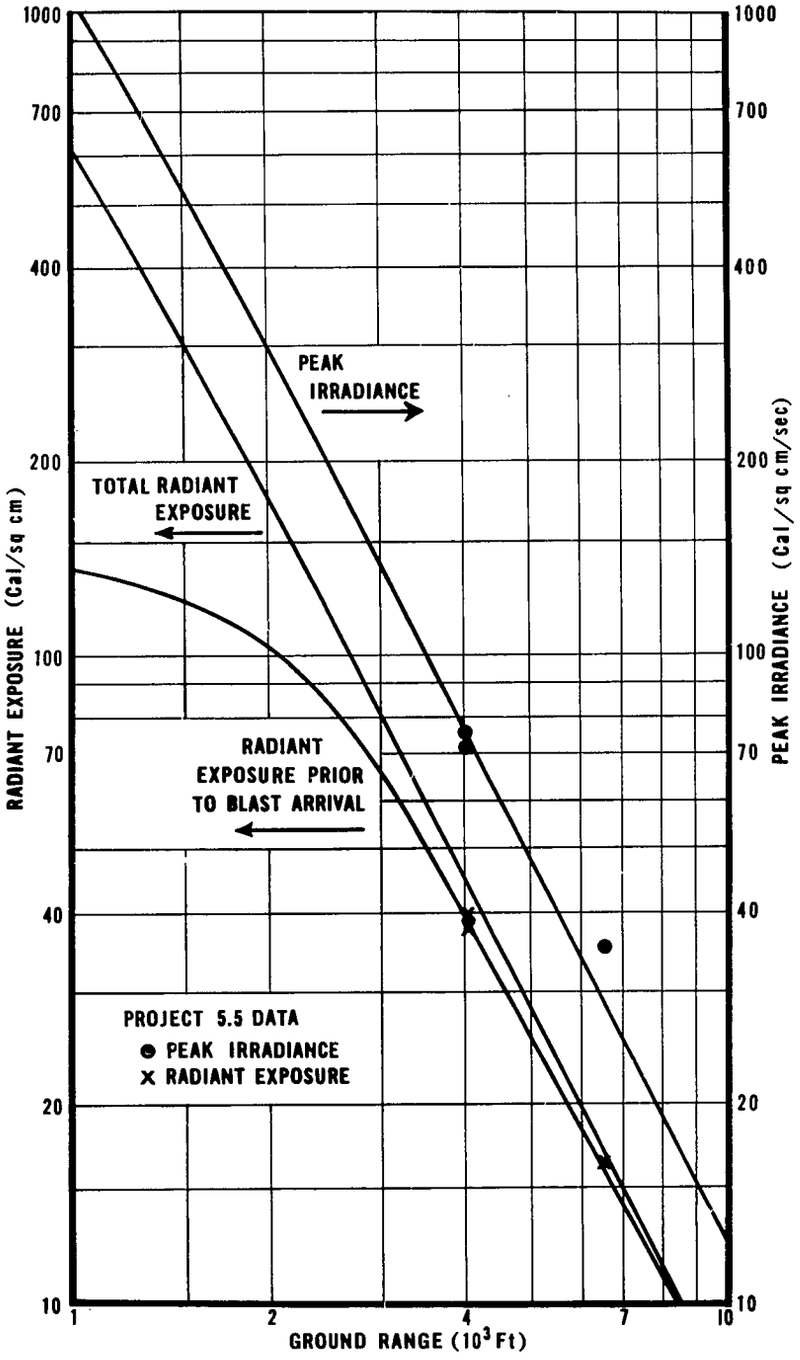

Figure 3.22 Calculated Radiant Exposure and Peak Irradiance versus Ground Range

Shot 12 and are presented in graphical form in Figure 3.22. The curve for unattenuated radiant exposure was calculated by use of a thermal yield of $44 \times 10^{10} W^{0.94}$ calories (where W is the total yield of the explosion, 23 KT) and assuming this energy is attenuated as the inverse square of the range. The approximate radiant exposure prior to blast arrival is represented by the lower curve in Figure 3.22. Dust, mud,

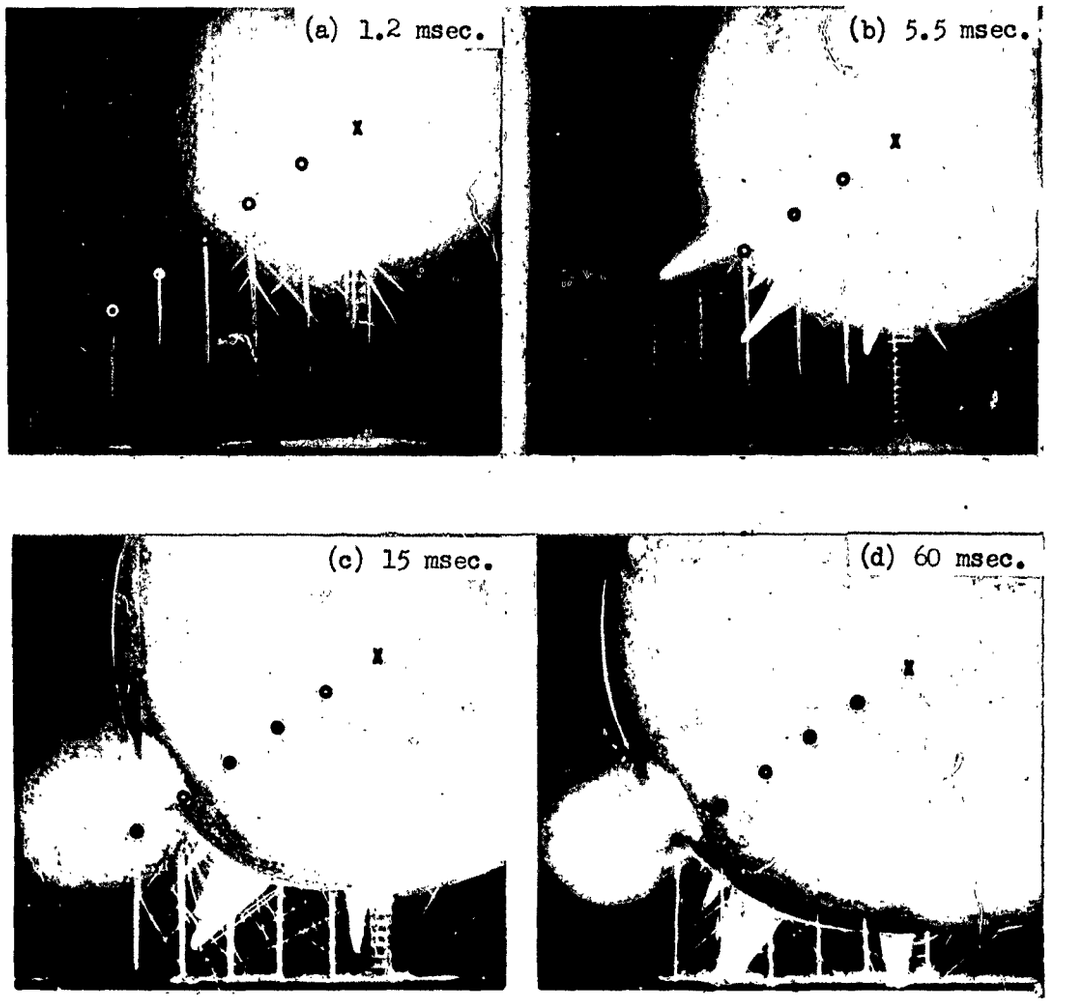

Figure 3.23 Sequence of Frames From a Film Showing Engulfment of Tower Specimens by Fireball.

and debris raised up by the blast wave would probably severely attenuate any thermal energy after blast arrival, especially at the close ranges. The peak irradiance was obtained by multiplying the total radiant exposure at any given range by about 1.8. Several thermal input measurements made by Project 5.5 during this shot are shown plotted on Figure 3.22 and appear to be in fair agreement with the calculated values. No

other measured data were available for comparison. Table 3.7 summarizes the thermal inputs at the various ranges used for the Thermal Shock Study.

The motion-picture cameras used to observe the response of the ceramic specimens at the 3,100-ft range operated satisfactorily; however, radiation fogging of the film caused considerable obscuration of the

TABLE 3.7 ESTIMATED THERMAL INPUTS FOR THERMAL SHOCK STUDY

Range (ft)	1,100	2,200	3,100	6,500	
				Station	Focal Spot
Radiant Exposure[a] (Cal/sq cm)	135	95	62	16.2[b]	1,300[c]
Peak Irradiance (Cal/sq cm/sec)	900	250	125	35.6[b]	2,800[c]

(a) Energy received prior to blast arrival
(b) Project 5.5 data for this range
(c) An approximate magnification factor of 80 was used.

images. There was not sufficient detail on the film to determine if there was any thermal damage sustained by the ceramics. Visual analysis of the ceramic materials after the test indicate that little, if any, thermal damage was incurred.

A few frames from a motion-picture film showing the engulfment of the lethality-study specimens by the fireball are presented in Figure 3.23. No time base was provided on this film; however, the approximate time of each frame given in Figure 3.23 was calculated from the curve of fireball radius versus time in "Capabilities of Atomic Weapons," TM 23-200. These photographs were touched up to show more clearly the tower legs, guy wires, and extent of the fireball and fireball spikes. The zeros indicate the pre-shot locations of the specimens and "x," the burst point.

Chapter 4
DISCUSSION

This chapter includes a brief discussion of the data obtained from both the lethality study and the thermal-shock study and is intended to point out any important peculiarities and limitations of the data. Where possible, the vulnerability data are presented in graphical form to illustrate their variation with distance from the burst point. A few conclusions are drawn on the basis of the data obtained and the need for further data is pointed out. With the exception of an elementary analysis of the trajectories of the lethality-study specimens in Appendix B, little analysis of the data is presented herein. An attempt is currently being made to determine the temperature time-history of exposure of the specimens exposed in the fireball as predicted from Problem "M." Further analyses and correlations will be attempted and if believed to be of general interest will be summarized in a future report. The Materials Laboratory of Wright Air Development Center (WADC) is currently performing a metallurgical analysis of a few of the lethality-study specimens in order to observe, by means of photomicrographs, possible variations in the crystalline structures of the materials. The results of this analysis will be summarized in a WADC Technical Note. It is hoped that personnel concerned with theoretical analysis find the data in this report useful and are encouraged to make further calculations which would be helpful in explaining various phenomena contributing to metal loss and which could be used to direct new or varied avenues of research in regard to fireball exposure.

4.1 LETHALITY STUDY

A particularly interesting result is the weight loss by the spheres. The weight loss of each of the spherical specimens is shown plotted in Figure 4.1 as a function of distance from the burst point. It can be seen from this plot that, for the particular conditions of exposure, the weight loss from the steel spheres is approximately the same as from the aluminum spheres. Whether this invariance of weight loss with material type can be extrapolated to other sizes of spheres and types of materials is not known. There are no known calculations which would predict this result or show that it is merely a result of chance by virtue of the particular metals used. Further data regarding this question should be obtained during Operation Redwing, in which various materials (copper, steel, molybdenum, titanium, plastic and graphite) of spherical configuration are being exposed within a nuclear fireball.

Figure 4.2 shows the apparent reduction in radius of the spherical specimens as calculated from weight measurements (Ref. formula 3.1). It can be seen from this figure that aluminum is about three times more vulnerable to material loss than steel. Because of the fracture of the

ceramic insert sphere from Tower 1 and the apparent loss of material on the surface of the fracture, the calculated reduction in radius for this sphere is probably too large; hence the curves of Figures 4.1 and 4.2 were drawn as if this point were approximately coincident with the data point for the solid aluminum sphere at Tower 1. Metal losses calculated from circumference measurements are slightly less than those calculated from weight measurements, and metal losses calculated from diameter measurements tended to be slightly higher than those calculated from weight measurements. This variation, it is believed, is due partly to surface irregularities and foreign materials and partly to asymmetry of the specimens. Circumference measurements are too large, because the measurements were made over the surface irregularities and extraneous surface materials; the diameter measurements are too small, because they were made between two opposite surface points without regard to surface irregularities and asymmetry.

The variation of weight loss with distance from the burst point for the steel cylinders is presented in Figure 4.3. These data were calculated from Table 3.4 and represent the total weight loss including loss from the end caps. For the cylinders on which one or more caps were lost, the estimated weights of the caps were added to the post-shot weights of the cylinders.

Because of the barreling effect, presentation of data on the reduction in size of the cylinders is difficult; however, with this in mind, a graph of the variation of average metal loss at the center of the cylinders with distance from the burst point is presented in Figure 4.4. These data were calculated as the difference between pre-shot and post-shot wall thicknesses in order to eliminate the error that would be introduced by measuring the external diameter of the squashed cylinders from Towers 1 and 2 and neglecting the reduction in size of the 1-in.-diameter holes. Particular attention should be given the cylinder configurations and exposure conditions under which the data of Figures 4.3 and 4.4 were obtained. The metal loss at the center of the cylinders as given in Figure 4.4 is probably not representative of a long or so-called infinite cylinder of the same diameter, because of the end effects which produced the barrel-shaped appearance. At Towers 3 and 4 the metal loss at the center of the cylinder was probably not influenced greatly by the end effects, as shown by the relatively flat profile near the center of the cylinder in Figure 3.11 and Table 3.4. A comparison of the data of Figures 4.2 and 4.4 indicates that at any given range there was from 50 to 100 percent more depth of metal lost from the steel spheres than from the center of the steel cylinders (neglecting end effects) which indicates that geometrical configuration is a definite parameter affecting metal loss.

There was a considerable variation in damage to the cylinders, especially between the cylinders on the right side of the tower and those on the left (as can be seen in Table 3.4 and in Figures 4.3 and 4.4). A certain part of this apparent damage variation may be due to possible inaccuracies in the measurements; however, the consistency with which the damage is greater on the left side of the tower than on the right

side tempts one to draw two curves through the data instead of the single curve shown, one curve for the left side of the tower and another for the right side. A possible explanation of the greater damage to the cylinders on the left side of the towers could be that these cylinders were heavier than the cylinders on the right side (except at Tower 1 where they had equal weights) and, as a consequence, should have had a smaller velocity and, hence, longer exposure in the fireball. However, this theory is not supported by measurements of the distances the specimens traveled from the tower, as seen in Table 3.1 and discussed in Appendix B. A possible explanation of the damage differential may lie in the particular materials used. All of the cylinders were made of "10" series steel; but as seen in Table 2.2, the carbon content of the cylinders on the right side of the tower was greater than the carbon content of the cylinders on the left. The last two figures in the steel designation represent the approximate carbon content in hundredths of percent, e.g., 1025 steel contains about 0.25 percent carbon. Further exposure of various cylinder types would aid in resolving some of these apparent discrepancies.

The profiles of the post-shot configurations of the hemispherical holes on the cylinders are shown in Figure 3.16, from which it can be seen that there was little difference in damage between the various holes. There was much less metal lost from the bottoms of all of these holes than from the general surface of the cylinder, which suggests that the molten and vaporized metal flowing past the holes afforded considerable protection to the bottoms of these holes. In some instances it appeared that some molten metal flowed into the holes and caused them to appear to have actually gained metal in the bottom.

Few quantitative data relative to material loss from the ceramic inserts were obtained, because of the difficulty in differentiating between thermal damage and mechanical damage. Most of the inserts sustained a certain degree of mechanical damage, in addition to any thermal damage, as evidenced by the chipped surfaces and absence of glaze on many of the surfaces. Probably the most-accurate statement which could be made without misleading the reader is that, under the conditions of exposure, the graphite and ceramic inserts were somewhat less vulnerable to material loss than aluminum. However, with the qualification that the apparent material loss data for the ceramics as given in Table 3.5 represent, in most cases, a combination of both mechanical and thermal damage, these data are tendered in Figure 4.5 in graphical form. The dashed curve represents the metal loss from the aluminum spheres in which the inserts were contained and is shown for comparison purposes. A curve is drawn for each of the material types through the lowest point (least amount of material loss) at the last three ranges.

These curves probably represent an upper limit for the amount of thermal damage which would have been inflicted on the materials had there been no blast impact or ground impact to cause the ceramics surfaces to be broken off or chipped. A comparison of the curves for the three material types suggests that the graphite is the least vulnerable and that the Battelle ceramic and Armour ceramic follow in order of

increasing vulnerability. In most instances, as seen in Table 3.5 and Figure 4.5, the front inserts lost more material than the rear inserts, probably because the front inserts were on the side of the sphere first impacted by the growing fireball and shock front and, hence, received a larger mechanical shock. It is the opinion of the author that the data on graphite and ceramic materials should be treated as only qualitative information from which the relative vulnerability of the materials can be estimated. In designing any further ceramic-exposure programs, particular attention should be given to protection of the materials from mechanical damage.

Little information was obtained on the variation of metal loss over the surface of the test specimens. The only quantitative data in this regard were from the cylinders, where the variation in wall thickness around the circumference was obtained. Table 3.4 summarizes the wall thicknesses on the cylinders, as measured on a circumference about 1 inch from the end of the cylinder. The measurements do not include large surface irregularities such as pock marks. Station 0° was taken at the center of the pock-marked area for the pock-marked cylinders and on the sides definitely facing the burst point for the cylinders which were provided with the hemispherical holes. The average of the data in Table 3.4 indicate that Station 0° sustained the most metal loss, Station 45° lost about 0.01 inch less, and from Station 90 to Station 180° there was about 0.03 inch less metal loss than at Station 0°.

From the variation of metal loss on the cylinders with hemispherical holes it is concluded that at least at Towers 3 and 4 metal loss was most severe on the sides of the cylinders facing the burst point. Further, since the metal loss was greatest on the sides of the cylinder facing the burst point at Towers 3 and 4, it is deduced that the pock marks were on the sides of the cylinders facing the burst point for, as seen in Table 3.4, this was the side with the most metal loss. The location of the relatively fewer pock marks observed on the cylinders provided with hemispherical holes is in agreement with this deduction. A further argument in support of this deduction was that at Tower 1 the sides of the cylinders which contained the pock marks were increased in length, i.e., the end faces were no longer parallel, as seen in Figure 3.9 (a). It is believed that this increase in length was due to the large acceleration force on the side of the cylinder, causing the material to yield on this side and to flow slightly toward the ends of the cylinder. The maximum variation of metal loss around a circumference on any one of the cylinders was less than 3/32 inch.

The cause and significance of the pock marks are not known. Spalling may have beer the cause; however, it was deduced in the preceding paragraph that these pock marks were on the side of the cylinder facing the burst point, which may indicate that the pock marks were caused by impact of high-velocity particles in the shock front. If the pock marks were caused by impact of debris in the shock front, however,

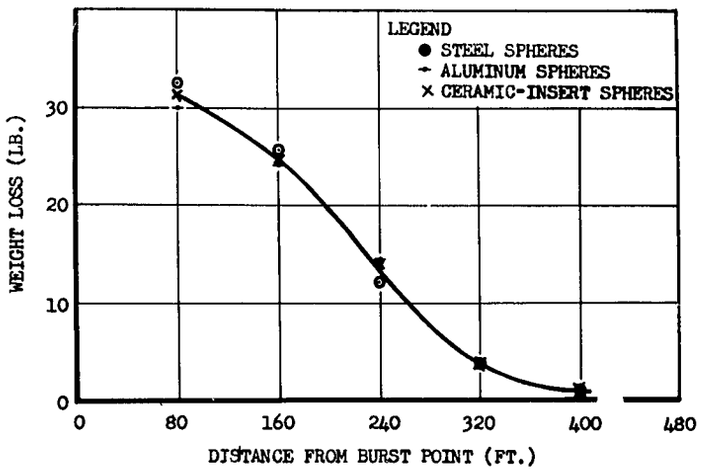

Figure 4.1 Variation of Weight Loss With Distance From the Burst Point for Aluminum and Steel Spheres

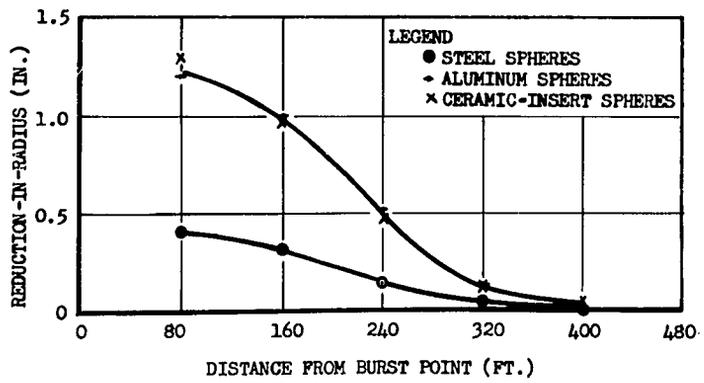

Figure 4.2 Variation of Reduction-of-radius With Distance From the Burst Point for Aluminum and Steel Spheres

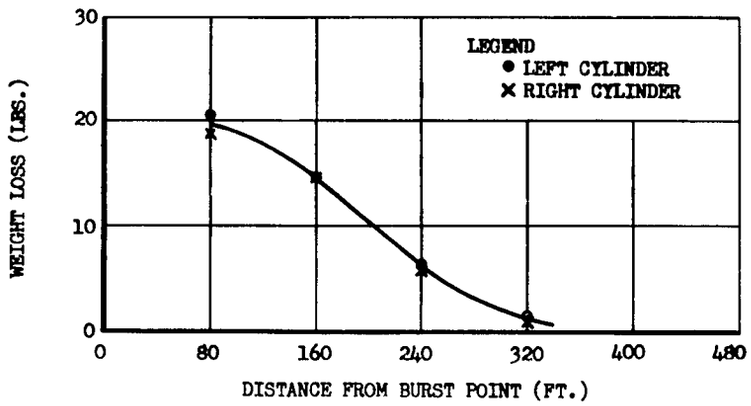

Figure 4.3 Variation of Weight Loss With Distance From the Burst Point for Steel Cylinders

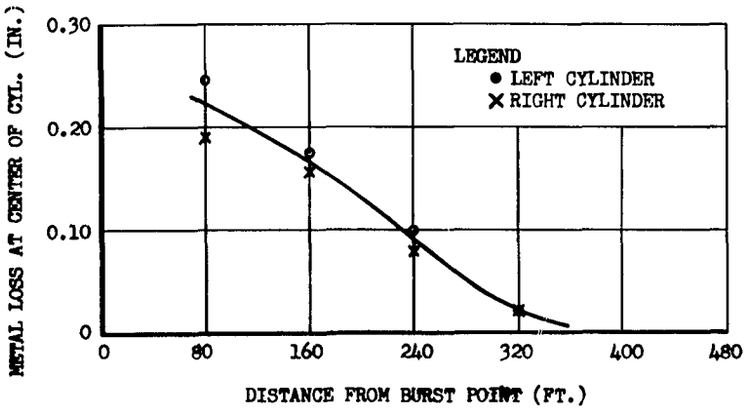

Figure 4.4 Variation of Average Metal Loss at the Center of the Cylinders (Reduction-in-wall-thickness) With Distance From the Burst Point for Steel Cylinders

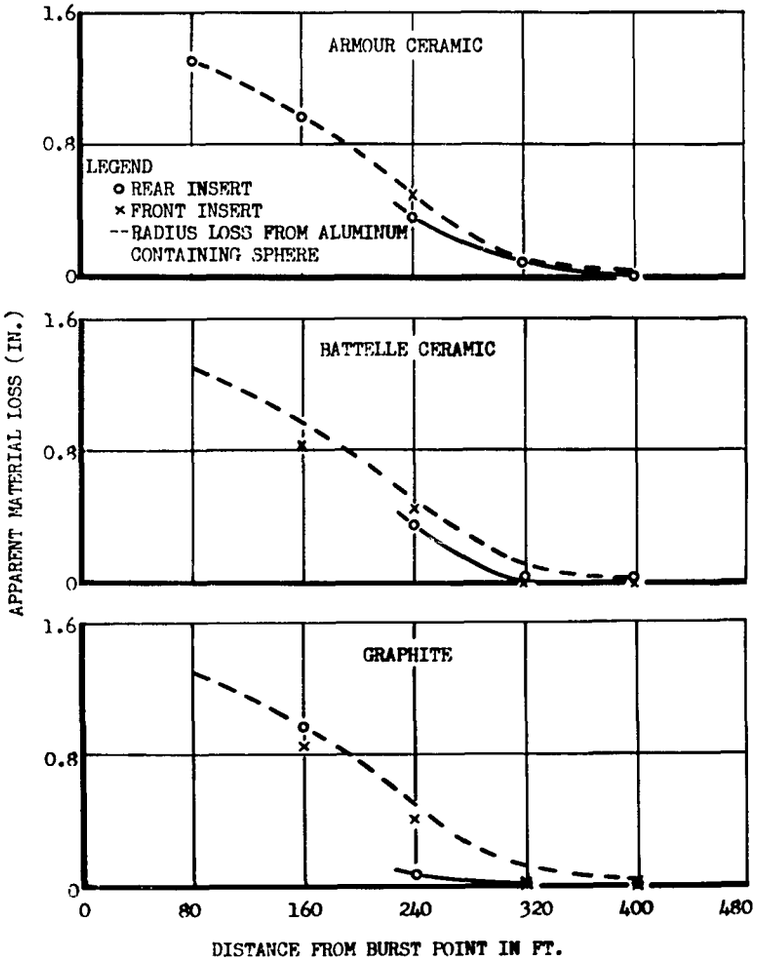

Figure 4.5 Apparent Material Loss From Armour Ceramic, Battelle Ceramic, and Graphite Inserts

it is peculiar that all of the cylinders at the close ranges were severely pock marked and the spheres were not noticeably affected.

The reduction in size of the 1-in. holes in the cylinders from Tower 1 is indicative that the overpressure in the fireball at this station was of sufficient magnitude to cause the material in the cylinders to yield.

Table 4.1 gives a summary of the yield strength of each of the cylinders and the external pressure which would cause the material to yield under static conditions. These pressures were calculated from the thick-walled cylinder forumla given at the bottom of Table 4.1.

TABLE 4.1 SUMMARY OF EXTERNAL PRESSURES REQUIRED TO YIELD CYLINDERS UNDER STATIC CONDITIONS

Tower	Location	Hole Dia- d_1-(in.)	Material (Steel)	Yield Strength- s-(psi)	Minimum External Pressure(p) to Yield Cylinder* (psi)
1	Left Side	1.0	1,015	44,000	21,000
	Right Side	1.0	1,045	59,000	28,500
2	Left Side	1.0	1,025	49,000	23,500
	Right Side	2.0	1,055	64,000	27,000
3	Left Side	2.0	1,020	46,500	19,500
	Right Side	3.0	1,045	59,000	19,000
4	Left Side	3.0	1,018	45,500	8,000
	Right Side	4.0	1,055	64,000	11,500

* $p = (d_2^2 - d_1^2)\, s/2d_2^2$ where d_2 is outside dia = 5 (in.) and d_1 is inside dia (in.)

As seen in this table, a constant overpressure of about 28,500 psi would cause the cylinders at Tower 1 to fail. Hence, it is concluded that peak pressure at a range of 82 feet from the burst point (Tower 1) was considerably in excess of 28,500 psi in view of the magnitudes of the deformations produced in the extremely short time the pressure was sustained.

The difference in the amount of squashing of the two cylinders from Tower 1, as seen in Table 3.4, is probably due to the difference in yield strengths of the two cylinders. There was only a slight amount of squashing of the cylinders from Tower 2. The fact that the left cylinder which had a 1-in. hole was squashed more than the right cylinder which had a 2-in. hole is attributed to the difference in yield strengths of the materials used, as seen in Table 4.1. In view of the small deformations of the cylinders from Tower 2, the peak overpressure at Tower 2 (Range 162 feet) was probably not much higher than the values of external pressure given in Table 4.1 for these cylinders; however, it should be noted that the pressures calculated in Table 4.1 were obtained from a static analysis of cylinders and are probably not entirely representative of the conditions of rapid application of pressure as realized during these exposures.

It is not known whether a dynamic analysis of a cylinder under external pressure exists; however, it is believed that the pressure

required to yield a cylinder, as calculated from a dynamic analysis, would be larger than that calculated from the static analysis given herein. The fact that some of the caps were detached from these cylinders is believed to be of little consequence, since the caps were probably not removed from the cylinders until after most of the crushing had been sustained and, hence, would not have afforded pressure relief during the crushing phase.

The elliptical cross section of the failed cylinders is believed to have been caused by the acceleration force imparted to the side of the specimen by the incident shock wave, for as can be seen in Table 3.4 and Figures 3.9 through 3.15, the minor axes of the elliptical cross sections of the cylinders points toward the pock-marked areas which, as deduced above, were on the sides of the cylinders facing the burst point. The overall reduction in hole diameter of the cylinders would probably still have occurred had there been no side acceleration loading (such as exposing the cylinders with one end pointed toward the burst point); however, the cross section of the cylinders under these conditions would not necessarily deviate from a circle.

There was probably a considerable variation in metal loss over the surface of the spheres, as evidenced by the variation in the diameter measurements given in Table 3.3. There were some slight indications that metal loss was most severe on the side of the spheres facing the burst point; however, because the centers of the spheres were not accurately located, no quantitative data were obtained.

Extrapolation of the steel-sphere-vulnerability data presented in Figures 4.1 and 4.2 indicates there is a possibility that the steel ball which was placed in the shot cab at a distance of about 13 feet from the weapon was not completely annihilated. At these close ranges, however, neutron heating becomes important. Some rough calculations indicate that neutron fluxes alone at this range could have nearly caused annihilation of this sphere. Further, the temperature of the fireball just before it breaks through the shot cab is probably much higher than just after it passes through the cab because of the large amount of steel and other materials engulfed by the fireball during this time interval. It is thus believed that the curves of metal loss as given in Figures 4.1 through 4.5 should start to rise rapidly for ranges close to the shot cab and inside the shot cab.

The success realized in exposure and recovery of the test specimens is an important result, for it shows that it is possible to position test specimens and equipment in a nuclear fireball with a reasonable assurance that recovery after the test will be feasible. As a consequence, the nuclear fireball represents an available source of high temperatures, pressures, and radiation fluxes which are currently not attainable in a laboratory for exposure of specimens. The light-weight television towers used for positioning the specimens in the fireball

during this test are believed to be a practical and relatively inexpensive means of assuring the location and orientation of test specimens at the time of engulfment by the fireball.

Because of the limited scope and exploratory nature of this program, only a relatively small amount of vulnerability data, as presented in Figures 4.1 through 4.4, were obtained. However, these data, it is believed, do define the relative vulnerability of some basic materials and structures and, as such, can be used to establish a preliminary estimate of the lethality of a nuclear explosion as applied to ballistic missiles under near sea-level conditions. Further theoretical calculations and test data on the vulnerability of other type materials and structures will be required to obtain the ultimate objective of predicting the lethal radius of a nuclear explosion at high altitude, if used to defend friendly target areas against incoming hostile intercontinental ballistic missiles.

Two parameters which affect metal loss and should be investigated further are material type and specimen configuration and orientation with respect to the burst point. Some specimens designed to maximize or minimize various mechanisms of heat transfer and metal loss and exposed in a nuclear fireball would aid in determining the relative importance of the various mechanisms and should give a better understanding of the physics involved in such exposures. Positioning of several types of specimens at various ranges within the fireball of a series of nuclear explosions covering a wide range of yields would be useful in determining the effects of the variation of weapon yield on metal loss and, at the same time, would aid in establishing empirical yield scaling laws for metal loss versus distance. Establishment of such scaling laws would be valuable in predicting the vulnerability of ballistic missiles and be useful in the planning phases of future test programs.

An attempt to develop time-history and peak-value instrumentation equipment and techniques to obtain measurements within a nuclear fireball appears to be the next logical step in the evolution of specimen exposure within a nuclear fireball. Such a development program is currently being carried out during Operation Redwing, wherein a miniature 8-channel magnetic-tape recorder is being used and tested. Development of suitable recording systems and techniques would be an invaluable asset in verifying or deriving theoretical predictions of metal loss for sea-level bursts and, later, for a high-altitude burst--which is the ultimate objective.

4.2 THERMAL-SHOCK STUDY

The most-significant result obtained from exposure of the ceramic materials external to the fireball was the surface glazing of the Armour and Battelle ceramics at the focal point of the parabolic mirror (Ref. Figure 3.20). There were several surface cracks observed which were attributed to cooling; however, there were no fractures noted in the parent material beneath the glaze. It is concluded that the thermal inputs at the mirror were not sufficient to cause thermal shock in these

ceramics. It is believed that at the two pylons and the pipe mount the ceramic materials sustained sufficient blast damage to obscure any thermal damage which may have been inflicted on the materials. Consequently, no damage threshold can be established.

The results obtained at the mirror were typical of those obtained from exposure of similar specimens in a solar furnace at lower flux levels but for longer time durations. From solar-furnace testing, it was determined that the Armour ceramic begins to emit a white smoke similar to that seen on the specimen holder in Figure 3.20 at a surface temperature of about 2200°C, and this smoke emission becomes profuse at surface temperatures of about 2400°C. Melting of the Armour ceramic occurs at about 2500 to 2700°C. It has been estimated that an absorbed step-input flux of 450 cal/sq cm/sec decaying lineraly to zero in 1 second would produce melting of the Armour ceramic. Melting of both ceramics did occur, as shown by the surface glaze and also by the slumping of the material toward the bottom of the holder. The estimated peak flux at the focal point of the mirror as given in Table 3.8 was about 2,800 cal/sq cm/sec and, assuming an approximate absorptivity of 0.2, the peak absorbed flux rate would have been about 560 cal/sq cm/sec.

The pitting of the Battelle ceramic is believed to have been caused by the charring of the asbestos fiber in the material producing a local area of high absorptivity. This would allow more energy to be absorbed and cause more material loss in these areas. Because of this pitting of the Battelle ceramic, it would be slightly inferior to the Armour ceramic, where surface smoothness after exposure is important. There were no results obtained during these exposures which would indicate that any of the materials tested would be unsuitable for use as protective surfaces for intercontinental ballistic missiles.

The technique of using parabolic mirrors to concentrate the thermal energy from a nuclear explosion is believed to be advantageous, for it permits the obtaining of high thermal inputs at relatively remote ranges, where blast damage is small. There is also a considerable saving realized in construction cost, for the mirrors can be mounted on relatively inexpensive structures. In most instances the mirror assemblies could be anchored by means of sand bags and cable tie-downs without the use of concrete bases.

A problem peculiar to this usage of parabolic mirrors is the determination of the distribution of energy over the focal spot as a function of time. This is due to the complicated optics of parabolic reflectors and to the rise of the fireball above the optical axis of the mirror, causing its image to move down over the specimens rather than remain fixed. In future tests it would be advisable to consider tracking the fireball by means of servo-mechanisms or, more simply, by a built-in cam drive which would cause the mirror to follow approximately the predicted fireball rise. An off-the-axis analysis of a parabolic mirror is time consuming and is probably best accomplished on computer equipment. Because of the limited results obtained, a thorough analysis of this type did not appear warranted. An on-the-axis analysis

of a parabolic mirror is given in "Analysis of Large Aperture Parabolic Reflectors for Solar Furnaces" by J. Farber and B. I. Davis, Consolidated Vultee Aircraft Corporation, Report No. TRM-77, 28 January 1954. The approximate magnification factor of 80 used in paragraph 3.4 was obtained from reference to this report.

The delta-wing pylons, although extremely low-drag structures, are not believed to be suitable designs for support structures because of their high sensitivity to side loading (angle of attack) and because such structures are relatively expensive to fabricate. The pylon which failed (range 1,100 feet), was designed for an angle of attack of 0.5°, and the calculated angle of attack which would have caused failure of the reinforcing rods as realized was about 1.3°. A survey of the pylon orientation before the test indicated that the front of the pylon was pointing to the left of ground zero by about $1/6^{\circ}$, but this misalignment alone should not have caused failure. There were no data on angle of attack measured at this range; however, there was apparently more pitting on the right side (facing ground zero) of the specimen holder than on the left side, which may indicate that the blast flow came from the right side and caused the pylon to fail.

Chapter 5
CONCLUSIONS AND RECOMMENDATIONS

5.1 CONCLUSIONS

5.1.1 Lethality Study.

1. Aluminum is about three times more vulnerable than steel in 10-in.-diameter spherical configuration when measured in terms of depth of metal lost; when measured in terms of net weight loss, steel and aluminum were of approximately equal vulnerability.

2. The depth of metal lost from 10-in.-diameter steel spheres is from 50 to 100 percent greater than the depth of metal lost from the center of 5-in.-diameter steel cylinders.

3. The cylinders at the closer ranges were not long enough to eliminate end effects and, as a result, the metal loss data from the cylinders at close ranges are not representative of metal loss from the so-called infinite cylinders.

4. Generally, the surface of the cylinder facing the burst lost more metal than the surface facing away from the burst.

5. The magnitudes of any thermally or thermomechanically induced shock waves in the cylindrical specimens were not sufficient to cause any noticeable spalling on the insides of the cylinders.

6. The high-velocity gases in the shock front did not cause any appreciable erosion of the hemispherical holes machined on the cylinders.

7. The bottoms of the hemispherical holes lost considerably less metal than the general surface of the cylinders on which they were machined, indicating that the molten and vaporized metals in the vicinity of the holes afforded some shielding effect.

8. The dynamic pressure and overpressure in the fireball were not sufficiently high to cause a noticeable increase in density of the test specimens.

9. The combined dynamic pressure and overpressure acting on the cylinders at Tower 1 was sufficient to cause considerable squashing and plastic flow of the metal. The peak overpressure at this range (82 feet) was considerably in excess of 28,500 psi, as estimated from the yield strength of the cylinders.

10. Graphite and the Armour and Battelle ceramic materials are less vulnerable to thermal damage than aluminum for the conditions of this test.

11. The technique of specimen exposure atop light-weight television towers is relatively inexpensive and is functional, assuring specimen position and orientation at detonation time.

5.1.2 Thermal-Shock Study.

1. The thermal energy received by the Armour and Battelle ceramics located at the focal point of the parabolic mirror did not cause any noticeable thermal-shock damage.

2. Where surface smoothness after exposure is important, the Armour ceramic is slightly superior to the Battelle ceramic.

3. There were no data obtained which would indicate that any of the materials tested would be unsuitable as protective surfaces for intercontinental ballistic missiles.

4. The technique of using parabolic mirrors to magnify the thermal flux at remote ranges is advantageous, since higher thermal energy levels and less blast interference are realized than by direct exposure and because the blast damage to the specimens is relatively small.

5. Pylons of the delta-wing type are not entirely suitable for use as specimen support structures because of their high sensitivity to side loading (angle of attack) and because of their relatively high cost and difficulty of construction.

5.2 RECOMMENDATIONS

Because of the narrow scope and exploratory nature of this test, relatively few specific recommendations can be made from test results alone; as a consequence, the suggestions tendered below are presented in a rather general fashion.

5.2.1 Lethality Study.

1. Further investigations, both theoretical and experimental, should be performed to determine the effects of various parameters on material loss from objects positioned in a nuclear fireball. Particular attention should be given the parameters of material type and composition, specimen configuration and orientation with respect to the burst point, and weapon yield and the distance from the burst point or, more correctly, the temperature-time-history of exposure. Various specimens should be designed to maximize or minimize possible mechanisms of material loss, so that the relative effectiveness of the various mechanisms can be determined.

2. An instrumentation development program should be included in future field testing in a nuclear-fireball specimen response and fireball phenomena.

5.2.2 Thermal-Shock Study.

1. Further exposure to high thermal fluxes of the material tested herein and of various other materials considered for use on intercontinental ballistic missiles should be made in order to determine the relative thermal vulnerability and damage threshold of each material type under conditions of rapid heating.

2. Where high thermal inputs are required, parabolic reflectors should be used to concentrate the thermal energy on the test specimens, if feasible in view of specimen size and such input requirements as spectral distribution of energy incident on the specimen.

3. In using parabolic reflectors, instrumentation should be provided to determine specimen response and the thermal energy realized at the focal spot. Photographic coverage of the fireball and its image at the focal spot should be provided to determine their size and location with respect to the optical axis and focal point of the mirror. Also, consideration should be given to designing mechanisms by which the mirror could be made to follow the fireball as it rises. Possible means of effecting this are by tracking the fireball or by elevating the mirror by means of a pre-set cam drive.

4. Pylons of delta-wing construction should not be used during nuclear test detonation unless justified by their low drag characteristics. If such usage is necessary, however, the pylons should be designed for relatively large side loads.

It should be noted that, at the time of this writing, many of the above recommendations have been acted upon and incorporated in a current program in Operation Redwing at the Pacific Proving Grounds and proposed for a future program in Operation Plumbbob which is scheduled for the spring of 1957 at the Nevada Proving Grounds.

Appendix A
DESCRIPTION OF DAMAGE TO LETHALITY-STUDY SPECIMENS

This appendix comprises a brief description of the damage and the surface condition of each of the lethality-study specimens and also serves as a repository for the large number of photographs showing the damage to individual specimens. Figures 3.4 and 3.8 in Chapter 3 present group photographs of the spheres and cylinders, respectively, and show the relative sizes of the specimens. The photographs of individual specimens are given in this appendix.

A.1 STEEL SPHERES

A.1.1 Tower 1 (Ref. Figure A.1). About 75 percent of the surface was very smooth. The remainder was splashed with once molten metal that had a sandy type of texture. No well defined streaming pattern was observed although there was a slight hint of one in the sandy appearance of the metal splashes. There was some out-of-roundness in this sphere as evidenced by the fact that the sphere would roll from certain positions when placed on a flat surface.

A.1.2 Tower 2 (Ref. Figure A.2). About two-thirds of the surface was quite smooth. The remaining area, which was centered near the mounting hole, was rough with a sandy type of texture in places. The periphery of the rough area had the appearance of radial streaming from the center of the area. There was a tendency to roll from various positions when placed on a flat surface indicating a slight out-of-roundness; however, this effect was much less noticed on the steel sphere from Tower 1.

A.1.3 Tower 3 (Ref. Figure A.3). Nearly two-thirds of the surface was very smooth. The remainder was covered with once molten metal in the form of smooth paint smears or runs about 1/32 in. thick. No streaming or obvious point of impact was observed.

A.1.4 Tower 4 (Ref. Figure A.4). The entire surface of this sphere was covered with patches of once molten steel in the form of paint smears approximately [illegible]/16 in. high. There was no streaming pattern observed. The mounting bolt was melted off about 1/4 inch below the surface.

A.1.5 Tower 5 (Ref. Figure A.5). Most of the sphere was smooth but there was a slight amount of thin metal splashes on the top. In addition, a considerable portion of the top half of the sphere was covered with a dark scale similar to that found on hot rolled steel.

SECRET

There was a radial streaming pattern which was clean and semi-shiny in appearance centered about the mounting hole. Some of the surface was rather bluish in color and was finely checked, probably due to surface contraction during cooling. The mounting bolt was melted off about 1/8 inch below the surface.

A.1.6 Base of Tower 1. This sphere was essentially undamaged. The surface was somewhat discolored but the machine marks were still visible.

A.2 ALUMINUM SPHERES

A.2.1 Tower 1 (Ref. Figure A.6). There was a large gash centered about 45° above the horizontal plane through the center of the sphere. The approximate dimensions were 1 1/4 in. deep, 1 1/4 in. wide, and 3 1/2 in. long. All of the corners were rounded and there was evidence of metal loss on the inside of this gash. It is thus believed that this deformation occurred prior to impact. There was a narrow crack which started at the top of the sphere and extended directly through the gash and mounting hole and ended about 3 1/2 inch on the other side of the mounting hole. No rounding of the corners of the crack was observed indicating that this probably occurred during or after impact with the ground. There was a large shiny streaming area centered on the surface in about the horizontal plane through the center of the sphere and approximately 90° from the large gash. This streaming pattern extended over nearly one half of the sphere. The remainder of the surface was dark in appearance and rough and sandy in texture. The shiny area on the surface was finely checked, probably due to surface contraction during cooling.

A.2.2 Tower 2 (Ref. Figure A.7). Most of the surface was lumpy or irregular in appearance. No shiny streaming pattern or obvious point of impact was observed. There was quite a bit of molten metal flow on the surface in the form of paint runs, in some places as much as 3/32 in. thick. The top portion of the sphere was dark in appearance and sandy in texture. This may have been the point of impact with the ground; however, no streaming pattern was observed.

A.2.3 Tower 3 (Ref. Figure A.8). The entire surface was rough and irregular in appearance. Some irregularities were nearly 1/8 in. deep. Molten metal flow in the form of paint runs was noticed over most of the surface. There was a shiny streaming area centered at a point about 20° above the horizontal plane through the center of the sphere.

A.2.4 Tower 4 (Ref. Figure A.9). Most of the surface was extremely rough and irregular. About one half of the sphere was quite dark in appearance. There was evidence of molten metal flow over most of the surface. There was a streaming pattern centered about 45° above the horizontal plane through the center of the sphere. This pattern was rather dull in appearance instead of shiny as on most of the other

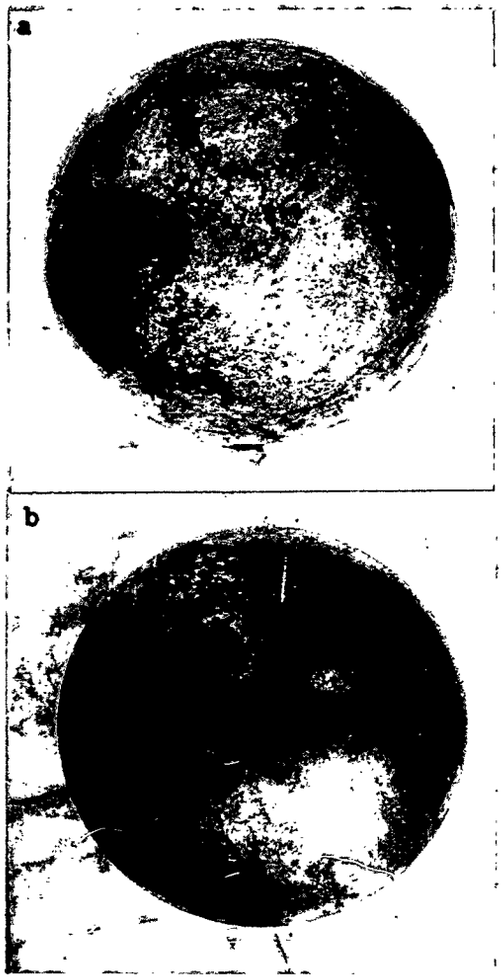

Figure A.1 Steel Sphere, Tower 1. (a) Bottom View; (b) Top View.

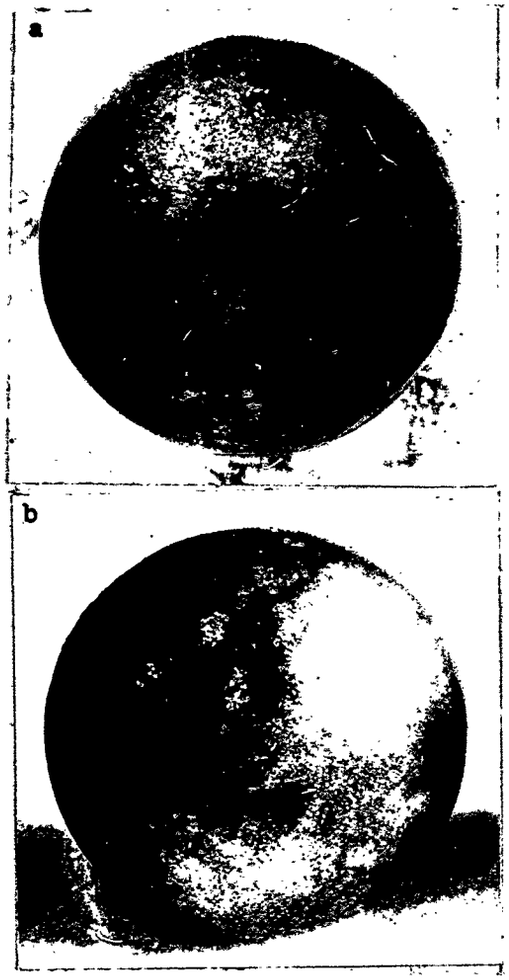

Figure A.2 Steel Sphere, Tower 2. (a) Bottom View; (b) Top View.

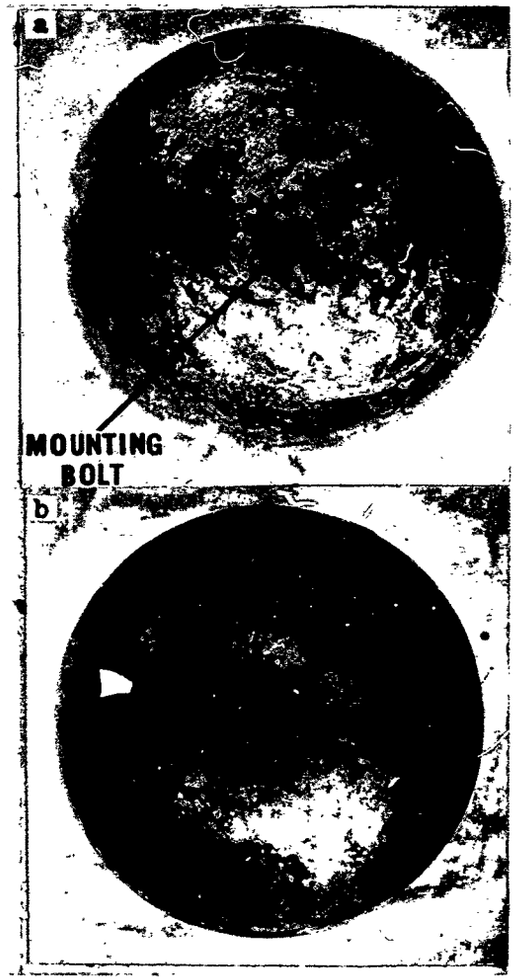

Figure A.3 Steel Sphere, Tower 3. (a) Bottom View; (b) Top View.

Figure A.4 Steel Sphere, Tower 4. Mounting hole is at bottom of pictures.

Figure A.5 Steel Sphere, Tower 5. (a) Bottom View; (b) Top View.

Figure A.6 Aluminum Sphere, Tower 1. (a) Showing Cut and Crack; (b) Showing Center of Shiny Streaming.

specimens. There was a peculiar "canyoning" effect which can be seen in Figure A.9 (a). The general surface in this area was nearly black, and it appeared that the surface had separated leaving a clean aluminum "canyon" about 3/32 in. deep.

A.2.5 Tower 5 (Ref. Figure A.10). The top half of the sphere was slightly rough, had a sandy texture, and was speckled with a dark material mixed in with the once molten aluminum. There was a shiny streaming pattern centered about 3 inches from the mounting hole and extended over nearly the entire bottom half of the sphere. There was a slight ridge of aluminum about 1/16 in. high and about 10-in. long which ran along the periphery of the shiny streaming area. This ridge is located in the upper right quarter of the photograph in Figure A.10 (b).

A.3 CERAMIC INSERT SPHERES

A.3.1 Tower 1 (Ref. Figure A.11). This sphere was broken into two pieces such that the plane of the fracture was roughly vertical and was perpendicular to a plane containing the Shot Tower and the specimen. There was evidence of metal loss on the fractured surface, especially near the periphery of the sphere as evidenced by the poor fit between the two pieces. This indicates that the fracture probably took place before impact with the ground. There was a shiny streaming pattern centered on the front half of the specimen near the front Battelle ceramic. This pattern appeared to extend onto the other half of the sphere. If these patterns were caused by impact with the ground, it could be surmised that either (a) the sphere was intact at time of impact with the ground, or (b) by chance the two portions happened to impact the ground in relatively the same positions. In addition to the main fracture, there was a crack in the front half of the sphere which started near the right rear graphite insert and extended to a point in front of the mounting hole where it split into a "Y" as can be seen in Figure A.11(b). The surface over this crack was routed out so that in places it was about 7/16 in. deep. In addition, there was another crack about 2-in. long starting from the same insert but located on the rear half of the sphere. On the inside of the front half of the sphere, cutting diagonally through the inside portion of the right front Battelle ceramic, was a shiny clean aluminum area as seen in Figure A.11(d). This area had the appearance of being cut, chiseled, or scraped; however, it had no mating part on the other half of the sphere. There was a large section of metal missing from the area around the left front graphite insert as shown in Figure A.11(c). Considerable metal was lost from each half of the sphere in this area. The general surface on the front half of the sphere on which the shiny streaming pattern was located was quite smooth and clean. The rear half, seen as the top half in Figure 3.33(b), was dark and rough in appearance.

CERAMICS: (See Figures A.16, A.17 and A.18)

Front Armour:

The ceramic was approximately flush with the retainer ring and the sphere in its immediate vicinity; however, the sphere was flattened out

in an area of about two inches in diameter around the insert. The top of the ceramic was thus actually about 1/8 inch below the nominal surface of the sphere. The shiny streaming pattern which was probably caused by ground impact passed across this insert. It is believed that this impact with the ground broke off any protruding ceramic.

Rear Armour:

The entire ceramic was covered with thick dark green glaze which had the appearance of slag or molten sand. This general area was flattened out over about a 2-in.-diameter area around the insert. The top of the glaze was about flush to 1/8 inch below the aluminum in the immediate vicinity, but about 1/4 inch below the nominal surface of the containing sphere.

Front Battelle:

The ceramic had a surface glaze which was brownish in color in some places and a greenish color in others. The surface was extremely irregular; the maximum protrusion was about 3/16 inch and maximum depth below the surface was about 3/16 inch. The surface averaged out to be approximately flush. Impact with the ground was probably very close to this ceramic as evidenced by the stream marks across the surface in this area.

Rear Bettelle:

The ceramic had a nearly complete surface glaze which was a gray-green color in most places and nearly black in others. The retainer ring was about 3/16 inch below the surface of the sphere. The top of the ceramic varied from about flush with the retainer to a maximum depth of about 7/16 inch below the nominal surface of the containing sphere.

Front Graphite:

Broken out of retainer ring entirely.

Rear Graphite:

The graphite insert was broken out about two inches below the surface. The insert retainer ring was partly torn away, also, to this depth.

A.3.2 Tower 2 (Ref. Figure A.12). The entire surface of this sphere was rough, containing much once molten aluminum. The area on the top front half of the sphere, centered about the point which is equidistant from the three front inserts (front radial point), contained an extreme amount of once molten aluminum which was quite rough and granular and in some places extended to heights of about 1/2 inch above

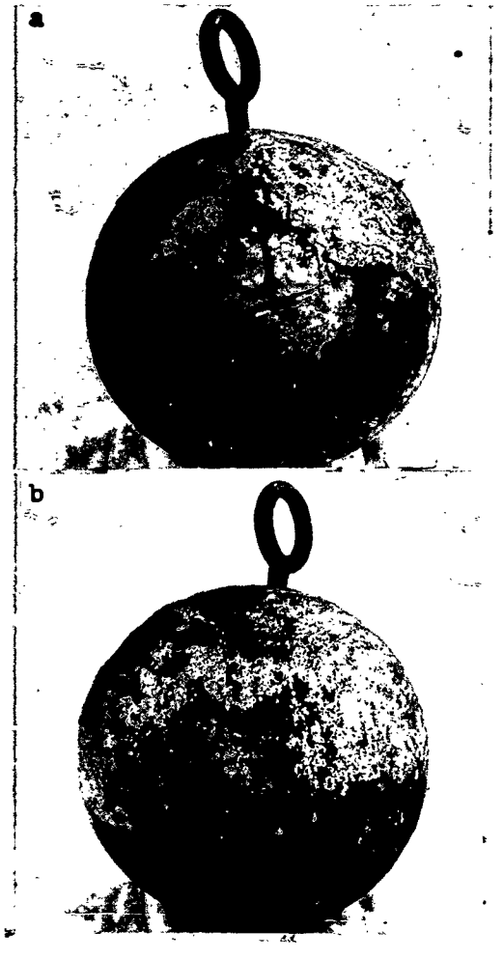

Figure A.7 Aluminum Sphere, Tower 2. (a) Showing Extreme Molten Metal Runs; (b) Side Opposite Metal Runs.

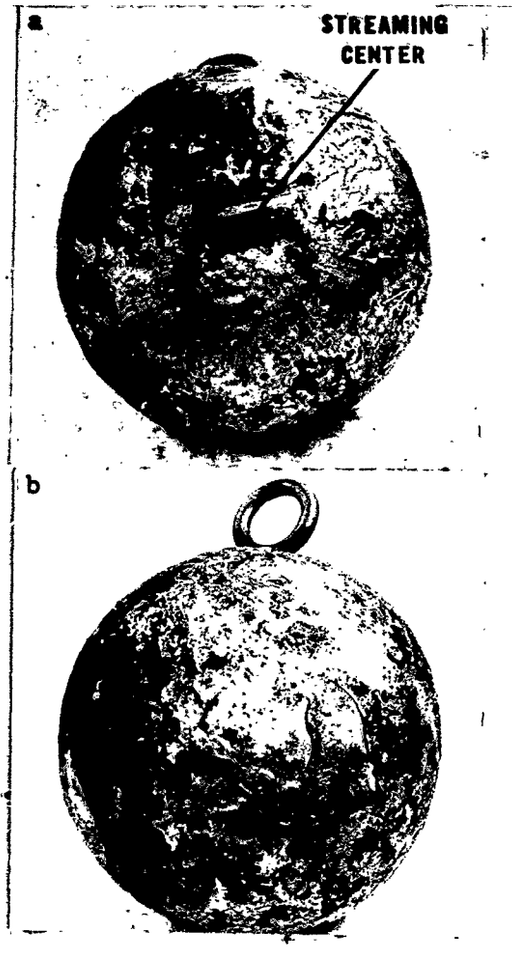

Figure A.8 Aluminum Sphere, Tower 3. (a) Center of Shiny Streaming Pattern; (b) Side Opposite Streaming Pattern.

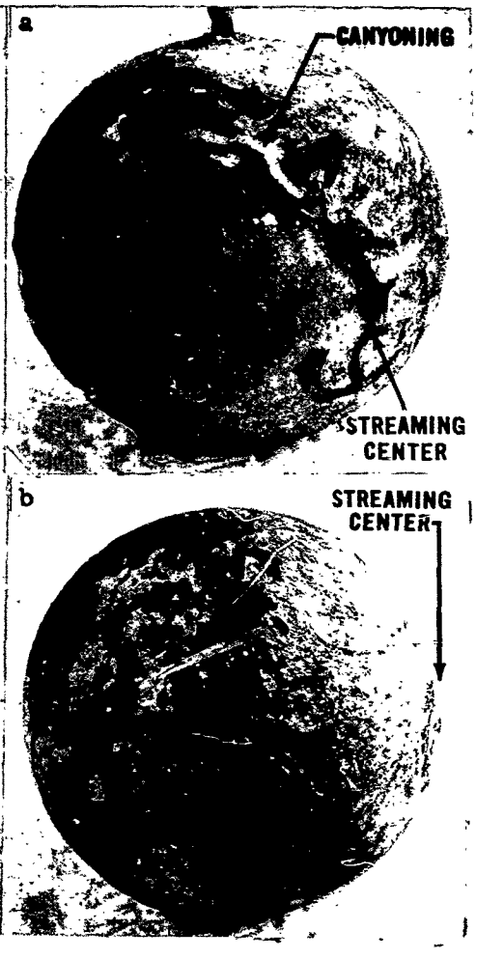

Figure A.9 Aluminum Sphere, Tower 4. (a) Canyoning Effect; (b) Top of Sphere.

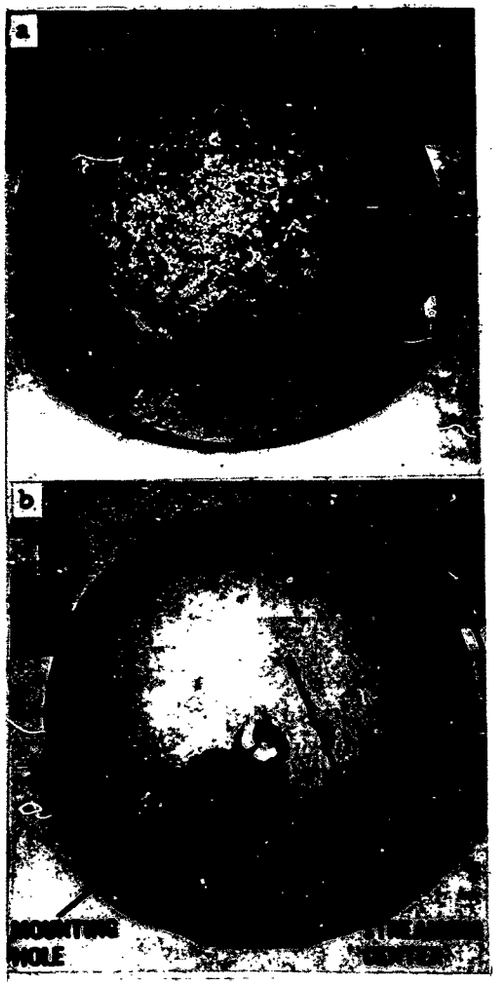

Figure A.10 Aluminum Sphere, Tower 5. (a) Top View; (b) Bottom View.

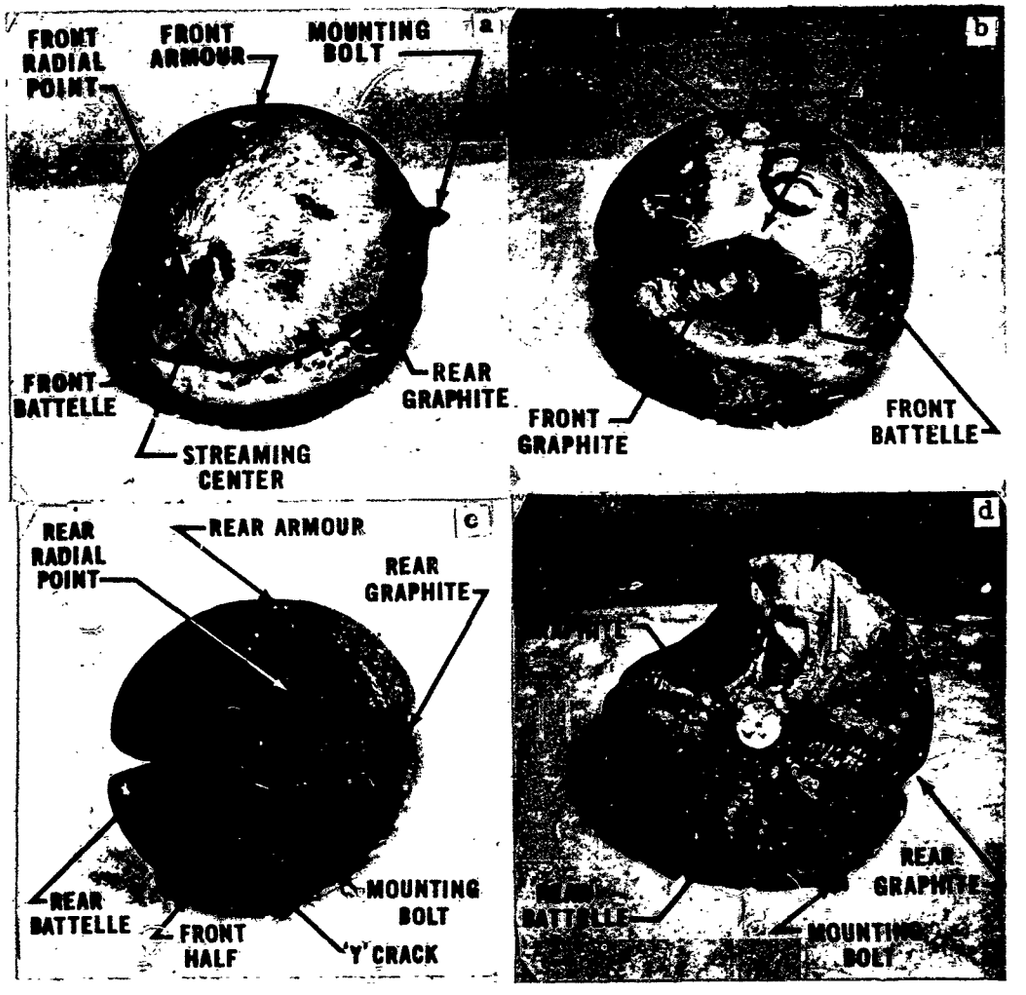

Figure A.11 Ceramic-Insert Sphere, Tower 1. (a) Center of Streaming; (b) Bottom View; (c) Front Radial View; (d) Inside of Front Half.

the surface. There was a shiny streaming pattern centered at about the right rear Battelle ceramic; however, most of this area was covered with a dark scale.

CERAMICS: (See Figures A.16, A.17 and A.18)

Front Armour:

The entire surface was covered with once molten aluminum quite granular in texture. A glaze could be seen in places under the molten aluminum. This glaze appeared to be about 1/32 in. thick. The top of the glaze was estimated to be about 1/4 inch below the nominal surface of the containing sphere.

Rear Armour:

There was a surface glaze about 1/64 to 1/32 in. thick remaining over part of the ceramic. The glaze was approximately flush with the containing sphere. The remaining surface appeared to be parent material and was slightly below the surface of the sphere. There was a slight streaming pattern noticed across this insert, probably caused by impact with the ground. This impact may have broken off any protruding portion of the ceramic.

Front Battelle:

The ceramic was completely covered with once molten aluminum and protruded about 1/8 inch above the nominal surface of the containing sphere. The insert retainer and aluminum immediately surrounding it were routed out to a depth of about 5/8 inch (see Figures 3.18(a) and 3.19). Thus, the top of the ceramic was about 3/4 inch above the aluminum in the immediate vicinity. An approximate measurement at the top of the ceramic insert indicates that its reduction in diameter was less than 1/8 inch.

Rear Battelle:

The ceramic protruded about 1/16 inch above the sphere in some places. There was no surface glaze observed. The ceramic appeared to have flowed onto the insert retainer ring and the main surface of the sphere in places as seen in the lower right corner of the photograph shown in Figure A.17(d).

Front Graphite:

The graphite was entirely covered with once molten aluminum. The insert was about flush with the sphere on one side of the retainer ring and about 1/8 inch below the surface on the opposite side. In some places the molten aluminum was nearly 1/8 inch above the surface of the graphite.

Rear Graphite:

The top of the insert was broken off nearly 7/16 inch below the surface of the containing sphere. This fracture probably occurred on

impact with the ground as evidenced by the streaming pattern over the sphere in this area. There was a light film of aluminum over most of the surface of the graphite.

A.3.3 Tower 3 (Ref. Figure A.13). The general surface of this sphere was rough and irregular to a depth of about 3/32 inch. The right rear quarter (between the rear Armour and rear graphite inserts) was quite dark and sandy in appearance. In many places it appeared that there was clean aluminum over a rather dark material. There was a shiny streaming pattern centered roughly between the three front ceramic inserts (front radial point) which would place it about on the front radial line (line to burst point). There was a crack which went completely around the sphere and was located approximately in a vertical plane which would be about perpendicular to a plane passing through the shot tower and the specimen. The width of the crack varied from 1/16 inch at the top to about 3/16 inch at the bottom of the sphere. This fracture probably occurred at or after impact with the ground, since the corners showed little or no evidence of metal loss.

CERAMICS: (See Figures A.16, A.17 and A.18)

Front Armour:

The surface of the ceramic was mostly below the nominal surface of the containing sphere. The retaining ring was also below the surface of the sphere and was about flush with the surface of the ceramic. One edge of the ceramic was about flush and the other side was about 1/4 inch below the nominal surface of the containing sphere. The streaming pattern, which probably resulted from impact with the ground, went directly over this insert and may account for the chipping off of the ceramic.

Rear Armour:

The surface of this ceramic was about 3/32 inch above the sphere and there was a glaze near the edge of the ceramic which was about 1/8 inch above the surface of the sphere. Most of the surface appeared to have cracked off leaving the parent material exposed.

Front Battelle:

The surface had essentially no glaze and appeared to have been scraped off during impact with the ground as evidenced by the streaming pattern across the sphere in this area. Most of the ceramic was about flush with the sphere; however, in some places it may have protruded about 1/32 inch.

Rear Battelle:

The center of the surface of the ceramic was about 1/8 inch above the surface of the sphere and had little, if any, glaze. The ceramic tapered down to the aluminum where it was nearly flush.

Front Graphite:

This insert was somewhat irregular and appeared to have been broken off. There was a streaming pattern across the insert which probably

indicates impact with the ground occurred close to this point. The surface of the graphite was very clean and protruded in places as much as 3/32 inch above the containing sphere.

Rear Graphite:

The maximum protrusion of this insert was about 7/16 inch. There was little rounding of the corners or metal loss on the side of the insert. The edges were not broken off and appeared to have a radius of about 1/8 inch. There was a slight layer of aluminum over a portion of the surface of the insert (see Figure 3.18).

A.3.4 Tower 4 (Ref. Figure A.14). There was a considerable amount of molten metal flow appearing in the form of "paint runs" and the direction of the "runs" appeared to be from the front radial point. About two-thirds of the surface was rough and irregular to depths of about 1/16 inch. The remainder of the surface located on the lower portion of the sphere (centered about on the rear radial) was quite clean with a slight sandy texture. In this general area a slight streaming effect was noticed. There was also a shiny streaming pattern about half-way between the rear Armour ceramic and the rear graphite inserts. This shiny surface was finely checked, probably because of cooling effects. The nut was still on the mount bolt flush with the surface and protected the aluminum under it. A measurement of the amount of protected metal indicated that about 5/64 inch of aluminum was lost from the bottom of the sphere.

CERAMICS: (See Figures A.16, A.17 and A.18)

Front Armour:

There was evidence near the periphery that there was once a glaze on the ceramic; however, most of this glaze was absent leaving parent material exposed. The maximum depth of material below the surface of the containing sphere was 5/32 inch.

Rear Armour:

Nearly all of the glaze was chipped off leaving parent material exposed. There appeared to have been some aluminum splatter over the surface glaze which remained. The ceramic was about 1/32 inch above the surface of the sphere in one place; however, most of the surface was well below the surface of the containing sphere.

Front Battelle:

Most of the ceramic was covered with a glaze which appeared to be 1/64 in. thick or less. In some places, the top of the glaze protruded about 1/8 inch above the surface of the sphere. The surface glaze was absent in some places, but all of the ceramic was above the nominal surface of the containing sphere.

Rear Battelle:

Nearly one-half of the surface was covered with a glaze of once molten aluminum. The protrusion of most of the ceramic was about 5/64

inch above the sphere. The portions of the ceramic where there was no glaze tapered down toward the edge of the insert where the ceramic was about flush with the retainer ring and containing sphere.

Front Graphite:

This insert was quite flat on top and protruded about 11/64 inch above the nominal surface of the containing sphere. The corners were slightly rounded but for the most part the insert looked undamaged. There was a very slight film of aluminum over the surface of the graphite.

Rear Graphite:

The insert protruded about 7/64 inch above the sphere and appeared to have incurred little damage. There were a few traces of once molten aluminum on the surface, and the corners had only a very small radius. Most of the corners appeared to have been chipped off rather than burned off.

A.3.5 Tower 5 (Ref. Figure A.15). Nearly one-half of the surface area was streaked with once molten aluminum in the form of "paint runs." This general area is centered about the top left graphite insert. A streaming pattern, slightly dull in appearance, was centered about the right rear graphite insert. There was a ridge of aluminum about 6-in. long running in a direction about perpendicular to the radial stream lines which can be seen in Figure A.15(b).

CERAMICS: (See Figures A.16, A.17 and A.18)

Front Armour:

The surface of the ceramic was unglazed and was below the nominal surface of the containing sphere. The maximum depth below the surface was about 7/64 inch. The surface was clean parent ceramic.

Rear Armour:

There was a dark material, unlike glaze, over part of the surface and may once have been over the entire surface. The maximum height of the ceramic above the surface of the sphere was about 1/32 inch. Most of the surface was about flush to 1/32 inch below the surface of the containing sphere.

Front Battelle:

There was a rather dark surface glaze about 1/32 in. thick which covered most of the ceramic. The area where the glaze was gone was apparently undamaged parent material. The top of the remaining glaze protruded approximately 1/32 inch above the sphere.

Rear Battelle:

There was a nearly complete light colored surface glaze which was

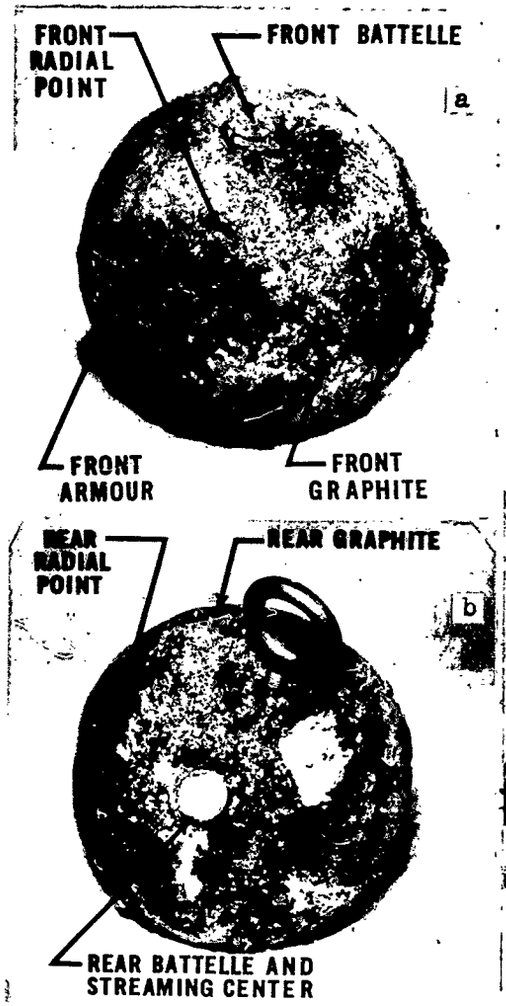

Figure A.12 Ceramic-Insert Sphere, Tower 2. (a) Front Radial View; (b) Center of Shiny Streaming.

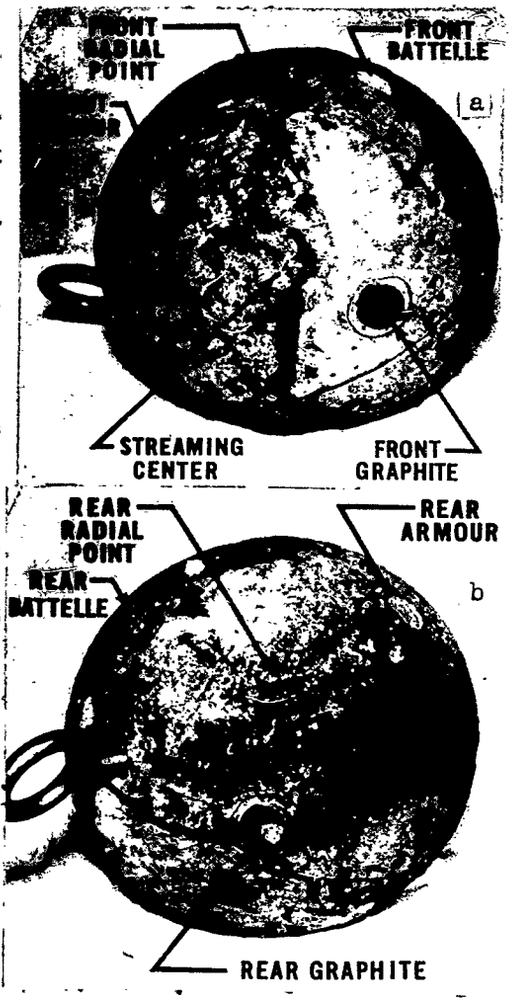

Figure A.13 Ceramic-Insert Sphere, Tower 3. (a) Front Radial View; (b) Rear Radial View.

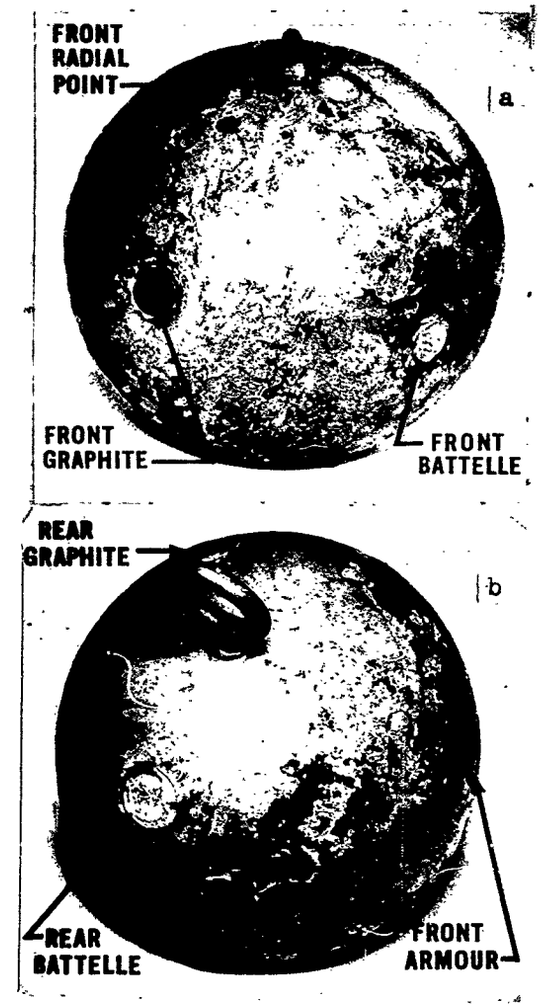

Figure A.14 Ceramic-Insert Sphere, Tower 4. (a) Front Radial View; (b) Bottom View.

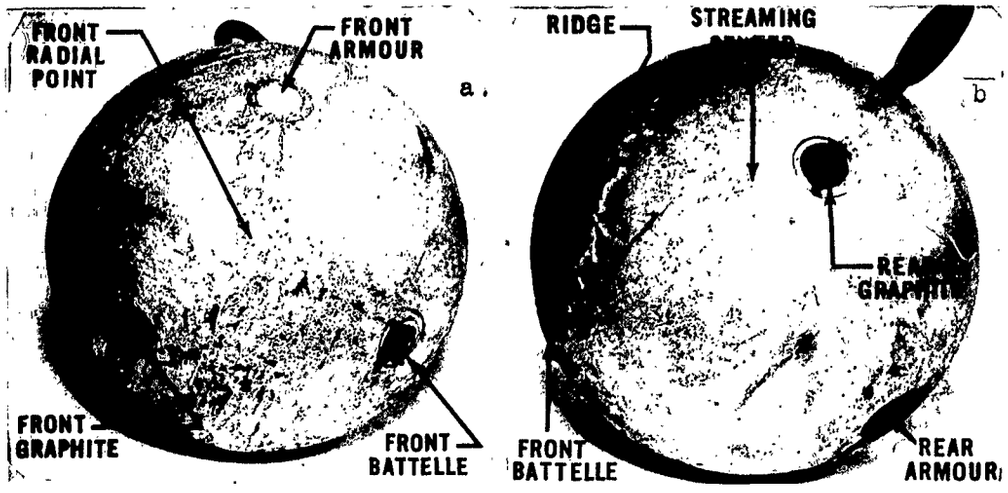

Figure A.15 Ceramic-Insert Sphere, Tower 5. (a) Front Radial View; (b) Center of Shiny Streaming.

about 1/32 in. thick. The top of the glaze was approximately flush with the surface of the sphere.

Front Graphite:

The surface of the graphite was very clean and the corners were relatively sharp. The top of the insert was flat and protruded approximately 3/64 inch above the surface of the sphere. There was a slight film of aluminum over a portion of the surface of the graphite.

Rear Graphite:

The surface of the insert was quite flat, and the corners were rounded very little. The insert protruded nearly 1/16 inch above the surface of the sphere and was covered with a very slight film of aluminum.

A.4 STEEL CYLINDERS

A.4.1 Tower 1, Left Side, 1-in. Hole (Ref. Figure A.19). There were approximately five large pock marks on the surface of the cylinder, some measuring about 7/16 in. deep and 1 1/2 in. in diameter. There were many more pock marks in this area which were not quite as large. This was the most severely pock marked of all the cylinders. There was a peculiar ridge of metal about 1/8 in. high extending from the center to one end of the cylinder near the periphery of the pock-marked area. This looked like an overlap of plastic flow of the metal and can be seen in Figures 3.13(a) and A.19(d). The remainder of the surface was slightly irregular to depths of about 1/32 inch. There was a streaming pattern (running from one end to the other) observed on the side opposite

(a) Tower 1, Front

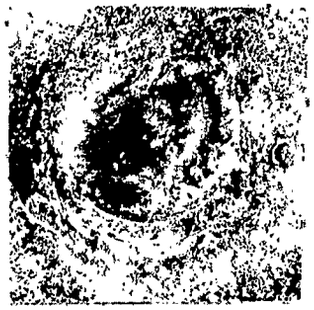

(b) Tower 1, Rear
(Note complete glaze.)

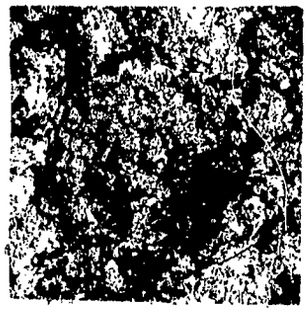

(c) Tower 2, Front
(Covered with Al.)

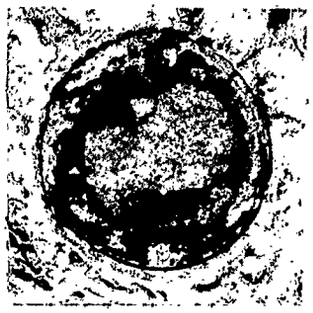

(d) Tower 2, Rear

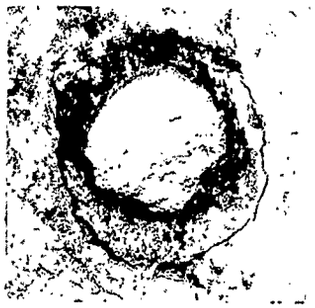

(e) Tower 3, Front

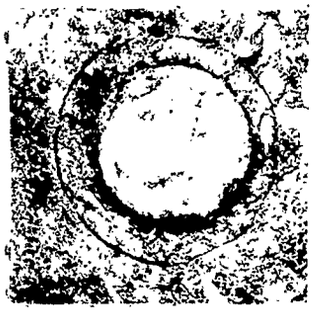

(f) Tower 3, Rear

(g) Tower 4, Front

(h) Tower 4, Rear

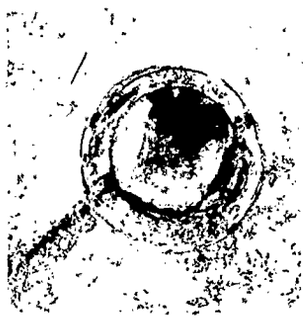

(i) Tower 5, Rear

Figure A.16 Armour Ceramic Inserts After Exposure

(a) Tower 1, Front

(b) Tower 1, Rear

(c) Tower 2, Front (Covered with Al. See Figure 3.18.)

(d) Tower 2, Rear

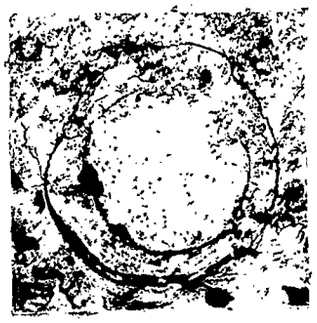

(e) Tower 3, Front

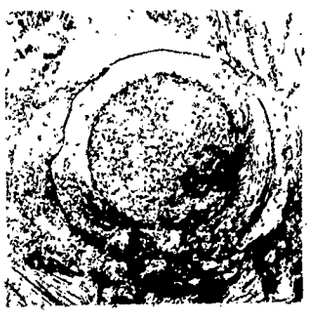

(f) Tower 3, Rear

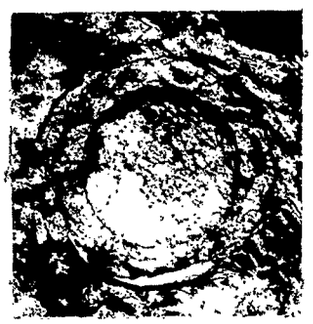

(g) Tower 4, Front

(h) Tower 4, Rear

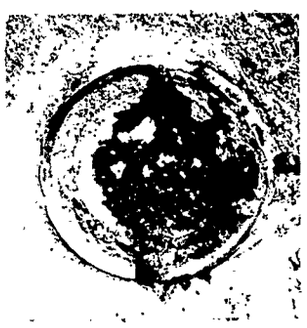

(i) Tower 5, Front

Figure A.17 Battelle Ceramic Inserts After Exposure

(a) Tower 1, Front (Completely Gone)

(b) Tower 1, Rear (Partially Broken Out)

(c) Tower 2, Front (Covered with Al.)

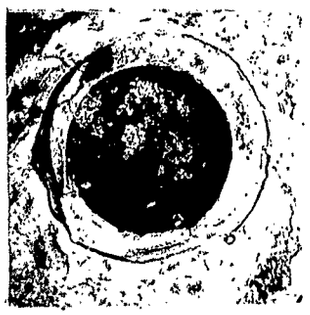

(d) Tower 2, Rear

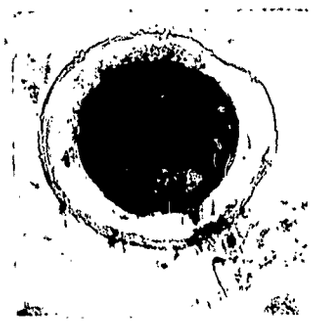

(e) Tower 3, Front

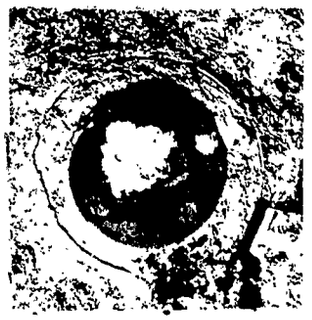

(f) Tower 3, Rear (See Figure 3.18)

(g) Tower 4, Front

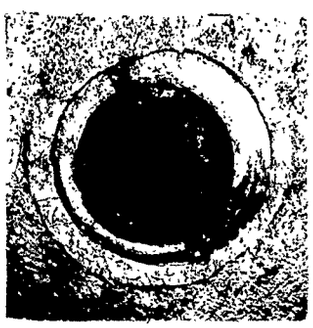

(h) Tower 4, Rear

(i) Tower 5, Front

Figure A.18 Graphite Inserts After Exposure

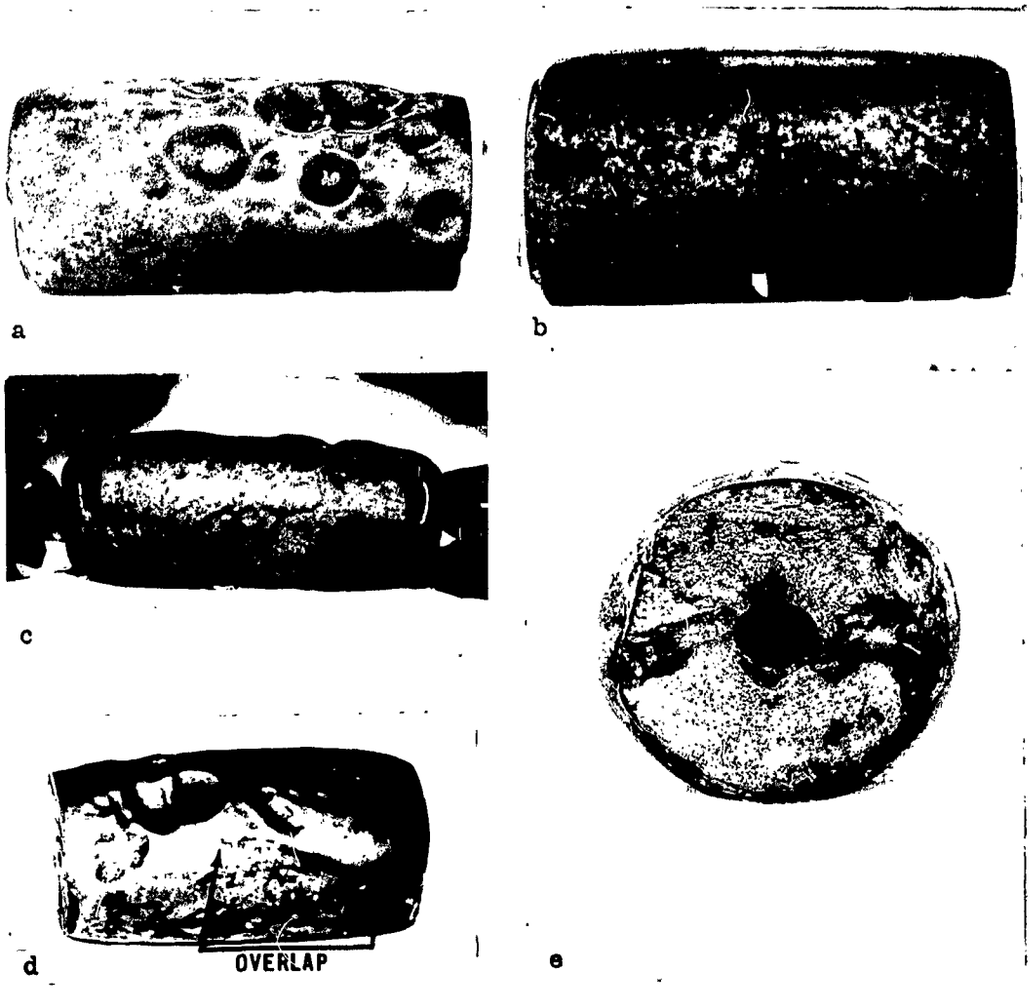

Figure A.19 Cylinder from Tower 1, Left Side, 1-in.-diameter Hole. (a) Pock-Marked Side; (b) Side Opposite Pock Marks; (c) Profile, Pock Marks Up; (d) Overlap of Metal; (e) End View, Pock Marks Up. See Figure 3.12 for Other End.

the pock marks. This streaming pattern, it is believed, was caused by impact with the ground. Both end caps were still attached to the cylinder even though the threads were burned off completely. The caps were held on by a layer of once molten steel which streamed under the cap and welded them in place. Both caps were removed by striking them sharply with a hammer. The molten metal which streamed under the cap came from the erosion of the joint between the cylinder and the cap, as can be seen in Figures 3.12 and A.19(c) and (e). The cylinder was squashed and became elliptical in cross-section as seen in Figures

3.12 and A.19. More surface metal was lost near the ends of the cylinder than at the center, thus giving the cylinder a barrel-shaped appearance.

A.4.2 Tower 1, Right Side, 1-in. Hole (Ref. Figure 3.20). There were about seven large pock marks on the surface of the cylinder, ranging in depth up to about 15/64 inch. Most of these pock marks were about 1/2 inch in diameter or less. The remainder of the surface was irregular to depths of about 1/32 inch. The surface was dark and had an appearance somewhat like hot rolled steel. Very little molten metal flow was observed. When recovered, the cylinder had only one end cap. Judging from the essentially undamaged condition of the end face, the cap probably came off during penetration in the ground or possibly even during recovery from its impact hole; however, if this happened during recovery, it was not noticed. The end face was not apparently discolored, and the machine marks were still visible. The other end cap could not be removed even by vigorous striking with a hammer. There was a very pronounced streaming pattern observed on the side opposite the pock marked area, probably caused by impact with the ground. This pattern appeared to start at the end with no end cap and fan out lightly to the other end of the cylinder. The cylinder was squashed such that it had an approximately elliptical cross-section as can be seen in Figure A.20(d). The cylinder was barrel-shaped as discussed in Section 3.2.2. There was some erosion of the seam between the end of the cylinder and the end cap to depths of about 1/4 inch below the nominal circumference of the cylinder. The numbered slug used for identification of the specimens can be seen in Figure A.20(c). The two small holes also seen in this picture and in other photographs were the holes from which pre-shot samples of the specimens were taken for chemical analysis. This was an alternate method of identification provided.

A.4.3 Tower 2, Left Side, 1-in. Hole (Ref. Figure A.21(a), (b), and (c). There were approximately eight pock marks in a relatively small area. The maximum depth below the surface was about 7/32 inch and most of the pocks were about 1/2 inch in diameter. Nearly all of the surface was wavy and irregular to depths of about 1/32 inch and was dark in color somewhat like hot rolled steel. There was some evidence of molten metal flow and splashes over the surface of the cylinder and especially over the ends as seen in Figure A.21(c). There was a slight streaming pattern observed on the side opposite the pock marks which, if attributable to impact with ground, would indicate the cylinder hit the ground approximately broad side. The inside of the hole was essentially undamaged with the machine marks still quite visible. The hole did not appear to be squashed but measurements given in Section 3.1.2 indicate that there was a slight amount of squashing sustained. The amount of barreling of the cylinder is shown pictorially in Figure A.21 (a) and is discussed in Section 3.1.2. Both caps were detached from the cylinder. The threaded shoulder was completely burned off leaving the corners rounded.

A.4.4 Tower 2, Right Side, 2-in. Hole (Ref. Figure A.21(d), (e), and (f). There were four large pock marks about 3/32 in. deep by 1/2 in.

in diameter. The surface in the vicinity of the pock marked area was rough and irregular to depths of 1/32 inch and was dark having an appearance somewhat like hot rolled steel. There was a streaming pattern over the area near the pock marks extending nearly the entire length of the cylinder. The remainder of the surface was rather spotty. In some places the surface was relatively clean steel and in other places it had a dark appearance similar to the pock marked area. Both of the end caps were detached from the cylinder. There was some evidence of molten metal flow, especially over the corners of the cylinder on to the first 3/16 inch of the end face as seen in Figure A.21(f). The machine marks on this end were still quite visible though discolored. The other end face was very clean with no molten metal flow. There was still a slight shoulder of the thread left in some places on this end. The face was very clean with only slight discoloration, and the machine marks were still visible. The barreling effect was quite pronounced as shown pictorially in Figure A.21(d). Data on the magnitude of barreling and squashing are given in Section 3.1.2.

A.4.5 Tower 3, Left Side, 2-in Hole (Ref. Figure A.22). There were two large indentations on the surface, one near the center of the cylinder and the other near one end. These indentations measured about 9/64 in. deep, 1 1/2 in. wide, and 2 1/4 in. long and 9/64 in. deep, 5/8 in. wide and 2 1/4 in. long, respectively. The general area in the vicinity of these pock marks was semi-shiny in appearance. Also, there was evidence of molten metal flow in this area. The apparent direction of metal flow on the surface was radially outward from the center of the large pock mark in the center of the cylinder and was probably caused by impact with the ground. The remainder of the surface was dark in appearance with some molten metal flow over it. There were two instances of erosion of the seam between the cap and the cylinder to depths of about 3/16 inch. One cap was easily removed; however, the other cap could not be removed because of the erosion mentioned above. There was no measurable squashing of the cylinder, and it became only slightly barreled in appearance.

A.4.6 Tower 3, Right Side, 3-in. Hole (Ref. Figure A.23). The 3/16 in. diameter hemispherical holes were practically indistinguishable from other surface irregularities. The 3/8 in. diameter holes were still plainly visible. There did not appear to be any appreciable erosion or streaming due to the flow of fireball gases across the holes. Some close-up photographs and various data relative to these hemispherical holes are presented in Section 3.1.2. There were two pock marks or indentations on the surface, one about 3/32 in. deep, 7/8 in. wide, and 1 3/4 in. long near the 3/16 in. diameter hole with 45° flow and the other about 3/64 in. deep, 1/2 in. wide, 1 3/8 in. long near the 3/16 in. diameter hole with tangetial flow. The general surface in the area facing the burst point (centered near the 3/16 in. and 3/8 in. holes which are closest together, see Figure 2.4) was dark and somewhat irregular in appearance. The remainder of the surface was fairly smooth and semi-shiny in appearance. Both end caps were still attached to the cylinder. The seam between the cylinder and cap was eroded in two places on each end of the cylinder. One cap could be forced off, but no

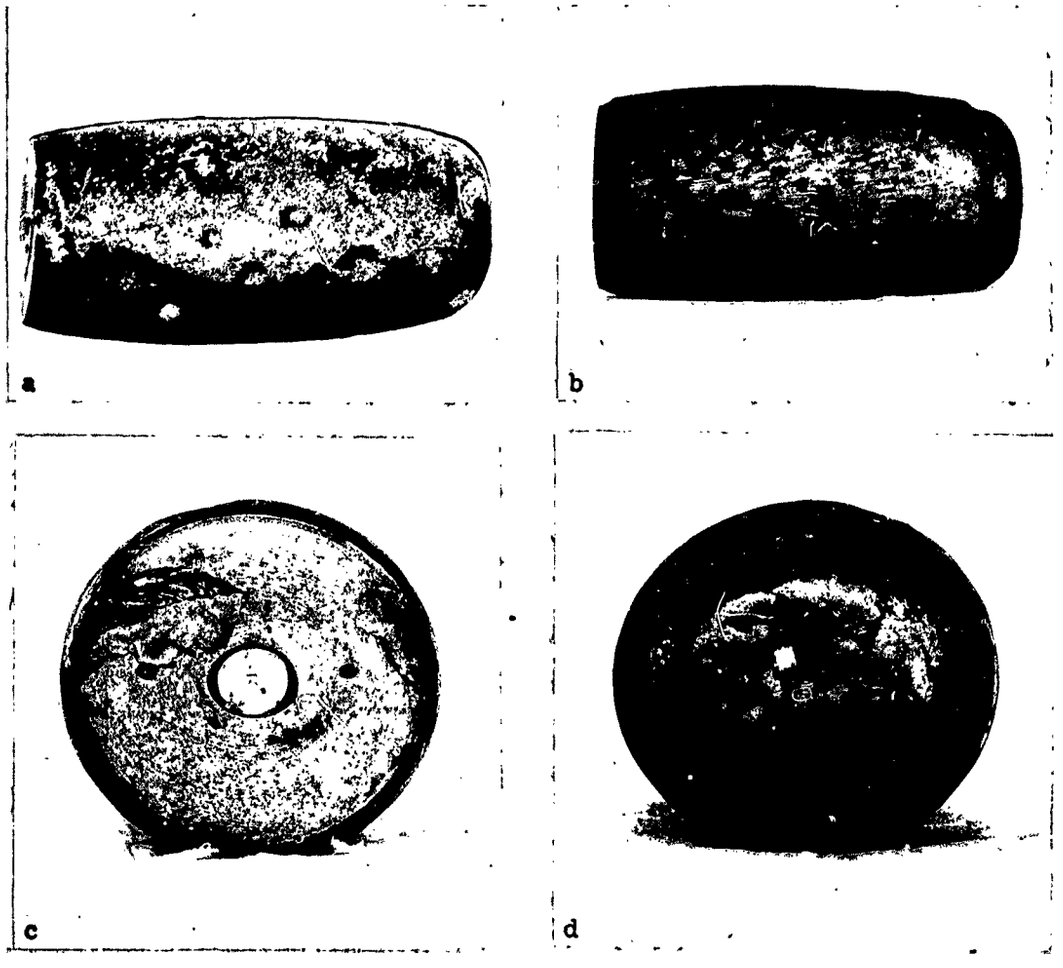

Figure A.20 Cylinder From Tower 1, Right Side, 1-in.-diameter Hole. (a) Pock-Marked Side; (b) Side Opposite Pock Marks (Note streaming pattern); (c) End Without Cap (Note numbered slug and two analysis holes); (d) End With Cap.

attempt was made to remove the other end cap because of the severity of the erosion at this seam. The inside of the cylinder was very clean and apparently sustained no damage. There was no squashing and only a slight amount of barreling.

A.4.7 Tower 4, Left Side, 3-in. Hole (Ref. Figure A.24). Both of the 3/8 in. diameter and 3/16 in. diameter hemispherical holes were plainly visible and there was little, if any, erosion or streaming caused by the shock flow over the cylinder. There was only a small amount of disconfiguration of these holes. Close-up photographs and general data on the damage to hemispherical holes is given in Section 3.1.2. The surface area between the centerline of the two hemispherical holes receiving tangential flow and the centerline of the two holes having 45°

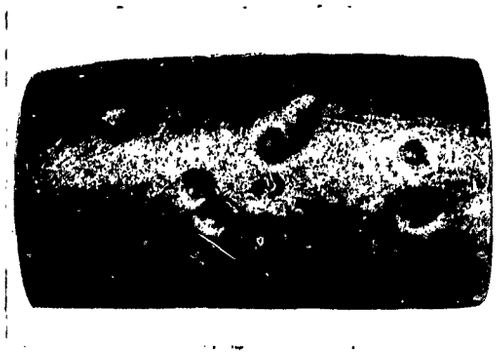

(a) Pock-Marked Side, Left Cylinder

(b) Pock-Marked Side, Right Cylinder

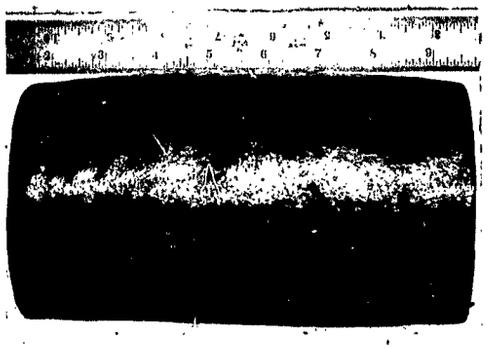

(c) Side Opposite Pock Marks, Left Cylinder

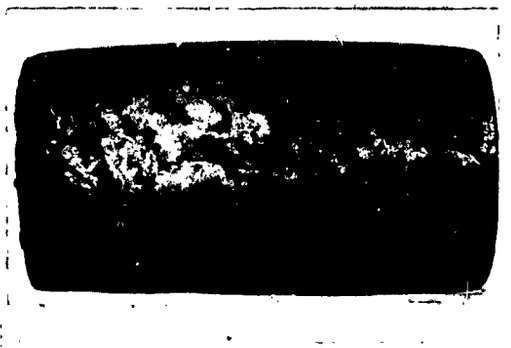

(d) Side Opposite Pock Marks, Right Cylinder

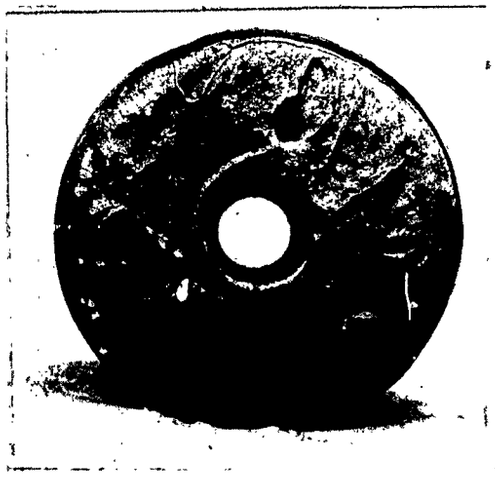

(e) End View, Left Cylinder

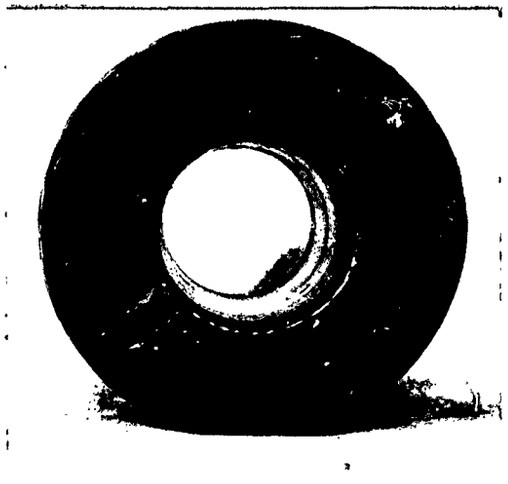

(f) End View, Right Cylinder

Figure A.21 Cylinders From Left Side (1-in. Hole) and Right Side (2-in. Hole) of Tower 2

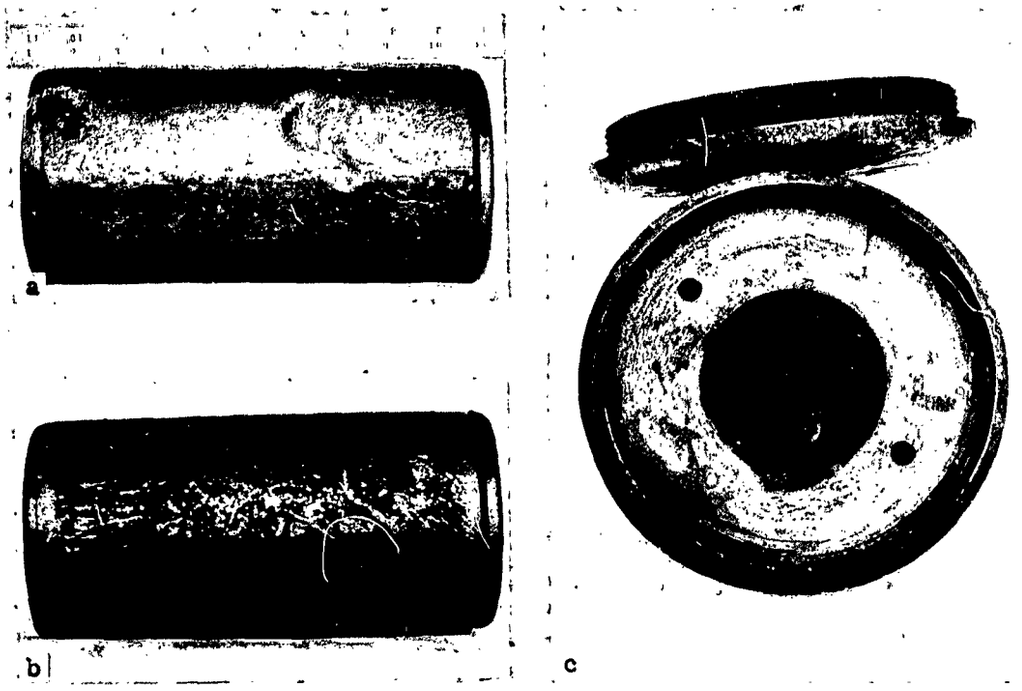

Figure A.22 Cylinder From Tower 3, Left Side, 2-in. Hole. (a) Pock Marked Side; (b) Side Opposite Pock Marks; (c) End View.

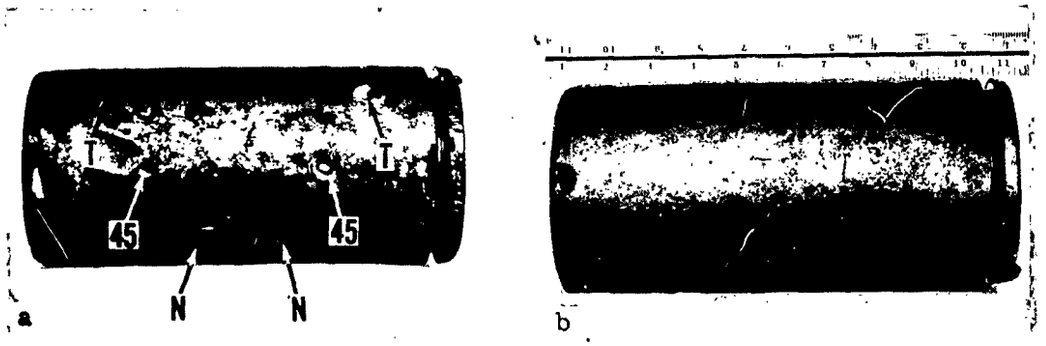

Figure A.23 Cylinder From Tower 3, Right Side, 3-in. Hole (Refer to Figure 3.17). (a) Front of Cylinder (Note hemispherical holes); (b) Rear of Cylinder.

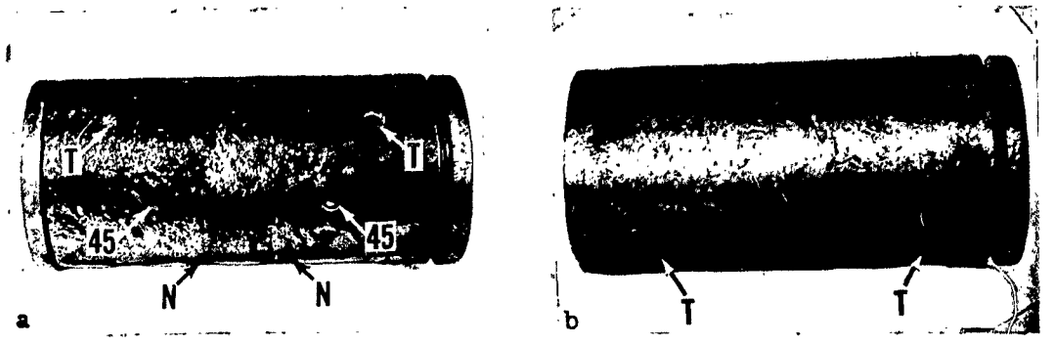

Figure A.24 Cylinder From Tower 4, Left Side, 3-in. Hole (Refer to Figure 3.17). (a) Front View (Note hemispherical holes); (b) Rear View (Note two holes which had tangential flow).

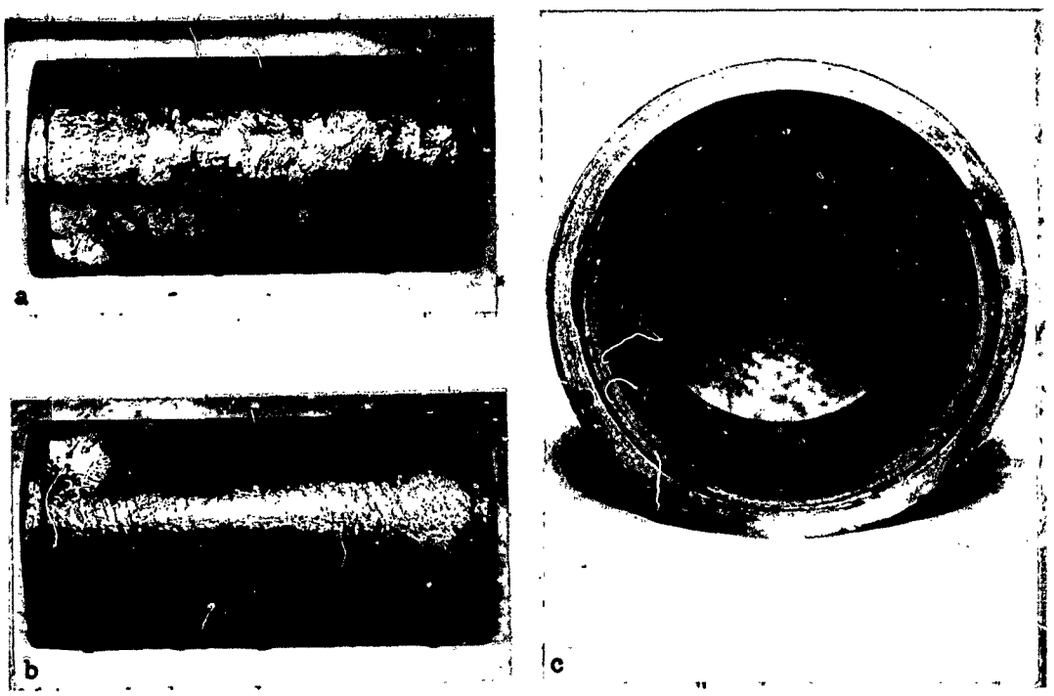

Figure A.25 Cylinder From Tower 4, Right Side, 4-in. Hole. (a) Side with Shiny Metal Splashes; (b) Side Opposite Shiny Metal Splashes (Note white spot is paint); (c) End View.

SECRET

flow was dark in appearance and fairly smooth. Most of the remainder of the surface, including the end caps, appeared to have been splashed and smeared with molten steel. The direction of this metal flow suggested that the specimen may have impacted with the ground on the side of the cylinder facing away from the blast; however, there was also evidence of a streaming pattern in the area near the two hemispherical holes which sustained 45° flow. Even though there was slight erosion of the seam under one cap, both end caps were easily removed and the interior of the cylinder was undamaged. There was no squashing or barreling observed.

A.4.8 Tower 4, Right Side, 4-in. Hole (Ref. Figure A.25). Nearly the entire surface was covered with dark streaks or splashes of once molten metal. There was one area which was rather heavily splashed with shiny steel as seen in Figure A.25(a). The surface opposite this shiny splashed area was streaked as if it were an impact pattern and had a slight brownish color somewhat like rust. There was no barreling noticed and only slight rounding of the corners. Both caps were easily removed. No internal damage or squashing of the cylinders was observed.

Appendix B
TRAJECTORIES OF LETHALITY-STUDY SPECIMENS

This appendix summarizes the equations and calculations used to determine the approximate trajectories of the various test specimens exposed in the fireball. Because of the many apparent irregularities in the trajectories, as indicated by the post-shot locations of some of the specimens, only a limited amount of analysis was possible and this primarily at the farther towers. The data, however, were extrapolated to the closer ranges, so that it was possible to obtain reasonable trajectories for nearly all of the specimens. A brief discussion of the trajectories is included in paragraph B.2.

In order to determine the trajectories of the specimens, it was necessary to know two quantities, the initial velocity (v_o) imparted to the specimens and the angle of departure (A) from the specimen tower as shown schematically in Figure B.1. Both of these quantities are unknown; however, since the distance the specimens traveled from their respective towers was measured, if one of these unknowns was determined, the other could be calculated. With a few assumptions regarding how the specimens received their initial velocity, it was possible to determine the approximate trajectories of most of the specimens without resorting to the description of relatively uncertain quantities such as the dynamic pressure and overpressure in the incident and reflected shock waves and the coefficient of drag and overpressure reflection factors for the particular specimen configurations and shock strengths.

B.1 DERIVATION OF EQUATIONS

A list of the various symbols used in this appendix is given in Table B.1. The important assumptions used in this analysis are that:

1. The specimens received their total impulse before any appreciable movement of the specimen occurred so that the specimens would appear to leave the tower with an initial velocity, v_o, at an angle, A, below the horizontal.

2. The weight and cross-sectional area of the specimens did not change appreciably during the time the specimens were receiving their impulse.

3. The resultant initial velocity can be expressed as

$$v_o = SgI/W,$$

where I is the magnitude of the effective total impulse, defined as the vector sum of the impulses imparted to the specimens by the dynamic pressure and overpressure in the incident and reflected shock waves.

4. The simple ballistic equations for a frictionless atmosphere are sufficiently accurate for this analysis.

If the specimen leaves the tower with a velocity, v_o, at an angle, A, as shown in Figure B.1, the distance y, it travels down and the distance, x, to the right from its initial position at any time, t, are

$$\begin{aligned} y &= gt^2/2 + v_o t \text{ Sin } A, \\ x &= v_o t \text{ Cos } A. \end{aligned} \qquad \text{(B.1)}$$

Eliminating the time variable between these two equations, the following equation is obtained.

$$v_o^2 = gx^2/2(y - x \text{ Tan } A)\text{Cos}^2 A. \qquad \text{(B.2)}$$

Substituting the values of x and y at impact (i.e., x=R and y=h), Equation B.2 becomes

$$v_o^2 = gR^2/2(h - R \text{ Tan } A)\text{Cos}^2 A. \qquad \text{(B.3)}$$

By assumption (3) above, gSI/W may be substituted for v_o, giving

$$S^2I^2/W^2 = R^2/2g(h - R \text{ Tan } A)\text{Cos}^2 A. \qquad \text{(B.4)}$$

Writing Equation B.4 for two different specimens at the same tower, denoted by subscripts 1 and 2, and taking the ratio of the two equations, the following equation is obtained

$$\begin{aligned} &(S_1/S_2)^2 (I_1/I_2)^2 (W_2/W_1)^2 \\ &\quad = (R_1/R_2)^2 (\text{Cos } A_2/\text{ Cos } A_1)^2 (h - R_2 \text{ Tan } A_2)/(h - R_1 \text{ Tan } A_1). \end{aligned} \qquad \text{(B.5)}$$

If Equation B.5 is applied to two spheres or two cylinders from the same station, by virtue of the symmetry of the specimens with respect to the incident and reflected shock waves,

$$\begin{aligned} A_1 &= A_2 = A, \\ S_1 &= S_2, \\ \text{and } I_1 &= I_2. \end{aligned}$$

Thus, the equation may be rewritten in the form

$$A = \text{Arctan } h(1 - F)/(R_2 - FR_1),$$

where

$$F = (W_2R_2/W_1R_1)^2. \tag{B.6}$$

Since h, F, R_1, and R_2 are known for any particular set of similar specimens from a given tower, it is possible to determine the apparent value of A from Equation B.6. Given the value of A, the initial velocity may be calculated from Equation B.3. The time to impact, t_i, may be calculated from Equation B.1 by letting x = R, obtaining

$$t_i = R/v_o \text{ Cos } A. \tag{B.7}$$

The x and y component velocities of the specimen at any time, t, are

$$\begin{aligned} v_y &= gt + v_o \text{ Sin } A, \\ v_x &= v_o \text{ Cos } A. \end{aligned} \tag{B.8}$$

The resultant velocity of the specimen at any time, t, is therefore

$$v = (g^2t^2 + 2\, gv_ot \text{ Sin } A + v_o^2)^{1/2}. \tag{B.9}$$

The terminal velocity, v_f, is given by Equation B.9 when t is replaced by the time of impact given by Equation B.7.

$$v_f = (g^2R^2/ v_o^2 \text{ Cos}^2 A + 2gR \text{ Tan } A + v_o^2)^{1/2}. \tag{B.10}$$

The angle of impact, B, is

$$B = \text{Arctan } v_x/v_y, \text{ at } t = t_i = R/v_o \text{ Cos } A, \tag{B.11}$$

or

$$B = \text{Arctan } v_o^2 \text{ Cos}^2 A/(gR + v_o^2 \text{ Sin } A \text{ Cos } A). \tag{B.12}$$

Since the burst point was three feet above the cab floor or 403 feet above the ground and the towers were positioned at ground range intervals of 60 feet as seen in Figure B.1, the line-of-sight angle C is given by

$$C = \text{Arctan } (403 - h)/60T,$$

where

$$T = \text{Tower No.} = 1, 2, 3, 4, \text{ or } 5. \tag{B.13}$$

B.2 SUMMARY OF TRAJECTORY DATA

The application of Equation B.6 to the three possible combinations of spheres at each tower (Steel-Aluminum, Steel-Ceramic, and Aluminum-Ceramic) resulted in a set of values of the apparent departure angle, A, which is summarized in Table B.2. The line-of-sight, or limiting angle, C, as calculated from Equation B.13 is also given in this table. The ceramic insert sphere at Tower 1 broke in two parts, and the two

TABLE B.1 LIST OF SYMBOLS

A (deg)	Angle of departure of specimen from tower. Measured positive downward.
B (deg)	Angle of impact of specimen with ground.
C (deg)	Angle of depression of the line through the burst point and the specimen.
F (lbs)	Resisting force of the ground on ten-inch-diameter spheres.
I (psi)	Effective total impulse imparted to the specimens.
R (ft)	Horizontal range specimen traveled at impact.
S (sq. in.)	Projected, flat-plate area of specimen.
T (no units)	Tower Number = 1, 2, 3, 4, or 5.
W (lbs)	Specimen weight.
g (ft/sec^2)	Gravitational acceleration (32.2).
h (ft)	Height of specimen above ground (tower height plus distance of specimen above tower).
L (ft)	Penetration of specimen in ground.
r (in.)	Radius of spherical specimen.
t (sec)	Time after specimen leaves tower.
t_i (sec)	Time of specimen impact with ground.
v_o (ft/sec)	Resultant initial velocity of specimen.
v_f (ft/sec)	Velocity of specimen at impact with ground.
v_i (ft/sec)	Velocity imparted to specimen by incident shock wave.
v_r (ft/sec)	Velocity imparted to specimen by reflected shock wave.
x (ft)	Horizontal distance measured positive radially outward from initial specimen position.
y (ft)	Vertical distance measured positive downward from initial specimen position.

TABLE B.2 SUMMARY OF INDIVIDUALLY CALCULATED DEPARTURE ANGLES, A

Tower No.	Departure Angle (A) - degrees			Angle (C) Degrees
	Stl.-Al.*	Stl.-Cer.*	Al.-Cer.*	
1	55.8	54.0	78.4	41.7
2	36.6	49.6	62.0	41.4
3	44.5	39.2	64.8	41.2
4	34.0	34.2	39.1	41.1
5	32.7	29.6	71.4	41.1

* Stl.-Al., Comparison of steel and aluminum spheres.
Stl.-Cer., Comparison of steel and ceramic insert spheres.
Al.-Cer., Comparison of aluminum and ceramic insert spheres.

SECRET

pieces landed at ranges differing by about 32 feet. The average range was considered to be the range at which the sphere would have landed had it not broken in half; it was used in the calculations for the angle A in Table B.2 and was used in the subsequent calculations. Usage of the average range in this sense indicates that this range is the center of mass of the two halves of the sphere, which is reasonable, since the two halves weighed approximately the same amount (the front half, range 245.4 feet, weighed 11 pounds and the rear half, range 277.3 feet, weighed 10 1/4 pounds). A comparison of the two cylinders from each tower would also be possible with Equation B.6, but these data would be of no value in obtaining an average value of departure angle since at Tower 1 the two cylinders had the same weight and size and yet landed at different ranges, and at the remaining towers the heavier (left) cylinder went farther than the light (right) cylinder even though the external dimensions were identical. It is assumed that the departure angle, A, can never be greater than the line-of-sight angle, C; for this would mean that the reflected shock would have pulled the specimen down rather than pushed it up. Using this philosophy, the departure angles in Table B.2 which were less than the line-of-sight angle were plotted in Figure B.2 and a curve was drawn through the data. This curve was made to approach the value of the limiting angle, C, at the close ranges, since the ratio v_i to v_r becomes large at close ranges, and the limit of the departure angle, A, as v_i/v_r increases as the angle, C, (see Figure B.1). The datum point for the steel and aluminum sphere comparison at Tower 2 was not plotted, even though it was less than the angle C; for it is believed that the aluminum sphere from this tower skipped out of its initial impact hole and rolled to its post-shot location. The fact that a calculated departure angle is greater than the limiting angle indicates (in view of the assumptions used in this analysis) the existence of a physical impossibility like a heavy object going farther than a similar light object for the same total impulse I (see assumption 3), such as noted above for the cylinders. The curve of departure angle versus distance from the burst point, as given in Figure B.2, however, is believed to be a reasonably good average value of A for each of the specimens at a given range and was used in the remaining calculations. That the departure angle should be representative of any of the specimens at a given tower is plausible in view of the symmetry of each of the specimens with respect to the incident and reflected shock waves.

Table B.3 summarizes the initial velocity, time to impact with the ground, and various other data relative to each of the specimens as calculated from the equations of paragraph B.1 using the curve value of A as given in Figure B.2. The calculated initial velocity of the aluminum sphere from Tower 2 was imaginary because the large value of R made the denominator of Equation B.3 negative. This sphere probably skipped out of its initial impact hole and rolled to this large range R. The initial velocity of each of the spheres is shown plotted as a function of distance from the burst point in Figure B.3. The velocities of the steel spheres appear to fall on a smooth curve with the possible exception of the velocity of the sphere from Tower 1 which may be somewhat high. This velocity calculation is particularly sensitive to the angle A since, because of the large value of R, the denominator, h - R Tan A,

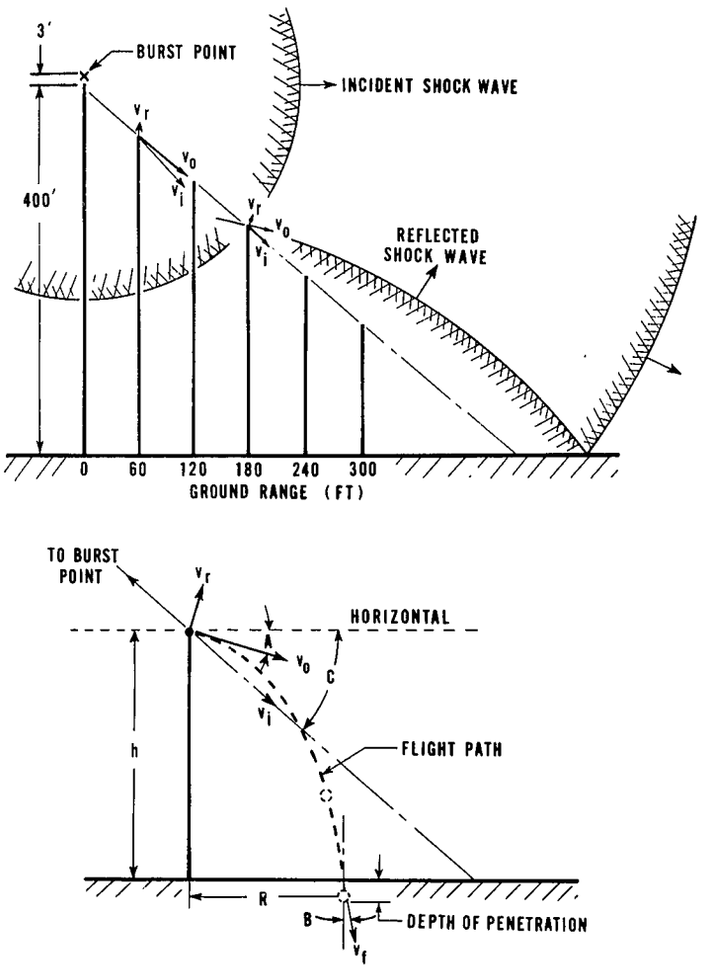

Figure B.1 Reference Sketch for Trajectory Calculations

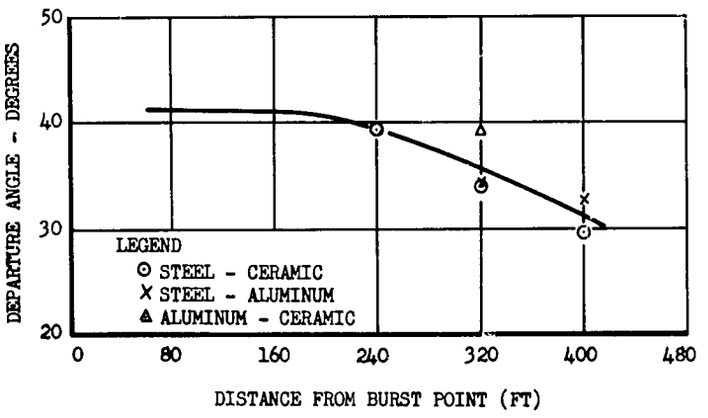

Figure B.2 Variation of Angle of Departure of Specimen From Tower With Distance From Burst Point

in Equation B.6 is very small and changes quite rapidly for a small change in A. For example, if angles 1 degree and 1/2 degree less were used, the calculated initial velocities would be, respectively, 510 and 640 ft/sec instead of 990 ft/sec, as shown in Figure B.3. The smaller specimen velocities are not as sensitive to the choice of the angle A: the ranges, R, of these specimens are relatively small, causing the factor, h - R Tan A, in the denominator to be large and to change only a small amount for a small change in A. The velocities of the aluminum and ceramic insert spheres at the close ranges appear to be inordinately low in comparison with the velocities calculated for the steel spheres and for the aluminum spheres at the farther towers. For a given total impulse, I, imparted to a steel sphere and an aluminum sphere at a particular tower, one would expect (see assumption (3)) that the ratio of the velocities of the two specimens would be inversely proportional to the ratio of their weights. Using average weights of 148 pounds for steel and 52 pounds for aluminum, the velocity of an aluminum sphere should be about 2.85 (= 148/52) times that of a steel sphere at any given range. The locus of velocities 2.85 times the velocity of the steel spheres is given in Figure B.3 by the dashed line. It can be seen that at the farther ranges the data points for the aluminum and ceramic spheres are quite close to this dashed curve but deviate considerably from the curve at the closer ranges. The heavy metal loss realized on the aluminum and ceramic insert spheres at the close ranges may have had a serious effect on the transmittal of the impulse of the shock waves to the specimens and, hence, caused them to receive a small velocity and to travel a shorter distance (horizontally, R). The solid curve is drawn through the average of the velocities of the aluminum and ceramic spheres at each range. No distinction was made between the aluminum spheres and the ceramic insert spheres, since the weights of these two types of spheres were practically the same as can be seen in Table B.3 and Figure B.3.

The initial velocities of the steel cylinders were not plotted because of the many different weights of these specimens. It can be seen in Table B.3 that each of the left cylinders had a calculated initial velocity greater than that of the right cylinder. This is peculiar in view of the fact that all of the cylinders had the same external dimensions and configuration and that the left cylinders were heavier than the right cylinders, except at Tower 1 where they had equal weights.

Figure B.4 shows a curve of impact velocity versus depth of penetration in the ground for 10-in.-diameter steel and aluminum spheres. The curve for the steel spheres was obtained by dropping a few steel spheres from a helicopter and measuring the depth of penetration of the sphere in the ground (from the level of the ground to bottom of sphere). A straight line correlation of these data points was considered to be within the accuracy of the data. Unfortunately, no drop tests were performed on the aluminum spheres; however, the curve for the aluminum spheres was obtained by multiplying the velocities of the steel spheres by 1.69, which is the square root of the weight ratio (148/52) for the two types of spheres. The scaling of the velocities by the square root of the weight ratio is an approximation based on the assumption that for

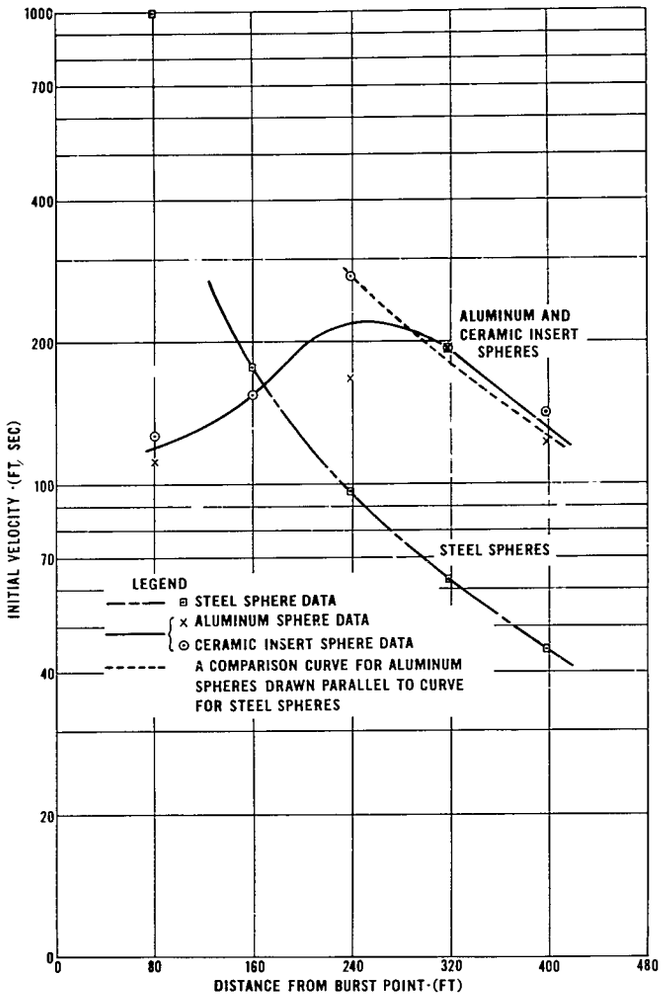

Figure B.3 Variation of Initial Velocities of Spheres With Distance From the Burst Point

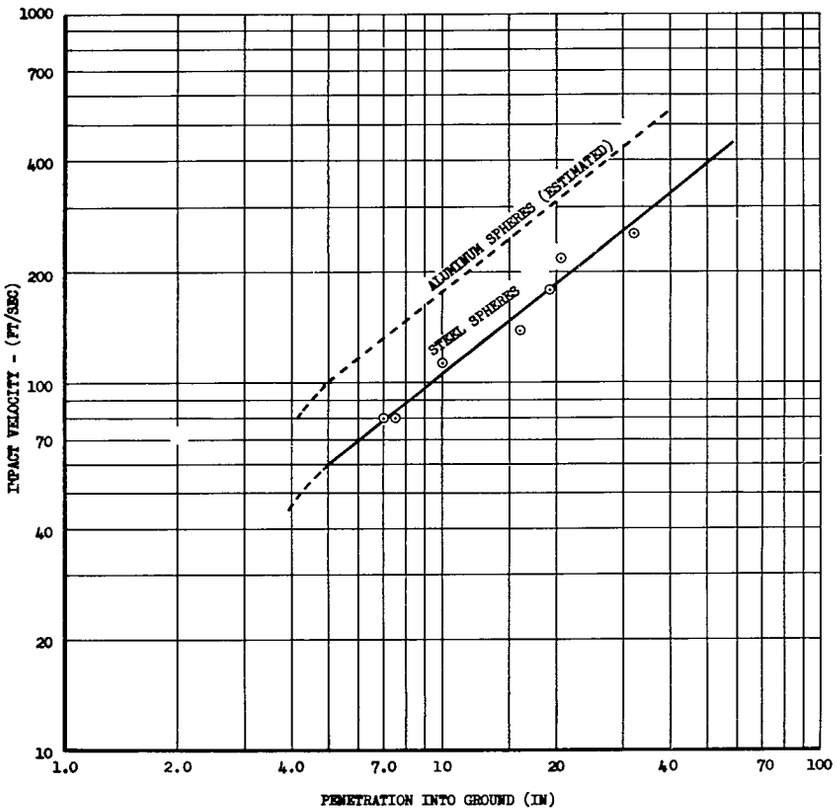

Figure B.4 Variation of Impact Velocity With Distance Penetrated in Ground for 10-in.-diameter Steel and Aluminum Spheres. Data points are drop test data for a steel sphere dropped on Frenchman's Flat Dry Lake bed.

10-in.-diameter spheres, the resisting force, F, of the ground is a function only of the penetration, L, into the ground. Using this assumption, the work done in penetrating to a depth L_1 in the ground is

$$\text{Work} = \int_0^{L_1} F dL. \tag{B.14}$$

If L_1 is the depth at which the sphere stops, the work done against this force should equal the energy of the sphere at the time of impact; i.e.,

$$\int_0^{L_1} F dL = (W/2g)v_f^2. \tag{B.15}$$

From this equation it can be seen that if a steel and an aluminum sphere both penetrate the same distance, L_1, they should have the same energy at impact. Thus,

$$(W_a/2g)v_{fa}^2 = (W_s/2g)v_{fs}^2, \tag{B.16}$$

where the subscripts a and s refer to aluminum spheres and steel spheres, respectively. Solving for v_{fa} from Equation B.16 gives

$$v_{fa} = (W_s/W_a)^{\frac{1}{2}} v_{fs}, \tag{B.17}$$

which, for $W_s = 148$ lbs and $W_a = 52$ lbs, reduces to

$$v_{fa} = 1.69 v_{fs}. \tag{B.18}$$

Table B.4 gives a comparison of the terminal velocities of the spheres as calculated from the ballistics Equation (B.10) with the velocities determined from the depths of penetration into the ground using the curves of Figure B.4. Nearly half of the velocities are in reasonable agreement but others differ appreciably. The differences in velocities, it is believed, is due in part to variations in the strength of the soil in which the specimens impacted. A small correction factor, given in Table B.4, was multiplied by the velocities as given by Figure B.4 in order to correct approximately for the loss in weight and reduction in size of the spheres. This correction factor was obtained by taking the square root of the ratio of the pre-shot to post-shot radii of the sphere and can be derived by replacing the force, F, in Equation B.14 by a force per unit area times the cross-sectional area, S, of the sphere. An equation similar to Equation B.16 can thus be written

$$(W_1/2S_1g)v_1^2 = (W_2/2S_2g)v_2^2, \tag{B.19}$$

TABLE B.3 SUMMARY OF TRAJECTORY PARAMETERS.

Tower		1	2	3	4	5
Angle A (Deg)		41.2	41.0	39.2	35.7	31.2
Steel Spheres	v_o (ft/sec)	990	177	97	63	45
	t_i (sec)	0.51	2.00	2.44	2.51	2.32
	v_f (ft/sec)	1000	225	159	128	106
	B (deg)	48.1	36.5	28.2	23.5	21.5
	R (ft)	394.1	268.1	183.4	128.2	90
	h (ft)	349.5	297.5	245.5	193.5	141.5
	W (lbs)	148.0	148.0	148.0	148.0	148.5
Aluminum Spheres	v_o (ft/sec)	112	(a)	167	194	123
	t_i (sec)	2.89	(a)	1.82	1.42	1.59
	v_f (ft/sec)	188	(a)	209	224	155
	B (deg)	26.4	(a)	38.3	44.7	42.5
	R (ft)	245.0	369.8	235.8	223.8	166.5
	h (ft)	349.5	297.5	245.5	193.5	141.5
	W (lbs)	53.5	51.5	53.0	53.5	51.5
Ceramic Insert Spheres	v_o (ft/sec)	127	155	273	195	143
	t_i (sec)	2.74	2.18	1.27	1.41	1.45
	v_f (ft/sec)	196	208	300	225	172
	B (deg)	29.1	34.3	44.7	44.8	45.3
	R (ft)	261.4	254.7	269.1	224.3	177.5
	h (ft)	349.5	297.5	245.5	193.5	141.5
	W (lbs)	52.5	50.5	52.5	52.5	50.5
Left Cylinders	v_o (ft/sec)	178	173	143	111	
	t_i (sec)	2.25	2.02	1.98	1.98	
	v_f (ft/sec)	233	221	190	157	
	B (deg)	35.2	36.2	35.7	35.0	
	R (ft)	302.2	263.7	219.6	177.5	
	h (ft)	346.5	294.5	242.5	190.5	
	W (lbs)	53.5	53.5	48.0	39.0	
Right Cylinders	v_o (ft/sec)	157	162	122	108	
	t_i (sec)	2.43	2.10	2.17	2.00	
	v_f (ft/sec)	217	212	175	154	
	B (deg)	33.0	35.1	32.8	34.5	
	R (ft)	287.0	257.0	204.7	175.0	
	h (ft)	346.5	294.5	242.5	190.5	
	W (lbs)	53.5	49.0	40.0	27.0	

(a) The calculated velocity was imaginary.

TABLE B.4 COMPARISON OF TERMINAL VELOCITIES OF SPHERES

Specimen	Tower	Angle of Impact B (deg)	Penetration in Ground (in.)		Velocity Correction Factor(a)	Terminal Velocity (ft/sec)	
			Vertical(b)	Slant(c)		From Ballistic Equation (B.9)	From Penetration in Ground (Fig. B.4)
Steel Spheres	1	48.1	37	55.3	1.04	1,000	447
	2	36.5	16	19.9	1.03	225	191
	3	28.2	13	14.7	1.01	159	146
	4	23.5	30	32.7	1.00	128	276
	5	21.5	10	10.1	1.00	106	107
Aluminum Spheres	1	26.9	14	15.7	1.14	188	292
	2	(d)	0	0.0	1.11	(d)	0
	3	38.3	9	11.5	1.10	209	220
	4	44.7	10	14.3	1.01	224	241
	5	42.5	11	14.9	1.00	155	245
Ceramic Insert Spheres	1	29.1	0	0.0	1.16	196	0
	2	34.3	12	14.5	1.11	208	267
	3	44.7	13	18.2	1.10	300	319
	4	44.8	12	16.9	1.01	225	275
	5	45.3	11	15.6	1.00	172	256

(a) Square root of pre-shot to post-shot radius ratio. This factor was multiplied by the velocities obtained from Figure B.4 to obtain the velocities in the last column.

(b) Measured penetration.

(c) Distance specimen traveled in ground (equals vertical penetration divided by Cos.B).

(d) No data available (see Table B.3).

SECRET

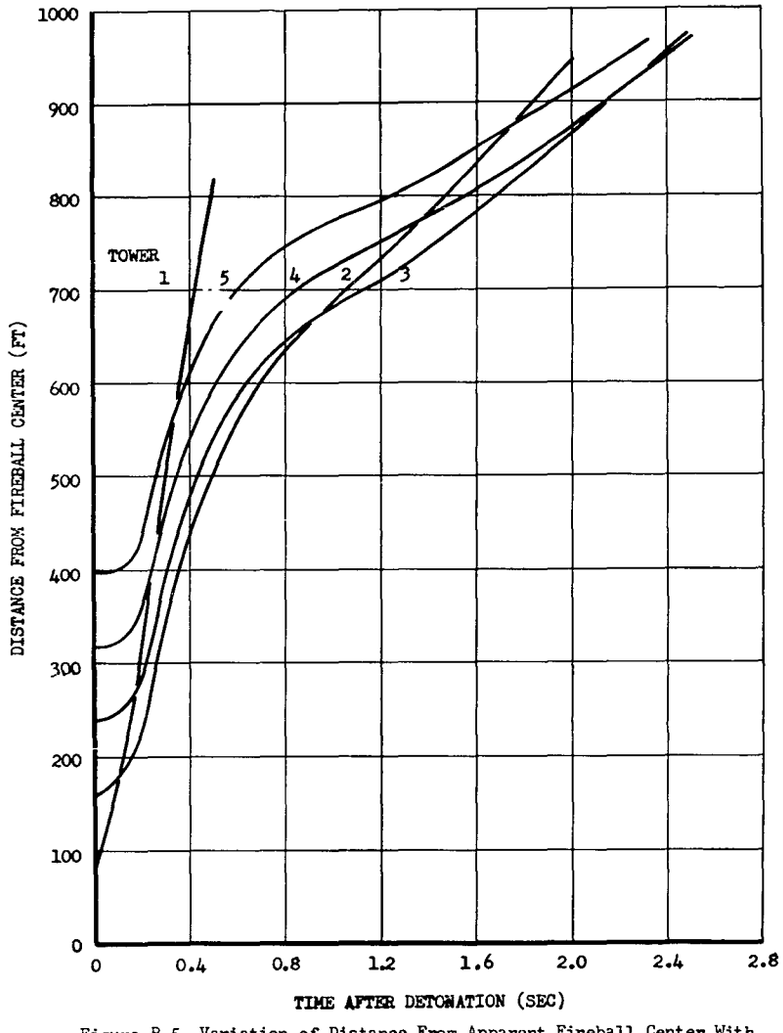

Figure B.5 Variation of Distance From Apparent Fireball Center With Time After Detonation for Steel Spheres. The curve for the sphere from Tower 1 is questionable because of the high initial velocity given in Table B.3.

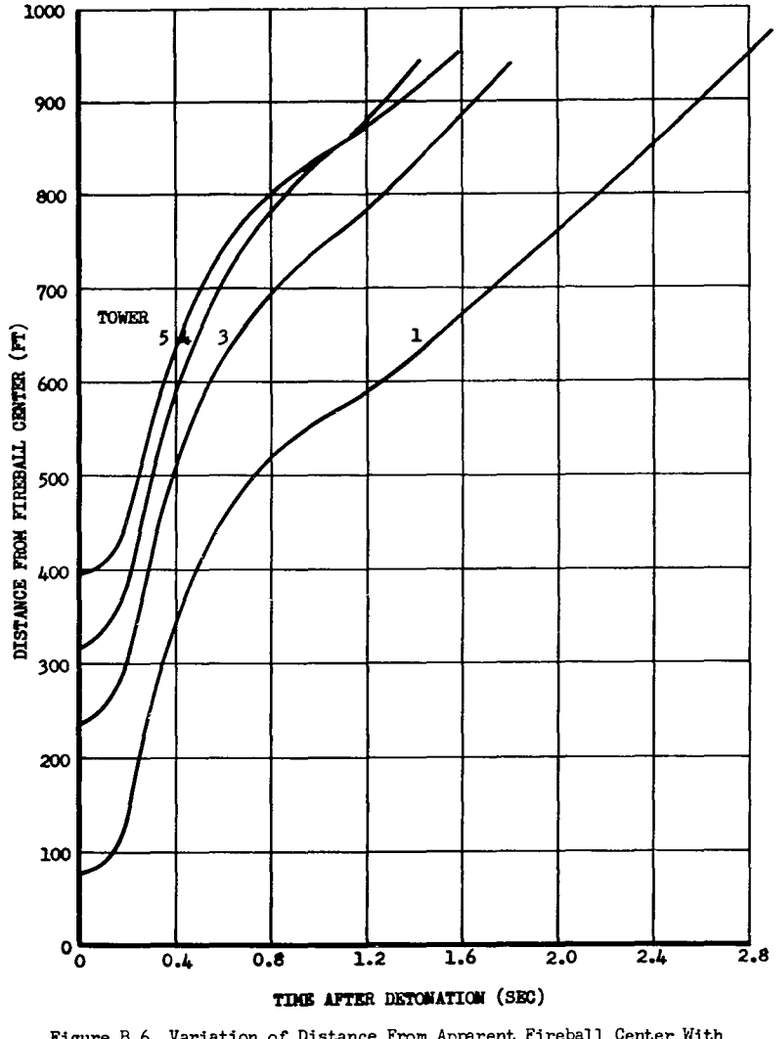

Figure B.6 Variation of Distance From Apparent Fireball Center With Time After Detonation for Aluminum Spheres. The calculated velocity of the sphere from Tower 2 was imaginary.

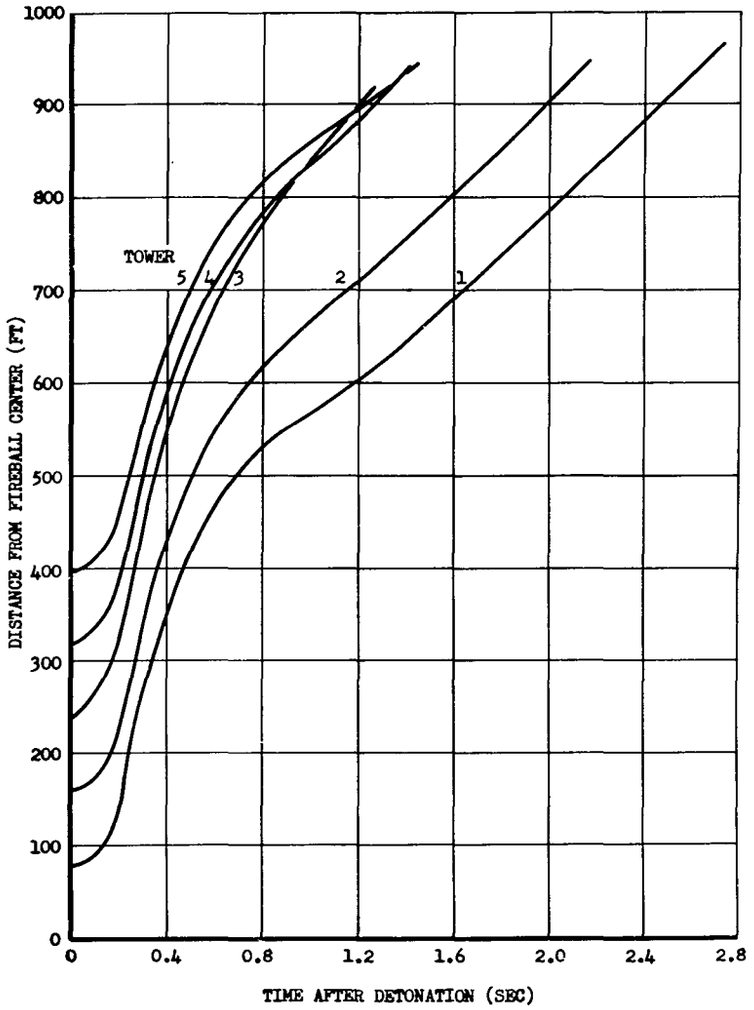

Figure B.7 Variation of Distance From Apparent Fireball Center With Time After Detonation for Ceramic-Insert Spheres. The curve for the sphere from Tower 1 represents the mid point of the two halves of this sphere.

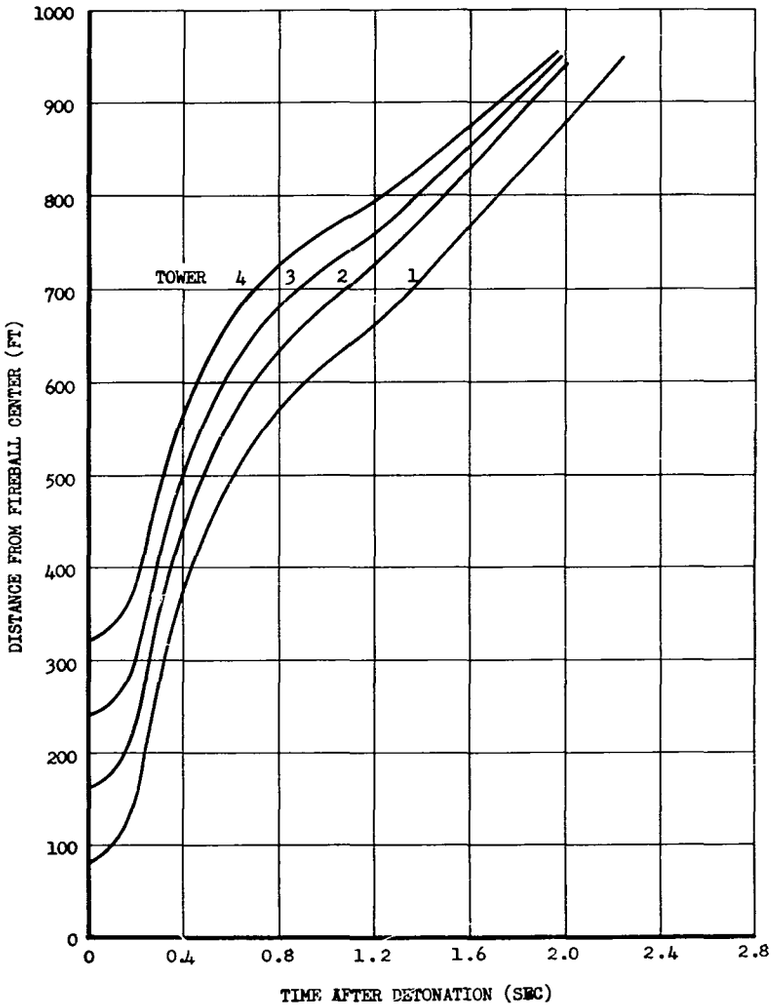

Figure B.8 Variation of Distance From Apparent Fireball Center With Time After Detonation for Cylinders From the Left Side of the Towers

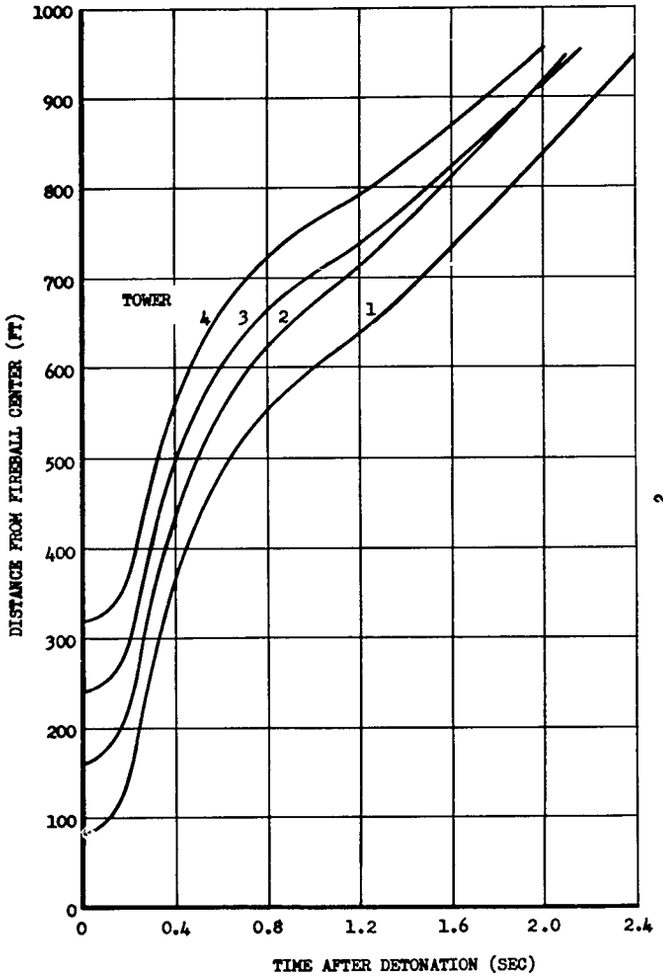

Figure B.9 Variation of Distance From Apparent Fireball Center With Time After Detonation for Cylinders From the Right Side of the Towers

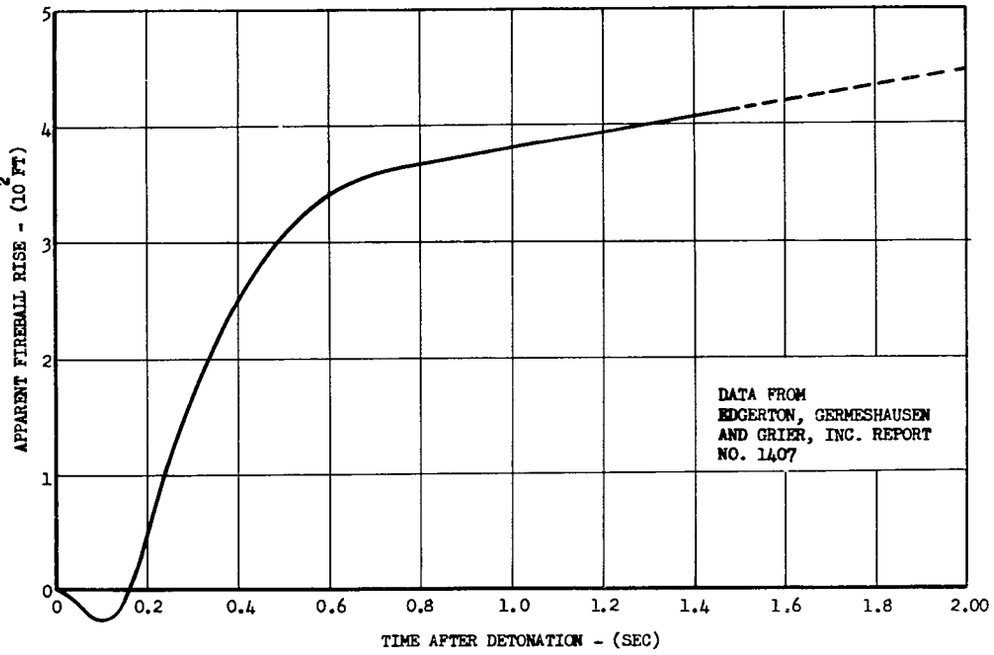

Figure B.10 Rise of Fireball Center Above Burst Point as a Function of Time After Detonation

where the subscripts, 1 and 2, refer, respectively, to pre-shot and post-shot values. Since the weight is proportional to r^3 (r = radius) and the area is proportional to r^2,

$$v = (r_1/r_2)^{\frac{1}{2}} v_1. \qquad (B.20)$$

Figures B.5 through B.9 show the variation of the distance of each specimen from the apparent fireball as a function of time after detonation. Each of the curves is terminated at the time the specimen impacts with the ground. These curves were calculated from the values of initial velocity and departure angle given in Table B.3 and from the apparent rise of the fireball center above the burst point as given in Figure B.10. The data on fireball rise, as given in Figure B.10, were obtained from an analysis of high speed motion picture photography presented in "Late Fireball - Early Cloud Analysis, Teapot MET," Report No. 1407, by Edgerton, Germeshausen, and Grier, Inc.

Appendix C
DESCRIPTION OF SHOT TOWER DAMAGE

This appendix comprises a brief description of the damage sustained by various shot towers used during Operation Teapot. The purpose of this study was to determine for each of the various type towers and weapon yields the extent to which the tower and guy cables were vaporized. This information was obtained to supplement the vulnerability data from the Lethality Study and should be of value in designing future exposure programs in a nuclear fireball. A description of the damage sustained by the television towers used for the Lethality Study is also included.

Operation Teapot consisted of 14 shots, numbered 1 through 14, of which ten were tower shots, three were air bursts, and one was a burst 67 feet underground. The air bursts were Shots 1, 9, and 10, and the underground burst was Shot 7. Table C.1 summarizes the yield, time and location of burst, and other data relative to each of the tower shots.

C.1 DESCRIPTION OF TOWERS

All of the shot towers were of steel construction, erected on concrete bases, and were guyed from each corner of the tower by wire ropes. With the exception of the tower used for Shot 2, all of the shot towers were square, 20 feet on a side. The tower for Shot 2 was of triangular cross-section, 20 feet on a side.

The main support members, or tower legs, of the triangular tower for Shot 2 were steel angles of sizes 8 x 8 x 7/8 in. up to the 50-ft elevation, 8 x 8 x 5/8 in. up to the 75-ft elevation, and 6 x 6 x 1 in. from the 75-ft elevation to the top of the tower (300 feet). Angles of 4 x 4 x 5/16 in. were placed horizontally at each multiple of 25-ft elevation. The criss-cross, diagonal tension members placed between these horizontal members were angles 2 1/2 x 2 x 1/4 in. A 3 1/2 x 3 x 1/4 in. angle was placed horizontally midway between the horizontal 4 x 4 x 5/16 in. angles at the 25-ft levels. A typical section of the upper portion of the 300-ft triangular tower is shown in Figure C.1(a). This tower was guyed at the 250-ft level from each of the three tower legs by 1 1/2 in. diameter cables going down at an angle of 45 degrees to concrete deadmen. The lengths of the guy cables were thus about 353 feet each.

The main support members and horizontal crossmembers of the square towers were box beams, formed by welding together two steel angles. The main support members were formed of 6 x 6 in. angles; the thickness

of the angles varied from 3/8 in. to 7/8 in. as determined by the height of the tower and the design load for the cab floor. All horizontal crossmembers were 4 x 4 in. square (outside dimensions) box beams and had a wall thickness of 1/4 inch. The criss-cross, diagonal tension members were either 1 1/8 in. or 1-in. diameter bar as determined by the tower height and design load for the cab floor. Figure C.1(b) shows a typical section of a square tower. With the exception of the tower for

TABLE C.1 SUMMARY OF DATA FOR TOWER SHOTS

	Shot 2	Shot 3	Shot 4	Shot 5	Shot 6	Shot 8	Shot 11	Shot 12	Shot 13	Shot 14
Date	22 Feb.	1 Mar.	7 Mar.	12 Mar.	22 Mar.	29 Mar.	9 Apr.	15 Apr.	5 May	15 May
Time (PST)	5:45:00.019	5:30:00.272	5:20:00.200	5:19:59.802	5:04:59.930	4:55:00.075	4:30:00.176	11:15:00.327	4:10:00.013	3:59:59.883
Location (Area)	T-3	T-9-b	T-2	T-3-a	T-7-1a	T-4	T-9-c	FF	T-1	T-7-1a
Elevation of Ground Zero	4026.00	4021.00	4491.00	4006.50	4245.00	4308.75	4235.80	3077.50	4236.00	4245.00
Yield (KT)	2.4±0.2	6.9±0.2	43±2	3.6±0.2	8.1±0.3	15±2	1.5±0.1	23±1.5	30±3	29±2
Tower Height (ft)	300	300	500	300	500	500	300	400	500	500
Tower Type	Triangular	Square 30 ton	Square 100 ton	Square 100 ton	Square 100 ton	Square 100 ton	Square 100 ton	Square 100 ton	Square 100 ton	Square 100 ton
Atmospheric Pressure										
Ground Zero (MB)	880	876	868	881	876	867	874	908	871.1	866
Burst Height (MB)	871	868	868.5	872.8	871	854.1	862.5	895.1	855.3	851
Air Temperature (C)										
Ground Zero	-7.8	-3.9	5.2	-1.0	1.0	9.1	1.0	19.5	7.5	3.0
Burst Height	-4.2	3.3	5.83	7.0	5.0	11.2	10.28	18.9	15.6	2.1

Shot 3, all square towers were designed for a total live cab floor load of 100 tons. The Shot 3 tower, which was 300-ft high was designed for a cab floor load of 30 tons. Table C.2 summarizes tl sizes of the angles used to form the main support members and the diameters of the tension members used for each of the several tower heights and design cab loads of the square towers. All of the square towers were guyed at the top of each of the four tower legs to concrete deadmen. The 400-ft and 500-ft towers were also guyed from each tower leg at the mid elevation of the tower. The lengths and diameters of these guy cables are included in Table C.2.

Other miscellaneous items which were on all of the shot towers include:

1. A lightweight ladder to the top of the tower. Small landings were provided at each 25-ft elevation interval.

2. A freight elevator. The two guide rails for the elevator were formed of a 5 1/4 x 5/8 in. plate with a 3 in., 5 lb/ft, channel welded on each side. These guide rails were suspended out about four feet from

one side of the tower. Two 3/4 in. wire ropes were used as hoist cables for the elevator cage.

3. A shot cab. The cab floor was constructed of heavy I-beams and covered with steel plate. The sides of the cabs were Acme Aluminum Rollaway Doors. The roof and upper portion of the sides were made of corrugated steel.

Table C.3 shows the type of material and distribution of weight of the 400-ft, 100 ton tower used for Shot 12. These data are typical of

TABLE C.2 SUMMARY OF MAIN SUPPORT MEMBER, TENSION MEMBER, AND GUY CABLE SIZES FOR SQUARE TOWERS*

Tower Height (ft)		300	300	400	500
Design Cab Load (Tons)		30	100	100	100
From Elevation 0 to 50 ft	l*(in.)	6 3/8	6 1/2	6 5/8	6 5/8
	t (in.)	1/2	3/4	7/8	7/8
	d (in.)	1 1/8	1	1 1/8	1 1/8
From Elevation 50 to 75 ft	l (in.)	6 3/8	6 1/2	6 1/2	6 1/2
	t (in.)	3/8	3/4	3/4	3/4
	d (in.)	1 1/8	1	1	1
From Elevation 75 to 250 ft	l (in.)	6 3/8	6 1/2	6 1/2	6 1/2
	t (in.)	3/8	3/4	3/4	3/4
	d (in.)	1	1	1	1
From Elevation 250 ft to Top	l (in.)	6 3/8	6 1/2	6 1/2	6 1/2
	t (in.)	3/8	3/4	5/8	5/8
	d (in.)	1	1	1	1
Upper Guy Cable Length (ft)		423	423	781	771
Upper Guy Cable Diameter		1 3/8	1 1/2	1 1/4	1 1/4
Lower Guy Cable Length (ft)		None	None	353	344
Lower Guy Cable Diameter (in.)				1 5/8	1 5/8

* Refer to Figure C.1

the 100 ton towers. Pre-shot photographs of various shot towers are presented in Figure C.2.

Some peculiarities in the construction of the various shot towers are as follows:

1. Shot 5. Two guy wires were used from the top of each tower leg instead of a single guy wire. One of the guys was joined to two separate guys near the ground and were anchored to two separate concrete deadmen, as seen in Figure C.7(c). The other guy ran directly to the center deadman as seen in Figure C.7(c).

2. Shot 8. There was a large tube in the center of the tower which went from the shot cab to the base of the tower and then out to a distant instrument shelter. In addition, there were seven large platforms suspended from one side of the tower as seen in Figure C.3(b).

An additional tower, 100-ft high, was erected near the base of the Shot 8 tower as can be seen in Figure C.2(c) and C.3(a).

3. Shot 11. Dual guys as seen in Figure C.2(a) were used from the top of each tower leg instead of single guys. The guys were anchored to separate deadmen.

4. Shot 13. There were seven large tubes in the center of the tower which ran from the shot cab to the base of the tower, as shown in Figures C.2(d) and C.3(c). In addition, there were five small platforms

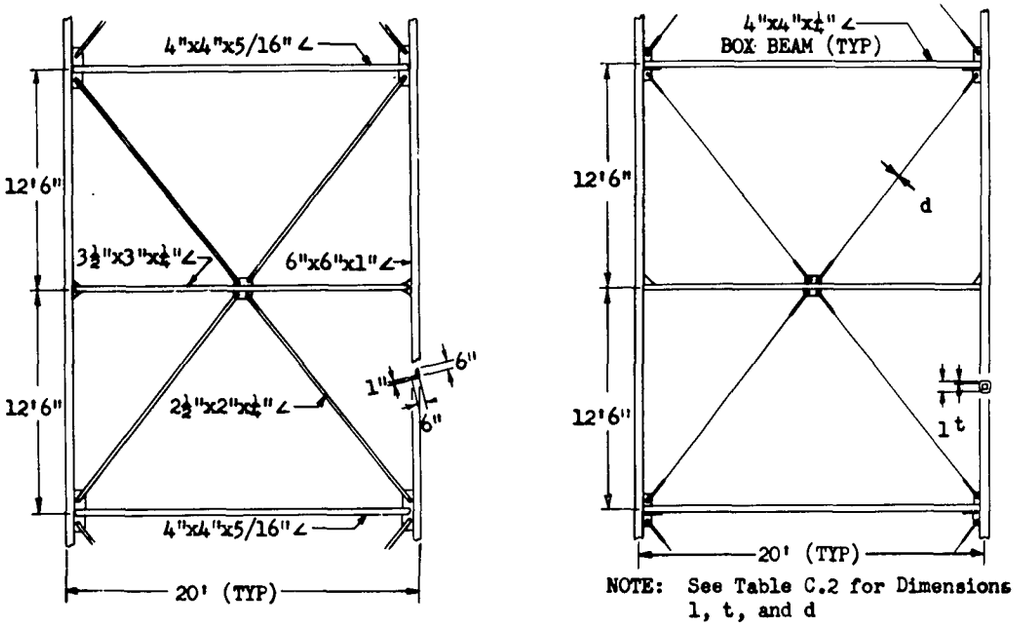

(a) Triangular Tower

(b) Square Tower

Figure C.1 Typical Tower Construction

suspended out from a corner of the tower as seen in the upper left corner of Figure C.3(c). Because of the additional weight of the tubes, etc., this tower was guyed very heavily as seen in Figure C.2(d). Dual guys were used at the 125-ft, 250-ft and 375-ft levels. Single guys were used from the top of the tower.

Photographs and drawings of the television towers used for the Lethality Study program during Shot 12 can be seen in Figures 2.1, 2.2, C.2(b), and C.3(d). These towers were of triangular cross-section, two feet on a side. The heights of the towers ranged from 348 feet for the closest tower (60-ft-horizontal range) to 140 feet for the farthest tower (300-ft-horizontal range) as discussed in Chapter 2. The main support members of these towers were 1 1/4 in. diameter solid steel rods and the diagonal members were 5/8 in. diameter steel rods. With the

exception of a few odd length tower sections which were necessary to obtain the required tower heights, all of the towers were made up of standard 20-ft sections which were fabricated at the factory. Each of the sections was of welded construction, but the individual sections were bolted together to form the tower. These towers were guyed at various levels from each of the three tower legs with 3/8 in. cable. Tower 1 was guyed at tower elevations of 108, 208, and 308 feet; Tower 2

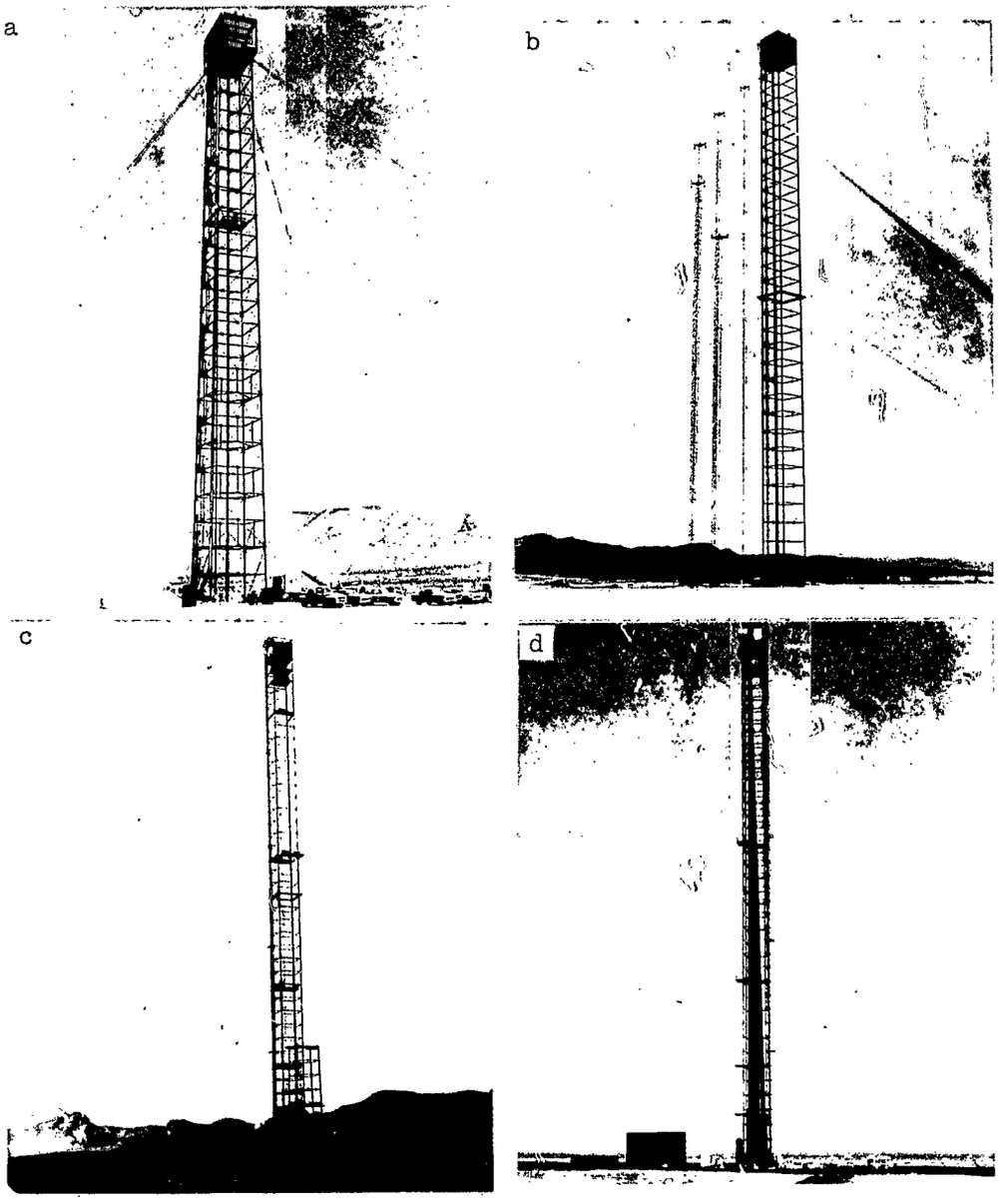

Figure C.2 Pre-shot Views of Typical Towers. (a) 300-ft, 100-Ton Tower, Shot 11. (b) 400-ft. 100-Ton Tower, Shot 12. Note TV Towers. (c) 500-ft. 100-Ton Tower, Shot 8, (See Fig. C.3). (d) 500-ft, 100-Ton Tower, Shot 13. Note 7 large tubes in tower (See Fig. C.3).

at 100, 180, and 260 feet; Tower 3 at 84 and 184 feet; Tower 4 at 80 and 160 feet; and Tower 5 at 100 feet.

C.2 SUMMARY OF TOWER DAMAGE

The damage descriptions included herein consist essentially of a brief summary of the approximate size and location of the post-shot wreckage of the various shot towers. Because of the high radiation levels near ground zero, it was necessary to limit the time spent near the tower wreckage, and, as a consequence, only approximate measurements

TABLE C.3 DISTRIBUTION OF WEIGHT AND MATERIAL FOR THE 400 FT, 100 TON TOWER (SHOT 12)

Location	Aluminum (lbs)	Steel (lbs)	Plastic (lbs)	Concrete (lbs)
Shot Cab	3,400	34,400	400	
Tower		111,600		
Guys		15,200		
Base				225,000
Total	3,400	161,200	400	225,000

of the lengths of some of the remaining guy cables and main support members were obtained. Each of the damage descriptions is supplemented with photographs of the tower remains.

C.2.1 Shot 2 (300-ft Triangular Tower). The three tower legs were laid out approximately radially from their pre-shot positions. The longest tower leg found was about 200-ft long. The other two legs appeared to be about 150-ft long. All three guy cables were still attached to their turnbuckle and deadmen such as seen in Figure C.4(c). All of the cables were about 100 to 150-ft long. The large piece of wreckage seen in the upper left corner of Figure C.4(a) was the I-beam and cable pulley from the top of the elevator cage. The elevator for this shot tower, as well as for all shot towers, was at the bottom of the tower at the time of detonation. The major portion of the tower remains was near ground zero with a very large pile of tower wreckage right on the base as seen in Figure C.4(b). A few large pieces of the tower, about 20 to 30-ft long, were strewn to ranges of about 200 feet.

C.2.2 Shot 3 (300-ft, 30-ton Square Tower). There was a relatively small amount of tower wreckage located right at the tower base as can be seen in Figure C.5(b). With the exception of the four tower legs, which were laid out radially from their original position, only a small amount of tower debris was found anywhere. There were, however, a few isolated pieces found at ranges of about 200 feet. Two of the tower legs were still attached to the concrete base; the others were detached but remained very close to their original position as seen in Figure C.5(b). The tower legs remained intact to lengths of about 125 feet. All four guy cables were still attached to the turnbuckles and deadmen as seen

in Figure C.5(c). The length of remaining guy cable was probably in excess of 150 feet.

C.2.3 Shot 4 (500-ft, 100-ton Square Tower). There were two large pipes about six feet high still on the tower base as seen in Figure C.6 (a) and (b). Only the main support members of this tower, however, remained to any extent. These members were scattered off to one side of the tower, as seen in Figure C.6(a), rather than laid out radially as

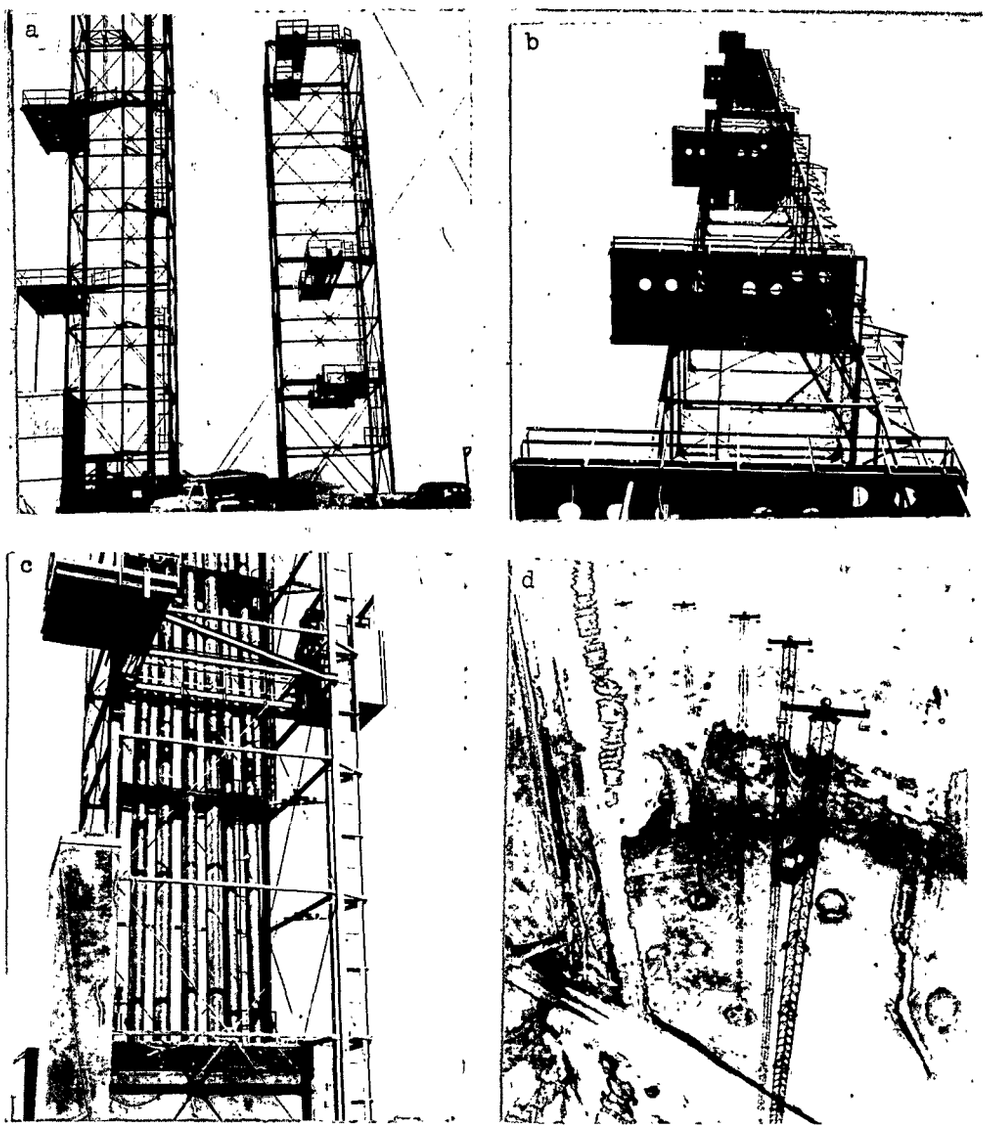

Figure C.3 Close-up Views of Various Towers. (a) Shot 8 Tower, Base Portion and Auxiliary Tower. (b) Shot 8 Tower, Steel Platforms. (c) Shot 13 Tower, Base Portion, Showing Seven Large Tubes. (d) View of TV Towers From Shot Cab of Shot 12.

noted on Shots 2 and 3. One piece of the tower leg which was still intact was about 100 feet as seen in the foreground of Figure C.6(a). The end of this was broken off at a tower splice with another tower member about 50-ft long also broken at a splice lying nearby. It is believed that these two members were from the same tower leg which indicates that nearly 150 feet of this tower leg was essentially undamaged. The other end of the 75-ft member was squashed, split, and showed evidence of thermal damage which is typical of the top of remaining main support members of all of the towers. Other main support members found were less than 150 feet; probably about 100 to 125-ft long. Most of the

a

b

c

Figure C.4 Shot 2 Tower Wreckage. (a) General View; (b) Close-up View; (c) Guy Anchor and Cable.

other tower remains were in relatively small pieces and were severely squashed, split and melted.

There was very little guy cable found. Probably the longest piece of any of the cables was less than 200 feet. Two of the lower cables and turnbuckles were still attached to their base, but the other two were broken off. All four of the upper guy cables and turnbuckles attaching them to the bases were broken off and hurled away from the base.

C.2.4 Shot 5 (300-ft. 100-ton Square Tower). Three of the main support members were about 100-ft long and the other was nearly 150-ft

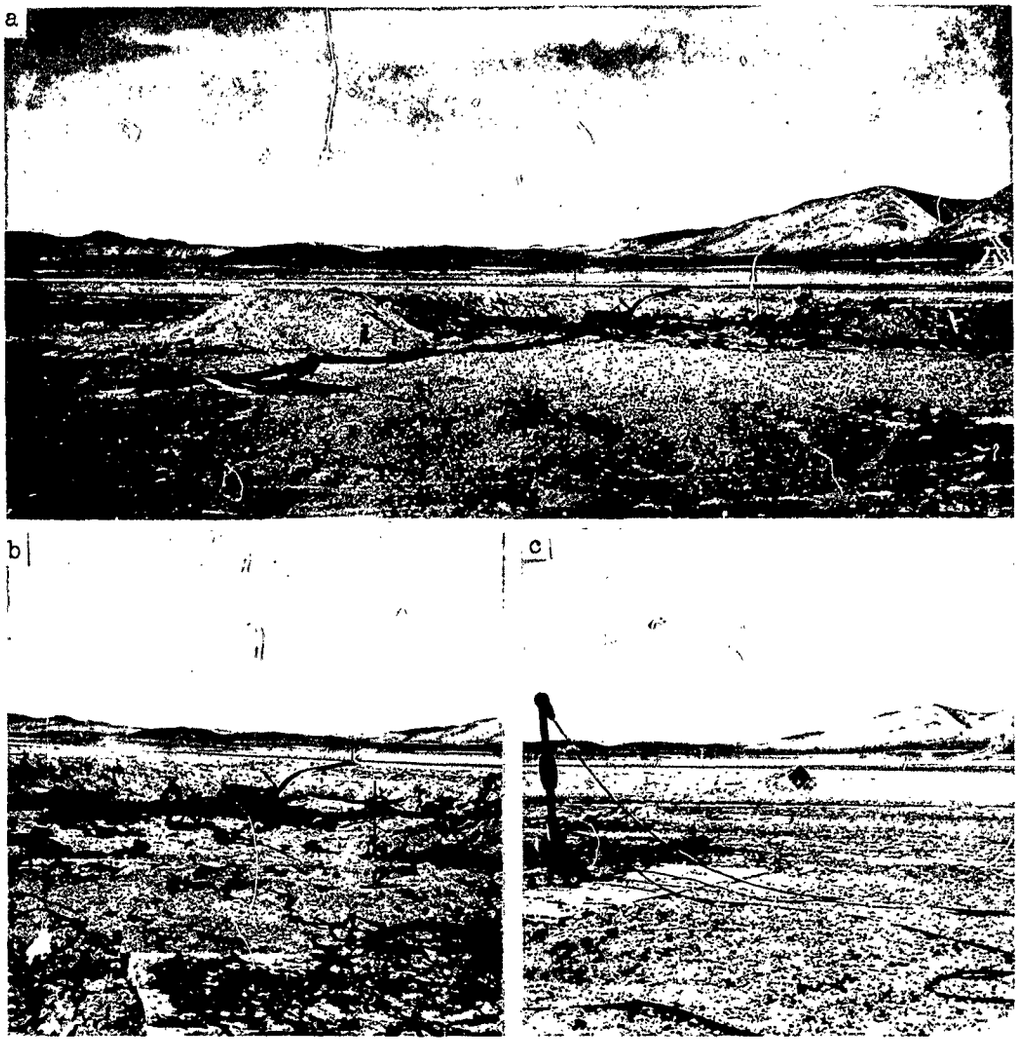

Figure C.5 Shot 3 Tower Wreckage. (a) General View; (b) Close-up View; (c) Guy Cable and Turnbuckle.

long. Most of these support members remained attached to the concrete base. There was very little indication of melting or squashing of these members. The tower legs were laid out generally radially from their initial position. A large portion of the tower wreckage was found very close to the tower base as seen in Figure C.7(a) and (b). Some portions of the tower remains, however, were strewn as far as 300 feet. All but two of the guy cables and turnbuckles still remained attached to the deadmen. From each tower leg there were two cables which were attached to three deadmen as seen in Figure C.7(c). One of the guy cables was attached about 30 feet above the deadmen to two cables (by a fixture which can be seen in the background of Figure C.7(c)) which in turn were anchored to two separate deadmen.

C.2.5 Shot 6 (500-ft, 100-ton Square Tower). A large portion of this tower was still standing after the shot. Unfortunately, however, no photographs were obtained before the tower was torn down. It is

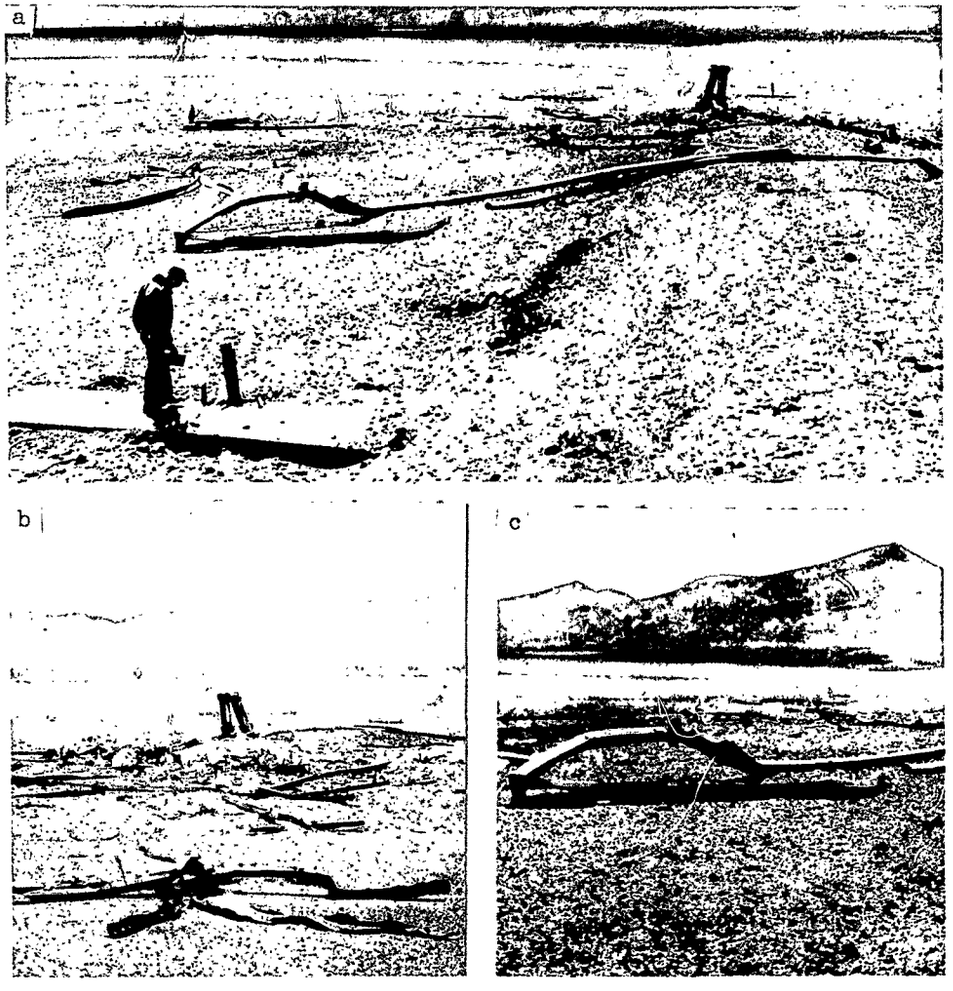

Figure C.6 Shot 4 Tower Wreckage. (a) General View; (b) Close-up View of Tower Debris; (c) Main Support Member.

estimated that at least 150 feet of the tower was essentially undamaged and standing erect with an additional 50 to 75 feet of the tower slightly melted and drooped over at the top. A general view of the wreckage of the tower after it was torn down is shown in Figure C.8. Some of the guy cables were undamaged to lengths of over 500 feet. The guy cable junction fixtures, such as seen in Figure C.8(c), were essentially undamaged. These fixtures were at a distance of about 350 feet from the burst point.

C.2.6 Shot 8 (500-ft, 100-ton Square Tower). Most of the wreckage of this tower and the 100-ft auxiliary tower remained close to ground zero. The main support members of the shot tower still remained to lengths of about 150 feet with the top 25 to 50 feet being crushed and

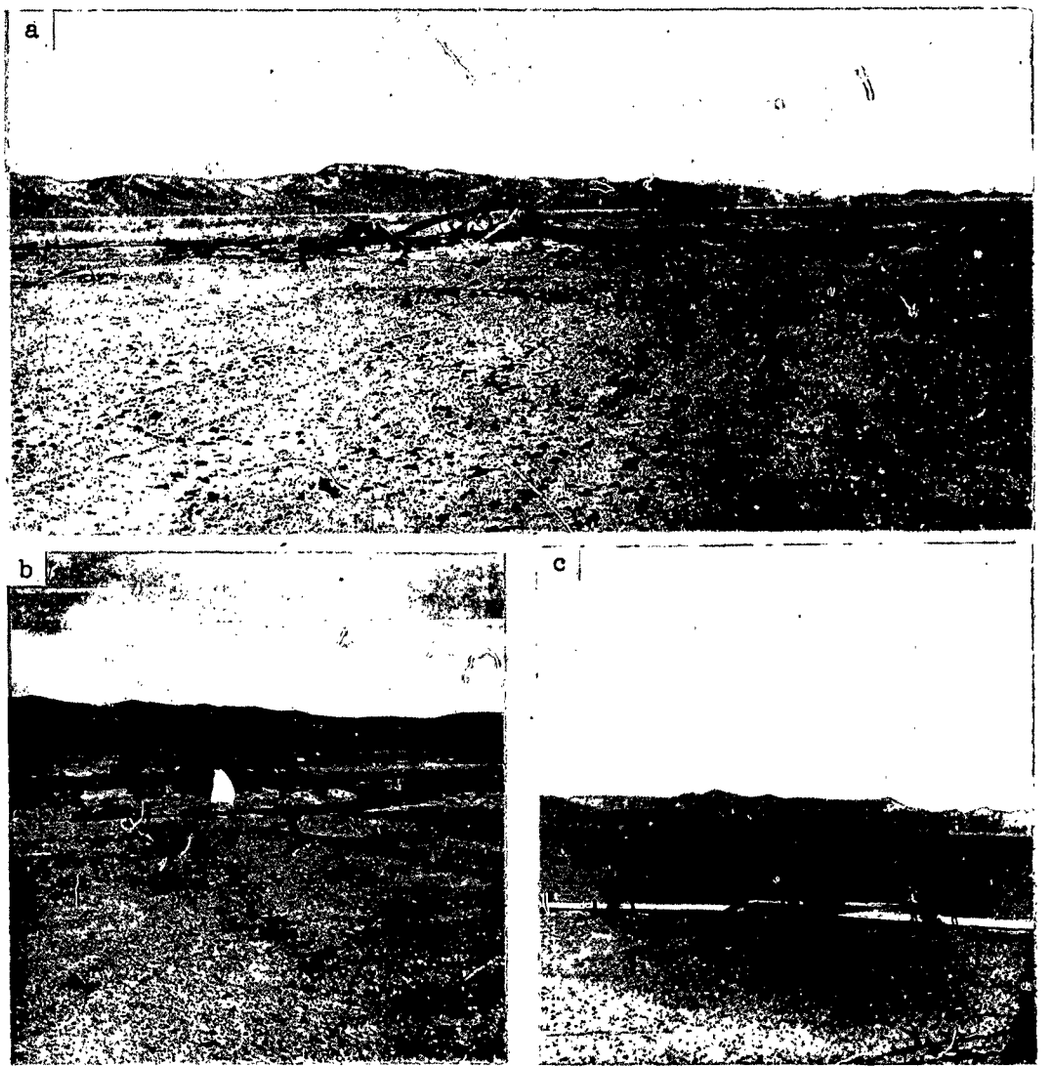

Figure C.7 Shot 5 Tower Wreckage. (a) General View; (b) Close-up View; (c) Deadmen, Turnbuckles, and Cables.

split as seen in the foreground of Figure C.9(a). Some of the legs still remained attached to the base. The auxiliary tower was blown down completely, but there was little evidence of any thermal damage. The portion of large pipe which went from the base of the shot tower to a distant instrument shelter was still in place except for the portion near the tower which was twisted somewhat. No portion of the pipe which went up the center of the tower was observed. All of the guy cables and turnbuckles were still attached to their bases. One turnbuckle, as seen in Figure C.9(c), was bent around over 90 degrees by the cable which was hurled outward. Nearly 200 feet of cable remained of some of the guy cables. It was noticed that all but about the 50 feet of cable closest to the deadman showed evidence of thermal damage. This was not noticed to this degree on the other shots.

C.2.7 Shot 11 (300-ft, 100-ton Square Tower). Most of the wreckage of this tower was mangled together right over the tower base.

a

b

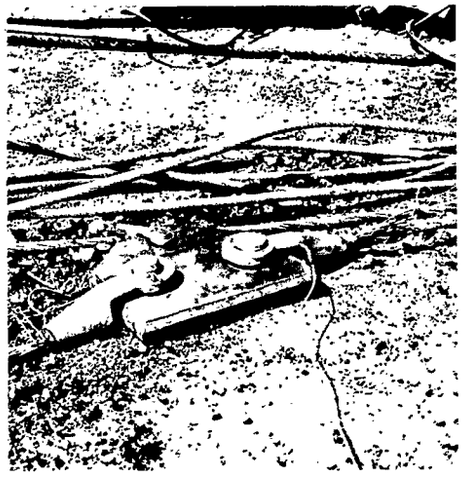

Figure C.8 Shot 6 Tower Wreckage. (a) General View of Wreckage after Tower was torn down; (b) Close-up View; (c) Guy Cable Junction.

Several of the main support members were still attached to the base and were about 150-ft long. One of the main support members was in the shape of an arch about 25 to 30-ft high, as seen in Figure C.10(c). Several 30 to 40-ft pieces of the tower were strewn to ranges of 200 feet or so. The expanded metal cage which was around the elevator at the base of the tower was severely bent and twisted but was still recognizable. All eight of the guy cables (two from each corner of the tower) were still attached to the turnbuckles and deadmen, as seen in Figure C.10(d). Some of the cables were essentially undamaged to lengths of nearly 150 feet.

C.2.8 Shot 12 (400-ft, 100-ton Square Tower). With the exception of the four main support members of the tower, nearly all of the tower

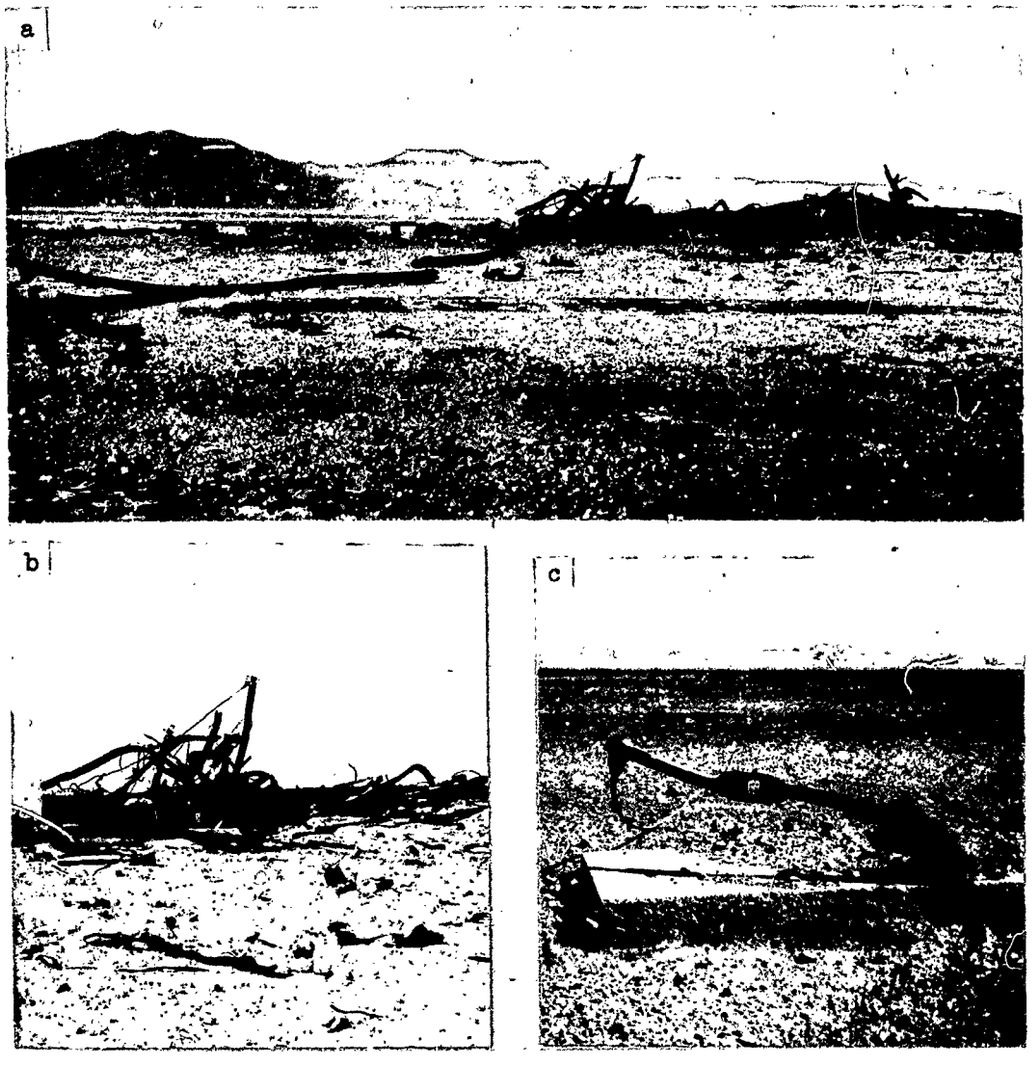

Figure C.9 Shot 8 Tower Wreckage. (a) General View; (b) Close-up View; (c) Guy Cable and Turnbuckle.

remains were at or near the base of the tower as seen in Figure 3.1 and C.11(a). About 225 feet of the tower legs were still intact with the top 25 to 50 feet being crushed, split, and slightly melted as seen in Figure C.11(b). This was typical of most of the shot towers. Much of the elevator cage could still be seen at ground zero. The hoist pulley from the top of the elevator cage was still attached and appeared to be essentially undamaged. All of the lower guy cables were still attached to the burnbuckle and deadmen and were about 300-ft long. All of the turnbuckles for the top guy cables were detached from their base but were located within 100 to 200 feet of their original position. Most of these turnbuckles were still attached to the guy cables. A cable junction fixture (similar to that seen in Figure C.8(c)) which was originally 353 feet from the burst point was found and showed only a small amount of

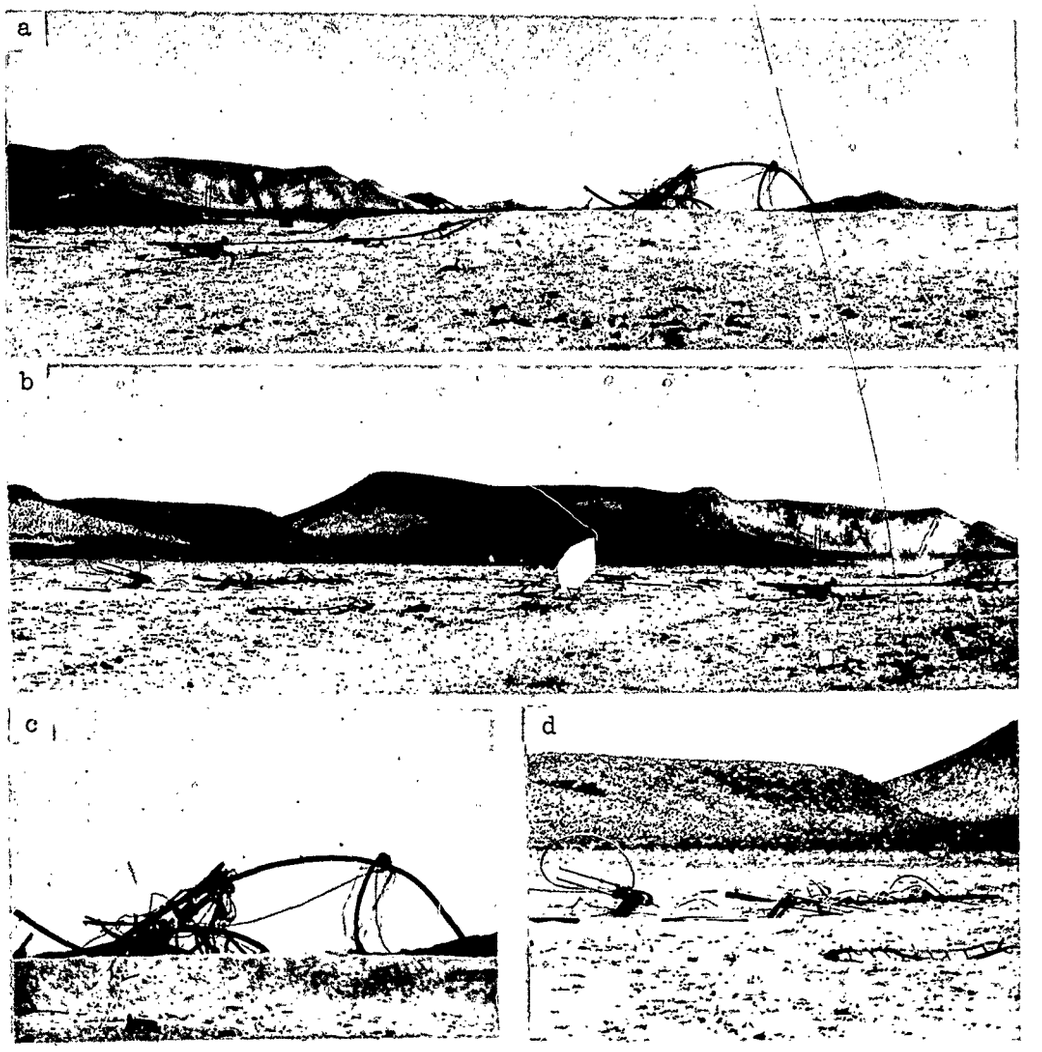

Figure C.10 Shot 11 Tower Wreckage. (a) General View; (b) Main Support Member and Guy Anchors; (c) Close-up View; (d) Guy Cables and Deadmen.

thermal damage (rounding of the corners). The main support cable was still fastened to both sides of this fixture. About 65 feet of cable, though slightly charred and untwisted, remained of the original 354 feet of cable on the side of the fixture nearest the burst point. All of the cable (427 feet) remained on the other side of the fixture. From this, it can be deduced that the cable survived to lengths of at least 490 feet or for distances of greater than about 290 feet from the burst point. Photographs of the fireball of Shot 12 in various stages of its development are given in Figure 3.23. The effects of fireball spikes are discussed briefly in Section 3.1 of Chapter 3.

C.2.9 Television Towers. The television towers were found in such a twisted form (see Figure 3.1 and C.11(c)) that it was difficult to

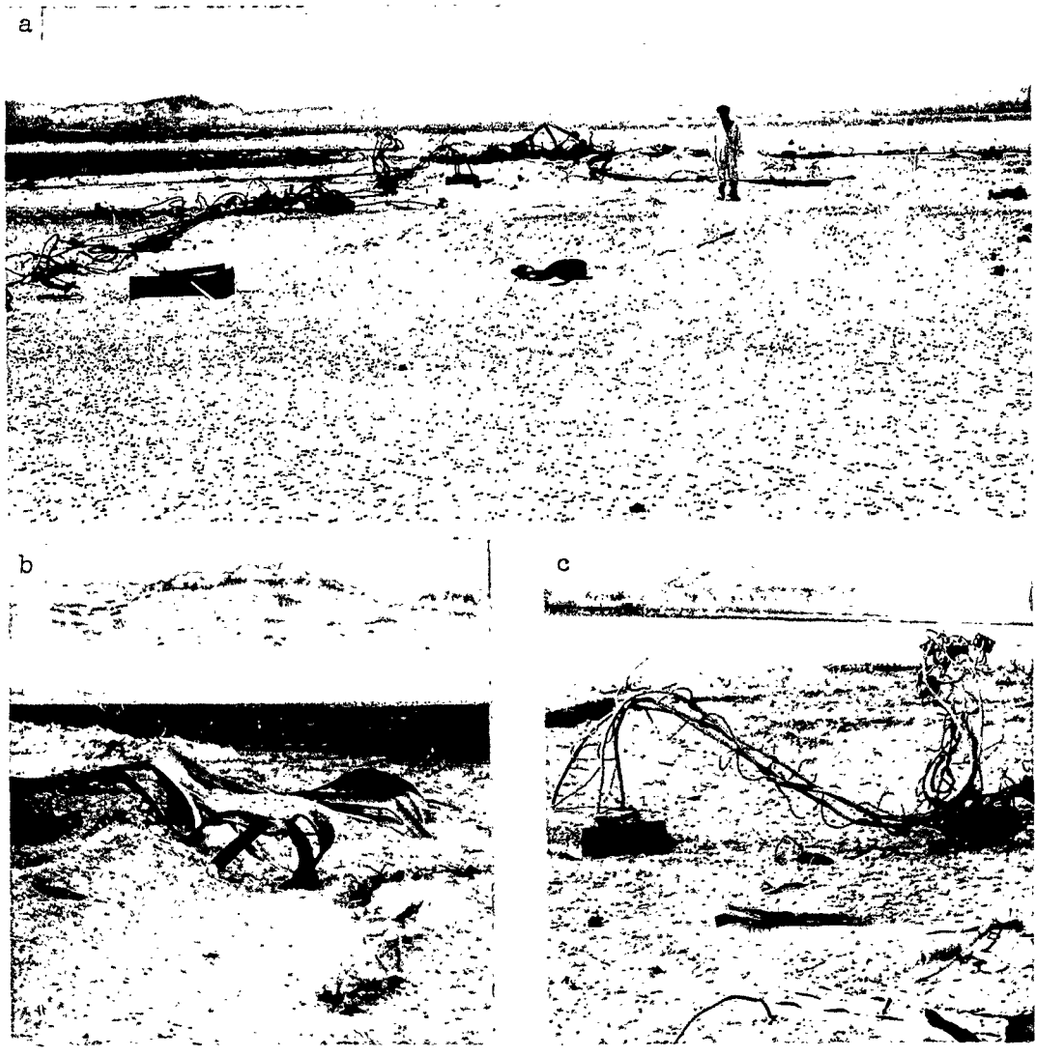

Figure C.11 Shot 12 Tower Wreckage. (a) General View; (b) Top End of Tower Leg; (c) Close-up View of TV Tower.

determine the amount of the towers still intact. As stated in Chapter 3, however, it is estimated that nearly 150 feet of both Towers 1 and 2 was still intact and attached to their base. There did not appear to be any thermal damage to the lower portions of these towers, but there were some slight indications of metal loss at the upper portion of the towers. Most of the remains of these towers were in small pieces, probably less than 40 feet, and were found at ranges of over 800 feet. Several of the top plates (1/2 in. thick) from these towers were located and measured

TABLE C.4 SUMMARY OF DAMAGE TO TOWER LEGS AND GUY CABLES

Shot No.	Yield KT	Tower Height (ft)	Cable Length (ft)	Post-shot Length (ft)		Apparent Reduction in Length (ft)	
				Tower Legs	Guy Cable	Tower Legs	Guy Cable
2	2.5	300	353	200	150	100	203
3	7	300	415	125	150	175	265
4	43	500	771	150	-	350	-
5	3.6	300	415	150	-	150	-
6	8.1	500	771	200	500	300	271
8	15	500	771	150	200	350	571
11	1.53	300	415	150	150	150	265
12	24	400	781	225	490	175	291

from about 3/8 to 1/2 in. thick. Two pieces of the cross-member which supported the lethality study specimens (see Figure 2.2) were also found but did not appear to have lost any appreciable amount of metal. Only a small amount of the guy cables from these towers was located.

No damage summary was obtained for the towers of Shots 13 and 14; however, these shots were similar to Shots 4 and 12 with respect to both tower type and weapon yield. Table C.4 summarizes the approximate lengths of remaining tower legs and guy cables for the various shot towers together with the apparent loss of material determined as the difference between the pre-shot and post-shot lengths of these members. The apparent reduction in length of these items is probably reasonably representative of the amount of material vaporized from the various towers; however, it should be remembered that there were many large pieces of cable and tower wreckage found which could not be associated with any particular tower member, and consequently the values of the lengths of tower legs and cables reported in Table C.4 may be somewhat low and the apparent reduction in length, somewhat high.

DISTRIBUTION

Military Distribution Category 5-10

ARMY ACTIVITIES

1 Asst. Dep. Chief of Staff for Military Operations, D/A, Washington 25, D.C. ATTN: Asst. Executive (R&SW)
2 Chief of Research and Development, D/A, Washington 25, D.C. ATTN: Atomic Division
3 Chief of Ordnance, D/A, Washington 25, D.C. ATTN: ORDTX-AR
4 Chief Signal Officer, D/A, P&O Division, Washington 25, D.C. ATTN: SIGRD-8
5 The Surgeon General, D/A, Washington 25, D.C. ATTN: MEDNE
6- 7 Chief Chemical Officer, D/A, Washington 25, D.C.
8 The Quartermaster General, D/A, Washington 25, D.C. ATTN: Research and Development
9- 11 Chief of Engineers, D/A, Washington 25, D.C. ATTN: ENGNB
12 Chief of Transportation, Military Planning and Intelligence Div., Washington 25, D.C.
13- 15 Commanding General, Headquarters, U. S. Continental Army Command, Ft. Monroe, Va.
16 President, Board #1, Headquarters, Continental Army Command, Ft. Sill, Okla.
17 President, Board #2, Headquarters, Continental Army Command, Ft. Knox, Ky.
18 President, Board #3, Headquarters, Continental Army Command, Ft. Benning, Ga.
19 President, Board #4, Headquarters, Continental Army Command, Ft. Bliss, Tex.
20 Commanding General, Headquarters, First U. S. Army, Governor's Island, New York 4, N.Y.
21 Commanding General, Headquarters, Second U. S. Army, Ft. George G. Meade, Md.
22 Commanding General, Headquarters, Third U. S. Army, Ft. McPherson, Ga. ATTN: ACofS, G-3
23 Commanding General, Headquarters, Fourth U. S. Army, Ft. Sam Houston, Tex. ATTN: G-3 Section
24 Commanding General, Headquarters, Fifth U. S. Army, 1660 E. Hyde Park Blvd., Chicago 15, Ill.
25 Commanding General, Headquarters, Sixth U. S. Army, Presidio of San Francisco, San Francisco, Calif. ATTN: AMGCT-4
26 Commanding General, U.S. Army Caribbean, Ft. Amador, C.Z. ATTN: Cml. Off.
27 Commanding General, USARFANT & MDFR, Ft. Brooke, Puerto Rico
28 Commanding General, Southern European Task Force, APO 168, New York, N.Y. ATTN: ACofS, G-3
29 Commanding General, Eighth U.S. Army, APO 301, San Francisco, Calif. ATTN: ACofS, G-3
30 Commanding General, U.S. Army Alaska, APO 942, Seattle, Wash.
31- 32 Commanding General, U.S. Army Europe, APO 403, New York, N.Y. ATTN: OPOT Div., Combat Dev. Br.
33- 34 Commanding General, U.S. Army Pacific, APO 958, San Francisco, Calif. ATTN: Cml. Off.
35- 36 Commandant, Command and General Staff College, Ft. Leavenworth, Kan. ATTN: ALLLS(AS)
37- 39 Commandant, Army War College, Carlisle Barracks, Pa. ATTN: Library
40 Commandant, The Infantry School, Ft. Benning, Ga. ATTN: C.D.S.
41 Commandant, The Artillery and Missile School, Ft. Sill, Okla.
42 Secretary, The U.S. Army Air Defense School, Ft. Bliss, Texas. ATTN: Maj. Ergan V. Roth, Dept. of Tactics and Combined Arms
43 Commandant, The Armored School, Ft. Knox, Ky.
44 Commanding General, Army Medical Service School, Brooke Army Medical Center, Ft. Sam Houston, Tex.
45 Director, Special Weapons Development Office, Headquarters, CONARC, Ft. Bliss, Tex. ATTN: Capt. T. E. Skinner
46 Commandant, Walter Reed Army Institute of Research, Walter Reed Army Medical Center, Washington 25, D. C.
47 Superintendent, U.S. Military Academy, West Point, N. Y. ATTN: Prof. of Ordnance
48 Commandant, Chemical Corps School, Chemical Corps Training Command, Ft. McClellan, Ala.
49- 50 Commanding General, U.S. Army Chemical Corps, Research and Development Command, Washington, D.C.
51- 52 Commanding General, Aberdeen Proving Grounds, Md. ATTN: Director, Ballistics Research Laboratory
53 Commanding General, The Engineer Center, Ft. Belvoir, Va. ATTN: Asst. Commandant, Engineer School
54 Commanding Officer, Engineer Research and Development Laboratory, Ft. Belvoir, Va. ATTN: Chief, Technical Intelligence Branch
55 Commanding Officer, Picatinny Arsenal, Dover, N.J. ATTN: ORDBB-TK
56 Commanding Officer, Frankford Arsenal, Philadelphia 37, Pa. ATTN: Col. Tewes Kundel
57 Commanding Officer, Army Medical Research Laboratory, Ft. Knox, Ky.
58- 59 Commanding Officer, Chemical Warfare Laboratories, Army Chemical Center, Md. ATTN: Tech. Library
60 Commanding Officer, Transportation R&D Station, Ft. Eustis, Va.
61 Commandant, The Transportation School, Ft. Eustis, Va. ATTN: Security and Information Officer
62 Director, Technical Documents Center, Evans Signal Laboratory, Belmar, N.J.
63 Director, Waterways Experiment Station, PO Box 631, Vicksburg, Miss. ATTN: Library
64 Operations Research Office, Johns Hopkins University, 6935 Arlington Rd., Bethesda 14, Md.
65 Commanding General, Quartermaster Research and Development, Command, Quartermaster Research and Development Center, Natick, Mass. ATTN: CBR Liaison Officer
66 Commanding Officer, Diamond Ordnance Fuze Laboratories, Washington 25, D.C. ATTN: Coordinator, Atomic Weapons Effects Tests
67 Commanding General, Quartermaster Research and Engineering Command, U.S. Army, Natick, Mass.
68- 72 Technical Information Service Extension, Oak Ridge, Tenn.

NAVY ACTIVITIES

73- 74 Chief of Naval Operations, D/N, Washington 25, D. C. ATTN: OP-36
75 Chief of Naval Operations, D/N, Washington 25, D.C. ATTN: OP-37
76 Chief of Naval Operations, D/N, Washington 25, D.C. ATTN: OP-03EG
77 Chief, Bureau of Medicine and Surgery, D/N, Washington 25, D.C. ATTN: Special Weapons Defense Div.
78 Chief, Bureau of Ordnance, D/N, Washington 25, D.C.
79 Chief of Naval Personnel, D/N, Washington 25, D.C.
80 Chief, Bureau of Ships, D/N, Washington 25, D.C. ATTN: Code 348
81 Chief, Bureau of Yards and Docks, D/N, Washington 25, D.C. ATTN: D-440
82 Chief, Bureau of Supplies and Accounts, D/N, Washington 25, D.C.
83- 84 Chief, Bureau of Aeronautics, D/N, Washington 25, D.C.

85 Chief of Naval Research, Department of the Navy Washington 25, D.C. ATTN: Code 811
86- 87 Commander-in-Chief, U.S. Atlantic Fleet, U.S. Naval Base, Norfolk 11, Va.
88 Commandant, U.S. Marine Corps, Washington 25, D.C. ATTN: Code A03H
89 President, U.S. Naval War College, Newport, R.I.
90 Superintendent, U.S. Naval Postgraduate School, Monterey, Calif.
91 Commanding Officer, U.S. Naval Schools Command, U.S. Naval Station, Treasure Island, San Francisco, Calif.
92 Director, USMC Development Center, USMC Schools, Quantico, Va.
93 Commanding Officer, U.S. Fleet Training Center, Naval Base, Norfolk 11, Va. ATTN: Special Weapons School
94- 95 Commanding Officer, U.S. Fleet Training Center, Naval Station, San Diego 36, Calif. ATTN: (SPWP School)
96 Commanding Officer, Air Development Squadron 5, VX-5, China Lake, Calif.
97 Commanding Officer, U.S. Naval Damage Control Training Center, Naval Base, Philadelphia, Pa. ATTN: ABC Defense Course
98 Commander, U.S. Naval Ordnance Laboratory, Silver Spring 19, Md. ATTN: EE
99 Commander, U.S. Naval Ordnance Laboratory, Silver Spring 19, Md. ATTN: EH
100 Commander, U.S. Naval Ordnance Laboratory, Silver Spring 19, Md. ATTN: R
101 Commander, U.S. Naval Ordnance Test Station, Inyokern, China Lake, Calif.
102 Officer-in-Charge, U.S. Naval Civil Engineering Res. and Evaluation La., U.S. Naval Construction Battalion Center, Port Hueneme, Calif. ATTN: Code 753
103 Commanding Officer, U.S. Naval Medical Research Inst., National Naval Medical Center, Bethesda 14, Md.
104 Director, Naval Air Experimental Station, Air Material Center, U.S. Naval Base, Philadelphia, Penn.
105 Director, U.S. Naval Research Laboratory, Washington 25, D.C. ATTN: Mrs. Katherine H. Cass
106 Director, The Material Laboratory, New York Naval Shipyard, Brooklyn, N. Y.
107 Commanding General, Fleet Marine Force, Atlantic, Norfolk, Va.
108 Commanding Officer and Director, U.S. Navy Electronics Laboratory, San Diego 52, Calif. ATTN: Code 4223
109-112 Commanding Officer, U.S. Naval Radiological Defense Laboratory, San Francisco, Calif. ATTN: Technical Information Division
113 Commanding Officer and Director, David W. Taylor Model Basin, Washington 7, D.C. ATTN: Library
114 Commander, U.S. Naval Air Development Center, Johnsville, Pa.
115 Commanding Officer, Clothing Supply Office, Code 1D-0, 3rd Avenue and 29th St., Brooklyn, N.Y.
116 Commandant, U.S. Coast Guard, 1300 E. St. N.W., Washington 25, D.C. ATTN: (OIN)
117 Commanding General, Fleet Marine Force, Pacific, Fleet Post Office, San Francisco, Calif.
118 Commander-in-Chief Pacific, Pearl Harbor, TH
119 Commander, Norfolk Naval Shipyard, Portsmouth 8, Va. ATTN: Code 270
120-124 Technical Information Service Extension, Oak Ridge, Tenn. (Surplus)

AIR FORCE ACTIVITIES

125 Asst. for Atomic Energy Headquarters, USAF, Washington 25, D.C. ATTN: DCS/O
126 Asst. for Development Planning, Headquarters, USAF, Washington 25, D.C.
127 Deputy for Materiel Atomic Energy Control, Asst. for Materiel Program Control, DCS/M, Headquarters, USAF, Washington 25, D. C. ATTN: AFMPC-AE
128 Director of Operations, Headquarters, USAF, Washington 25, D.C. ATTN: Operations Analysis
129 Director of Operations, Headquarters, USAF, Washington 25, D.C.
130 Director of Plans, Headquarters, USAF, Washington 25, D.C. ATTN: War Plans Div.
131 Director of Requirements, Headquarters, USAF, Washington 25, D.C. ATTN: AFDRQ-SA/M
132 Director of Research and Development, DCS/D, Headquarters, USAF, Washington 25, D.C. ATTN: Combat Components Div.
133-134 Director of Intelligence, Headquarters, USAF, Washington 25, D.C. ATTN: AFOIN-IB2
135 The Surgeon General, Headquarters, USAF, Washington 25, D.C. ATTN: Bio. Def. Br., Pre. Med. Div.
136 Asst. Chief of Staff, Intelligence, Headquarters, U.S. Air Forces-Europe, APO 633, New York, N.Y. ATTN: Directorate of Air Targets
137 Commander, 497th Reconnaissance Technical Squadron (Augmented), APO 633, New York, N.Y.
138 Commander, Far East Air Forces, APO 925, San Francisco, Calif. ATTN: Special Asst. for Damage Control
139-140 Commander, Alaskan Air Command, APO 942, Seattle, Wash. ATTN: AAOIN
141 Commander-in-Chief, Strategic Air Command, Offutt Air Force Base, Omaha, Nebraska. ATTN; OAWS
142 Commander, Tactical Air Command, Langley AFB, Va. ATTN: Documents Security Branch
143 Commander, Air Defense Command, Ent AFB, Colo.
144-145 Research Directorate, Headquarters, Air Force Special Weapons Center, Kirtland Air Force Base, New Mexico, ATTN: Blast Effects Res.
146 Commander, Air Materiel Command, Wright-Patterson AFB, Dayton, O. ATTN: MCSW
147 Director of Installations, DCS/O, Headquarters, USAF, Washington 25, D.C. ATTN: AFOIE-E
148 Commander, Air Research and Development Command, Andrews AFB, Washington 25, D.C. ATTN: RDDN
149 Commander, Air Proving Ground Command, Eglin AFB, Fla. ATTN: Adj./Tech. Report Branch
150-151 Director, Air University Library, Maxwell AFB, Ala.
152-159 Commander, Flying Training Air Force, Randolph AFB, Texas. ATTN: Director of Observer Training
160 Commander, Crew Training Air Force, Randolph Field, Tex. ATTN: 2GTS, DCS/O
161-162 Commandant, Air Force School of Aviation Medicine, Randolph AFB, Tex.
163 Commander, Wright Air Development Center, Wright-Patterson AFB, Dayton, O. ATTN: WCOSI
164-165 Commander, Air Force Cambridge Research Center, LG Hanscom Field, Bedford, Mass. ATTN: CRQST-2
166-168 Commander, Air Force Special Weapons Center, Kirtland AFB, N. Mex. ATTN: Library
169 Commander, Lowry AFB, Denver, Colo. ATTN: Department of Special Weapons Training
170 Commander, 1009th Special Weapons Squadron, Headquarters, USAF, Washington 25, D.C.
171-172 The RAND Corporation, 1700 Main Street, Santa Monica, Calif. ATTN: Nuclear Energy Division
173 Commander, Second Air Force, Barksdale AFB, Louisiana ATTN: Operations Analysis Office
174 Commander, Eighth Air Force, Westover AFB, Mass. ATTN: Operations Analysis Office
175 Commander, Fifteenth Air Force, March AFB, Calif. ATTN: Operations Analysis Office
176 Commander, Western Development Div. (ARDC), PO Box 262, Inglewood, Calif. ATTN: WDSIT, Mr. R. G. Weitz
177-181 Technical Information Service Extension, Oak Ridge, Tenn. (Surplus)

OTHER DEPARTMENT OF DEFENSE ACTIVITIES

182 Executive Secretary, Joint Chiefs of Staff, Washington 25, D.C.
183-184 Asst. Secretary of Defense, Research and Engineering. D/D, Washington 25, D.C. ATTN: Tech. Library
185 U.S. Documents Officer, Office of the U.S. National Military Representative, SHAPE, APO 55, New York, N.Y.
186 Director, Weapons Systems Evaluation Group, OSD, Rm 2E1006, Pentagon, Washington 25, D.C.
187 Asst. for Civil Defense, OSD, Washington 25, D.C.
188 Chairman, Armed Services Explosives Safety Board, D/D, Building T-7, Gravelly Point, Washington 25, D.C.
189 Executive Secretary, Military Liaison Committee, PO Box 1814, Washington 25, D.C.
190 Commandant, National War College, Washington 25, D.C. ATTN: Classified Records Library
191 Commandant, Armed Forces Staff College, Norfolk 11, Va. ATTN: Secretary
192 Commandant, Industrial College of the Armed Forces, Ft. Lesley J. McNair, Washington 25, D.C.

193 Commander, Field Command, Armed Forces Special Weapons Project, PO Box 5100, Albuquerque, N. Mex.

194 Commander, Field Command, Armed Forces Special Weapons Project, PO Box 5100, Albuquerque, N. Mex. ATTN: Technical Training Group

195-199 Commander, Field Command, Armed Forces Special Weapons Project, P.O. Box 5100, Albuquerque, N. Mex. ATTN: Deputy Chief of Staff, Weapons Effects Test

200-210 Chief, Armed Forces Special Weapons Project, Washington 25, D.C. ATTN: Documents Library Branch

211 Commanding General, Military District of Washington, Room 1543, Building T-7, Gravelly Point, Va.

212-216 Technical Information Service Extension, Oak Ridge, Tenn. (Surplus)

ATOMIC ENERGY COMMISSION ACTIVITIES

217-219 U.S. Atomic Energy Commission, Classified Technical Library, Washington 25, D.C. ATTN: Mrs. J. M. O'Leary (For DMA)

220-221 Los Alamos Scientific Laboratory, Report Library, PO Box 1663, Los Alamos, N. Mex. ATTN: Helen Redman

222-226 Sandia Corporation, Classified Document Division, Sandia Base, Albuquerque, N. Mex. ATTN: H. J. Smyth, Jr.

227-229 University of California Radiation Laboratory, PO Box 808, Livermore, Calif. ATTN: Clovis G. Craig

230 Weapon Data Section, Technical Information Service Extension, Oak Ridge, Tenn.

231-240 Technical Information Service Extension, Oak Ridge, Tenn. (Surplus)